Title
Integration of benchwork, clinical trials, and real world data to investigate drug interactions

Author
Vora, Bianca

Publication Date
2021

Integration of benchwork, clinical trials, and real world data to investigate drug interactions

by

Bianca Vora

DISSERTATION

Submitted in partial satisfaction of the requirements for degree of

DOCTOR OF PHILOSOPHY

in

Pharmaceutical Sciences and Pharmacogenomics

in the

GRADUATE DIVISION

of the

UNIVERSITY OF CALIFORNIA, SAN FRANCISCO

Approved:

DocuSigned by:

Marina Sirota — Marina Sirota

925B61AB9C41499...

Chair

DocuSigned by:

Kathleen Giacomini — Kathleen Giacomini

[illegible]48C...

DocuSigned by:

Radojka Savic — Radojka Savic

7EC091D1336044E...

Committee Members

ACKNOWLEDGMENTS

"The journey is more important than the destination." This quote could not be more accurate to describe the path to a PhD. However, my journey could not have come to fruition without the constant support and love from my family, friends, and mentors.

First, I would like to thank my dissertation advisor and mentor, Dr. Kathleen Giacomini, for her endless support and encouragement. Kathy's scientific curiosity, creativity, and leadership has been a strong source of inspiration and encouragement. Her mentorship style provided me the freedom and opportunity to develop as an independent scientist, allowing me to embark on a variety of projects across a spectrum of scientific topics as well as foster ideas on my own accord. I would not be the scientist I am today without her and I could not have envisioned a better mentor for my PhD journey.

Next, I would like to thank Dr. Rada Savic and Dr. Marina Sirota, members of my dissertation committee, for their helpful insight and support for my research projects and professional development. I would also like to thank Dr. Deanna Kroetz and Dr. Nadav Ahituv, PSPG program directors, whose leadership contributed to my development as well.

I was fortunate to work with a variety of collaborators during my time at UCSF and this dissertation would have not been completed without their hard work. I would like to thank Dr. Natalia Khuri, Dr. John Newman, Dr. Andrew Greenberg, Dr. Russ Altman, Anita Wen, Kim

Trinh, Dr. Theresa Pedersen, Dr. Maria Garcia-Cremades Mira, Dr. Tomiko Oskotsky, Dr. Stefano Rensi, and Adam Lavertu for all their contributions.

Being a part of the Giacomini lab was an absolute pleasure and I find myself fortunate to have been surrounded by such wonderful and intelligent scientists during my time here. I would like to thank all members of the Giacomini lab, both past and present, for their scientific expertise and mentorship, but especially for the coffee breaks and spontaneous conversations.

To my fellow PSPG classmates and friends (old and new), especially Jennifer Stokes and Megan Koleske, I am incredibly grateful for your support and encouragement. Thank you for believing in me when I did not believe in myself. And more importantly, thank you for the countless happy hours, FaceTimes (especially during the time of COVID), belly-aching laughs, and unforgettable memories.

To my family, especially mom, dad, and Vineet, thank you. The magnitude of love and support I have received from you is immeasurable. I am immensely thankful for the confidence and opportunity you have provided to allow me to succeed and follow my dreams. Thank you for being my biggest fans and I hope to continue to make you proud.

CONTRIBUTIONS

Several chapters in this dissertation contain material that has been published previously or is currently under consideration/review. They do not necessarily represent the final published form and in all cases have been edited slightly.

Chapter 1 of this dissertation is a reprint of previously published work: Lavertu A and Vora B, Giacomini KM, Altman R, Rensi S. (2021) "A New Era in Pharmacovigilance: Towards real world data and digital monitoring." *Clinical Pharmacology and Therapeutics*. doi: 10.1002/cpt.2172. A.L., B.V., K.G., S.R., and R.A. wrote the manuscript; A.L. and B.V. contributed equally to writing the text and designing the figures and tables; K.G., R.A., S.R. provided direction, reviewed and edited drafts, and contributed text.

Chapter 2 of this dissertation is a reprint of previously published work: Vora B and Green EAE, Khuri N, Bällgren F, Sirota M, Giacomini KM. (2020) "Drug-nutrient interactions: discovering prescription drug inhibitors of the thiamine transporter ThTR-2 (SLC19A3)." *American Journal of Clinical Nutrition*. doi: 10.1093/ajcn/nqz255. BV, EAEG, and KMG conceived of the study and the designed research; BV, EAEG, NK, and FB conducted research and carried out experiments; BV, EAEG, NK, and FB performed data analysis; all authors contributed to writing and editing the manuscript; KMG had primary responsibility for final content; and all authors read and approved the final manuscript.

Chapter 4 of this dissertation is a reprint of material recently accepted for publication: Vora B and Brackman DJ, Zou L, Garcia-Cremades M, Sirota M, Savic RM and Giacomini KM. (2021) “Oxypurinol Pharmacokinetics and Pharmacodynamics in Healthy Volunteers: Influence of BCRP Q141K polymorphism and patient characteristics.” *Clinical and Translational Science*. BV, DJB, LZ, MGC, and KMG wrote the manuscript; DJB, BV, LZ, MGC, RMS, MS, and KMG designed the research; BV, DJB, LZ, and MGC performed the research; BV, DJB, LZ, and MGC analyzed the data; MS, RMS, and KMG contributed new reagents/analytical tools.

Chapter 5 of this dissertation is a reprint of material currently in review for publication: Yee SW and Vora B, Oskotsky TT, Zou L, Jakobsen S, Enogieru OJ, Koleske ML, Kosti I, Rödin M, Sirota M, Giacomini KM. “Drugs in COVID19 clinical trials: Predicting transporter-mediated drug-drug interactions using in vitro assays and real-world data.” S.W.Y, B.V, T.T.O, L.Z, S.J, and K.M.G wrote the manuscript; S.W.Y, B.V, and K.M.G designed the research; S.W.Y, B.V, T.T.O, L.Z, O.J.E, and K.M.G performed the research; S.W.Y, B.V, T.T.O, L.Z, S.J, O.J.E, M.L.K, M.R, and K.M.G analyzed the data; I.K, M.S, and K.M.G contributed new reagents/analytical tools.

Integration of benchwork, clinical trials, and real world data to investigate drug interactions

Bianca Vora

ABSTRACT

Real world data (RWD), data from various sources other than clinical trials, is increasingly being integrated into the research setting. In particular, electronic health records (EHRs), which serve as a clinical record to document a patient's medical history as well as support administrative functions, have been an invaluable resource rich with patient data. Here we present three projects spanning four chapters where EHRs, in combination with clinical trials and pharmacokinetic and pharmacodynamic (PKPD) modelling, were used to extend and complement studies and findings in the laboratory focusing on transporter-mediated drug interactions. Transporter-mediated drug interactions have the potential to influence both drug efficacy as well as toxicity. During the clinical development of the Janus Kinase 2 (JAK2) inhibitor fedratinib, several patients developed symptoms similar to Wernicke's encephalopathy, a life-threating disease caused by Vitamin B1 (thiamine) deficiency; subsequent *in vitro* studies showed that fedratinib is a potent inhibitor of ThTR-2. Motivated by this drug-nutrient interaction (DNI) observed in the fedratinib trial, we investigated if commonly used prescription drugs can inhibit ThTR-2. Using a multifaceted approach, we started with an *in vitro* high-throughput screen which was further complemented by quantitative structure activity relationship (QSAR) modelling and real world

data. Our comprehensive analysis suggested that several marketed drugs inhibit ThTR-2 and may contribute to thiamine deficiency, especially in at-risk populations. In order to further explore the impact of these potential inhibitors in humans, we designed and conducted a clinical study in healthy volunteers. Interestingly, we observed that thiamine concentrations were higher when co-administered with trimethoprim, one of the potent, clinically relevant inhibitors identified in our screen. The maximum concentration achieved (C_{max}) and area under the curve from 0 to 24 hours (AUC_{0-24}) were 2.7- and 4.6-fold higher in the combination arm, respectively. We hypothesized that trimethoprim may inhibit OCT1, a hepatic uptake transporter, in addition to ThTR-2, which was supported using EHR data by comparing laboratory values of endogenous OCT1 biomarkers in patients prescribed trimethoprim versus patients not prescribed trimethoprim. Next, we shifted our focus to pharmacogenomics, that is, genetic factors that affect drug response. Response to allopurinol, the first line treatment for gout, is highly variable; the reduced function variant BCRP p.Q141K has been associated with poor response to allopurinol. Thus, we aimed to characterize the relationship between BCRP p.Q141K, allopurinol/oxypurinol, and serum uric acid (SUA) levels by performing a clinical trial, building a PKPD model, and mining EHRs. Our clinical study found that p.Q141K associated with longer half-life of oxypurinol and our PKPD model found that gender affected oxypurinol volume of distribution while BCRP genotype and kidney function were significant covariates for baseline SUA levels. Additionally, using RWD, we found that drugs that were clinical inhibitors of BCRP associated with increased SUA levels, suggesting the potential of these drugs to cause hyperuricemia. Finally, given the ongoing COVID19 pandemic, we conducted extensive *in vitro* experiments aimed at predicting the potential for 25 small molecule drugs in clinical trials for COVID19 to cause transporter-mediated drug-drug interactions (DDIs). We found that 21 of the drugs were predicted to cause a clinically relevant DDI, and we were able to provide preliminary validation of these *in vitro* findings using EHR data, including a database representing nearly 120,000 COVID19 patients.

Collectively, my dissertation research demonstrates how the integration of benchwork, clinical trials, and real world data provides us a new approach to translational research, bridging findings from the laboratory to patients.

TABLE OF CONTENTS

CHAPTER 1: A New Era in Pharmacovigilance: Towards real world data and digital monitoring....1

1.1 ABSTRACT 1

1.2 INTRODUCTION 2

1.3 ESTABLISHED PHARMACOVIGILANCE SYSTEMS....3

1.4 EMERGING PHARMACOVIGILANCE SYSTEMS 5

1.5 EXPERIMENTAL PHARMACOVIGILANCE SYSTEMS....7

1.6 CONCLUSION 12

1.7 STATEMENT OF PURPOSE 13

1.8 FIGURES....15

1.9 TABLES....17

1.10 REFERENCES....18

CHAPTER 2: Drug-Nutrient Interactions: Discovering prescription drug inhibitors of the thiamine transporter ThTR-2 (SLC19A3) 21

2.1 ABSTRACT 21

2.2 INTRODUCTION 22

2.3 METHODS 24

2.3.1 Chemicals and reagents 24

2.3.2 Radiometric cell uptake screen 24

2.3.3 Radiometric cell uptake dose-response curves......26
2.3.4 Data analysis for radiometric cell uptake assays......26
2.3.5 Clinical relevance ratios......27
2.3.6 Data preparation for the QSAR model......27
2.3.7 Analysis of physicochemical properties for QSAR model......28
2.3.8 QSAR model development with machine learning......28
2.3.9 Substructure similarity search......29
2.3.10 EHR data and analysis......29
2.4 RESULTS......32
2.4.1 Overview......32
2.4.2 In vitro radiometric thiamine inhibition screen identified 146 potential thiamine inhibitors......32
2.4.3 Potency studies of top inhibition hits validate primary screen......33
2.4.4 Selected clinically relevant screen hits maintain predicted potency......34
2.4.5 Computational characterization of properties of hit compounds......34
2.4.6 EHRs validate identified clinically relevant inhibitors......36
2.5 DISCUSSION......38
2.6 FIGURES......44
2.7 TABLES......56
2.8 REFERENCES......66
CHAPTER 3: Intersection of Pre-Clinical, Clinical, and Real World Data: A multi-faceted approach to understand complex transporter-mediated drug-nutrient interactions......74

3.1 ABSTRACT 74
3.2 INTRODUCTION 75
3.3 METHODS 77
3.3.1 Clinical study design 77
3.3.2 Bioanalytical methods 79
3.3.3 Data cleaning and pharmacokinetic analyses....................................81
3.3.4 Transporter inhibition studies 82
3.3.5 Prediction of transporter-mediated inhibition 82
3.3.6 Thiamine Pyrophosphokinase 1 (TPK1) enzyme assay..........................83
3.3.7 Real world data analyses 84
3.4 RESULTS 86
3.4.1 Thiamine concentrations increase when co-administered with trimethoprim 86
3.4.2 Trimethoprim prevents metabolism of thiamine by inhibiting OCT1 and potentially TPK1..........87
3.4.3 Electronic health record analyses complement in vitro OCT1 inhibition findings....87
3.5 DISCUSSION 88
3.6 ACKNOWLEDGEMENTS 92
3.7 FIGURES...93
3.8 TABLES..99
3.9 REFERENCES..103
CHAPTER 4: Oxypurinol Pharmacokinetics and Pharmacodynamics in Healthy Volunteers: Influence of BCRP Q141K polymorphism and patient characteristics.............108

4.1 ABSTRACT 108

4.2 INTRODUCTION 109

4.3 METHODS 111

4.3.1 Study participants 111

4.3.2 Genotyping 111

4.3.3 Clinical study design 112

4.3.4 Bioanalytical methods 113

4.3.5 Non-compartmental PK analysis 114

4.3.6 Collection of mouse luminal contents 114

4.3.7 Xanthine oxidase assay 115

4.3.8 Population PKPD model 115

4.3.9 Electronic health record analyses to evaluate uric acid levels in patients prescribed clinical inhibitors of BCRP 117

4.4 RESULTS 119

4.4.1 Study cohort 119

4.4.2 BCRP p.Q141K associates with a longer half-life of oxypurinol and the concentration-time profile of oxypurinol demonstrates enterohepatic recycling 120

4.4.3 PKPD covariate model shows a significant effect of gender on oxypurinol volume of distribution and genotype and SCr on baseline SUA 121

4.4.4 Electronic health record analyses show clinical inhibitors of BCRP can phenocopy the p.Q141K variant 122

4.5 DISCUSSION 124

4.6 FIGURES 129

4.7 TABLES 139

4.8 REFERENCES 143

CHAPTER 5: Drugs in COVID19 Clinical Trials: Predicting transporter-mediated drug-drug interactions using in vitro assays and real world data 147

5.1 ABSTRACT 147

5.2 INTRODUCTION 148

5.3 METHODS 150

5.3.1 Selection of COVID19 drugs used in clinical trials 150

5.3.2 Cell lines used for inhibition studies 150

5.3.3 Transporter inhibition studies 150

5.3.4 Prediction of transporter-mediated inhibition 151

5.3.5 Electronic health record analyses 151

5.3.6 Statistical analyses 153

5.4 RESULTS 153

5.4.1 In vitro studies determine inhibition potencies of 25 drugs used in clinical trials for COVID19 153

5.4.2 Clinically relevant transporter-mediated drug-drug interactions are predicted for 21 drugs 155

5.4.3 Electronic health record analyses complement in vitro findings on clinically relevant transporter-mediated DDIs 156

5.5 DISCUSSION 160

5.5.1 Drugs in clinical trials for COVID19 inhibited membrane transporters that are targets for clinical DDIs 161

5.5.2 Most of the drugs (21 out of 25) tested were predicted to cause at least one transporter-mediated clinical DDI 162

5.5.3 Real world data from electronic health records were consistent with our predictions of transporter-mediated DDIs 163

5.6 FIGURES 166

5.7 TABLES 172

5.8 SUPPLEMENTARY INFORMATION 206

5.9 REFERENCES 215

CHAPTER 6: Conclusions and Perspectives 223

List of Figures

Figure 1.1 Overview of pharmacovigilance methods at varying stages of development 15

Figure 1.2 General pharmacovigilance workflows for emerging and experimental systems........16

Figure 2.1 Workflow of experimental and computational methods for primary screen and identification of clinically relevant hits 44

Figure 2.2 Classification of drug library by therapeutic class 45

Figure 2.3 Total number of hits and nonhits in each therapeutic class...46

Figure 2.4 IC_{50} curves of a subset of (A) potent and (B) clinically relevant hits. IC50 values were determined for selected drugs in HEK293 cells stably overexpressing ThTR-2 47

Figure 2.5 Thiamine laboratory values in patients on 1 or more clinically relevant inhibitors compared with concentrations in patients in vulnerable populations but not on a clinically relevant inhibitor..48

Supplemental Figure 2.1 Frequency distribution of predicted intestinal concentrations for 175 commonly used drugs 49

Supplemental Figure 2.2 Distribution of inhibition of thiamine uptake across all plates in primary screen..50

Supplemental Figure 2.3 Additional dose response curves of top hits from primary screen 51

Supplemental Figure 2.4 Additional dose response curves of top hits with high clinical interaction ratios...52

Supplemental Figure 2.5 Differences in physicochemical properties between hits and nonhits ...53

Supplemental Figure 2.6 Receiver Characteristic Operating (ROC) curves of double-loop cross-validation experiments using (A) 18 features and (B) 770 molecular descriptors 54

Figure 3.1 Average thiamine concentrations and pharmacokinetic parameters after administration of thiamine alone or in combination with trimethoprim in 6 healthy volunteers ..93

Figure 3.2 Inhibition of [^{3}H]-thiamine uptake by trimethoprim in HEK293-FlpIn cells overexpressing human OCT1 (SLC22A1)...95

Figure 3.3 Results of the thiamine pyrophosphokinase 1 (TPK1) activity assay 96

Figure 3.4 Endogenous biomarker levels in patients prescribed trimethoprim compared with levels in patients not prescribed trimethoprim using electronic health record data.......................97

Supplemental Figure 3.1 Average thiamine pyrophosphate to thiamine ratio after administration of thiamine alone or in combination with trimethoprim in 6 healthy volunteers ..98

Figure 4.1 Concentration time profiles for (A) allopurinol and (B) oxypurinol after a single dose of allopurinol to healthy volunteers...129

Figure 4.2 Evaluation of oxypurinol PK and PKPD models through visual predictive checks ..130

Figure 4.3 Simulated plasma concentrations of serum uric acid (SUA) at (A) baseline and (B) following allopurinol administration 131

Figure 4.4 Uric acid levels in patients prescribed at least one clinical inhibitor of BCRP compared with levels in patients not prescribed a clinical inhibitor of BCRP from electronic health record data...132

Supplemental Figure 4.1 Individual concentration-time profiles for oxypurinol up to 8 hours post-dose after a 300mg single dose of allopurinol in 19 healthy volunteers 134

Supplemental Figure 4.2 Xanthine oxidase activity in mouse intestinal contents 135

Supplemental Figure 4.3 Goodness of Fit (GoF) plots for (A) oxypurinol PK and (B) serum uric acid levels 136

Supplemental Figure 4.4 Visual predictive checks (VPCs)..137

Supplemental Figure 4.5 Sensitivity analysis comparing patients prescribed at least one clinical inhibitor of BCRP vs patients not prescribed a clinical inhibitor of BCRP at a 1:1 ratio 138

Figure 5.1 Overall study approach to assess the risks for transporter-mediated drug-drug interactions (DDI) of 25 drugs in clinical trials to treat COVID19 patients 166

Figure 5.2 Results of predictions of 25 drugs in COVID19 clinical trials to cause *in vivo* transporter-mediated drug-drug interactions (DDIs) 168

Figure 5.3 Endogenous levels of transporter biomarkers in patients prescribed drugs that are predicted to cause a transporter-mediated DDI 170

Supplemental Figure 5.1 Schematic for Cerner Real World COVID19 data mining and real world data analysis...171

List of Tables

Table 1.1 Select examples of successful pharmacovigilance studies in which ADR and RWD database studies played a prominent role........17

Table 2.1 Prescription drug inhibitors predicted to be clinically relevant based on experimental and computational methods 56

Table 2.2 Physicochemical descriptors of hit and nonhit compounds identified in a screen of ThTR-2........58

Supplemental Table 2.1 Z-prime and number of hits for each plate 59

Supplemental Table 2.2 Detailed dose response curve parameters for a subset of top hits from primary screen........60

Supplemental Table 2.3 Detailed dose response curve parameters for selected hits with high clinical interaction ratios........61

Supplemental Table 2.4 Molecular descriptors used to train QSAR models 62

Supplemental Table 2.5 Detailed dose response curve parameters for selected compounds from QSAR........63

Supplemental Table 2.6 Analysis of discrepancies between *in vitro* screen and QSAR model....64

Supplemental Table 2.7 Demographics for on and off groups used in EHR analysis........65

Table 3.1 Demographics of study cohort analyzed as part of the clinical trial........99

Table 3.2 Summary of pharmacokinetic parameters of thiamine in six healthy volunteers with or without trimethoprim 100

Table 3.3 Summary table of electronic health record analyses comparing laboratory values in patients prescribed trimethoprim versus patients not prescribed trimethoprim 101

Supplemental Table 3.1 Demographics for on and off groups used in EHR analysis 102

Table 4.1 Demographics and clinical characteristics of study cohort 139

Table 4.2 Summary of the effect of the BCRP p.Q141K variant allele on the pharmacokinetic parameters of allopurinol and oxypurinol computed by non-compartmental analysis 140

Table 4.3 Parameter estimates in the final oxypurinol PKPD covariate model..........................141

Supplemental Table 4.1 Demographics for on and off groups used in EHR analysis 142

Table 5.1 Summary table showing the inhibition potencies of drugs in COVID19 clinical trials against transporters that are mediators of drug-drug interactions (DDIs) 172

Table 5.2 Summary of drugs in clinical trials for COVID19 predicted to cause a transporter-mediated DDI 175

Table 5.3 Summary table of electronic health record analyses comparing endogenous biomarkers in patients prescribed predicted clinical inhibitors of transporters versus patients not prescribed predicted clinical inhibitors..180

Table 5.4 Table of electronic health record analyses comparing serum creatinine levels in patients prescribed hydroxychloroquine (HCQ) and chloroquine (CQ) versus patients not prescribed hydroxychloroquine and chloroquine (control)...182

Supplemental Table 5.1 Results of screening 25 drugs used in COVID19 clinical trials at one concentration across eleven transporters 183

Supplemental Table 5.2 Pharmacokinetic characteristics for the 25 drugs used in computing the [I] value for I/IC_{50} determinations 188

Supplemental Table 5.3 Demographic for on and off groups used in EHR analyses..................190

Supplemental Table 5.4 Comparison of IC_{50} values from this study to data in the literature 192

Supplemental Table 5.5 Expansion of Table 5.2, showing DDI predictions for each drug with I/IC_{50} for each organ (intestine, liver, and kidney) and their respective transporters 194

Supplemental Table 5.6 Evidence from the literature on potential biomarkers of transporter-mediated DDIs 200

Supplemental Table 5.7 Sensitivity analyses comparing patients prescribed sildenafil vs patients not prescribed sildenafil at a 1:5, 1:10, and 1:20 ratio between the “on” drug and “off” drug groups 202

Supplemental Table 5.8 Prescription frequencies of drugs that are substrates for transporters listed in the FDA Drug Development and Drug Interactions: Table of Substrates, Inhibitors, and Inducers 204

CHAPTER 1

A New Era in Pharmacovigilance: Towards real world data and digital monitoring

1.1 ABSTRACT

Adverse drug reactions (ADRs) are a major concern for patients, clinicians, and regulatory agencies. The discovery of serious ADRs leading to substantial morbidity and mortality has resulted in mandatory Phase IV clinical trials, black box warnings, and withdrawal of drugs from the market. Real World Data, data collected during routine clinical care, is being adopted by innovators, regulators, payors, and providers to inform decision making throughout the product life cycle. We outline several different approaches to modern pharmacovigilance, including spontaneous reporting databases, electronic health record monitoring and research frameworks, social media surveillance, and the use of digital devices. Some of these platforms are well established while others are still emerging, or experimental. We highlight both the potential opportunity, as well as the existing challenges within these pharmacovigilance systems that have already begun to impact the drug development process, as well as the landscape of postmarket drug safety monitoring. Further research and investment into different and complementary

---

*Modified from the publication: Lavertu A and Vora B, Giacomini KM, Altman R, Rensi S. (2021) “A New Era in Pharmacovigilance: Towards real world data and digital monitoring.” *Clinical Pharmacology and Therapeutics*. doi: 10.1002/cpt.2172.

pharmacovigilance systems is needed to ensure the continued safety of pharmacotherapy.

1.2 INTRODUCTION

The safety of a drug continues to be monitored after approval and marketing in an ongoing process of pharmacovigilance (*1*). This postmarket drug safety monitoring is especially important with regards to ADRs that are rare, only occurring in certain subgroups, and/or only develop after long-term drug exposure. In some cases, serious ADRs are not recognized until long after a drug has been approved for market, as seen in the case of thalidomide where its use in pregnant women led to congenital malformations. Accordingly, the importance of postmarket monitoring is highlighted by the finding that one-third of newly identified safety issues in the postmarketing period are added to the Warnings and Precautions section of the label, the second highest tier of severity, indicating the serious nature of newly identified ADRs (*2*).

The passage of the 21st Century Cures Act has modernized clinical trials and requires the evaluation of the potential use of Real World Data (RWD), data collected during routine clinical care in the form of EHRs, medical billing, and other data generating activities, in the regulatory decision making and approval process. Real World Evidence (RWE) is the evidence of the potential benefits of the medical product in a clinical setting derived from RWD. Results from various study designs and analyses, both prospective and retrospective, that use RWD are accepted as RWE. The US Food and Drug Administration (FDA) guidance on RWE describes several contexts in which it can be used during the product life cycle, such as proving an unmet medical need, substituting for a control group, as supporting evidence for a label expansion, and as a part of postmarketing studies. The multiple emergency use authorizations EUAs granted to drugs during the COVID19 pandemic highlights a situation where postmarket pharmacovigilance becomes pivotal to maintaining long-term patient safety. Collectively, the legislative acts and regulatory practices have led to an increased reliance on postmarket pharmacovigilance to inform drug safety. Innovation in pharmacovigilance is needed to address these challenges and complement clinical trials by improving the sensitivity and specificity of ADR detection and streamlining the process of refining real world data into real world evidence that supports regulatory decision-making.

1.3 Established Pharmacovigilance Systems

Published case reports have been circulated among physicians since the late 1960s and continue to serve an important role in pharmacovigilance. They are typically rich in information because physicians are trained in the rigorous evaluation of medical histories, drug exposures, and outcomes; additionally, peer review provides a form of quality control. However, case reports are fundamentally anecdotal data points, and as such cannot support conclusions in broader populations. The digitization of written media and advent of databases and search engines make it possible to collect, store, and rapidly retrieve relevant and comprehensive case series, but the data are unstructured text, which is not suitable for rigorous quantitative analysis. Despite these limitations, case reports published in journals are useful for generating hypotheses, and pharmacovigilance studies often start with a search of the relevant case literature.

Medwatch has been the principal means of collecting and analyzing information about ADRs since 1993 and is used by the FDA to collect information on both small molecule drugs and biologics. Data are collected using standardized individual case safety reports forms, which are submitted physically or electronically to the FDA Adverse Event Reporting System (FAERS). The aggregate data are then mined for safety signals, which generate hypotheses for further investigation. FAERS has successfully identified previously unreported ADRs, with FAERS data contributing to more than 50% of all postmarket safety-related label changes (*3*). **Table 1.1** lists a selection of additional pharmacovigilance studies in which FAERS or other ADR databases have played a prominent role. In addition to FAERS, the FDA has event reporting systems for (1) foods, dietary supplements, and cosmetics, (2) medical devices, and (3) vaccines, via CAERS, MAUDE, and VAERS, respectively.

However, FAERS case reports as a source of data are limited by incompleteness, bias, and inconsistency. Prescribing decisions are often influenced by factors that affect clinical outcomes such as comorbidities, insurance, and access to primary care, information that is not available in the publicly available FAERS data. The Institute for Safe Medical Practices (ISMP) found that over half of the reports in FAERS were missing basic information, such as age, gender, exposure date, and outcome. Additionally, FAERS does not measure the total number of exposures in the population, so there is no “denominator” to estimate the frequency of adverse events. While adverse events are generally underreported, stimulated reporting driven by news, social media, and advertising can increase reporting rates for certain drugs. Incorrect hypotheses generated from erroneous or incomplete adverse event report data can be costly, with false positives resulting in resources wasted on unnecessary studies and false negatives leading to harm to patients.

1.4 EMERGING PHARMACOVIGILANCE SYSTEMS

Another component of the data revolution within healthcare has been the adoption of information technology by the health insurance industry and the adoption of electronic health records (EHRs) by healthcare systems as a result of the 2009 HITECH Act (**Figure 1.1**). Insurance claims capture prescription and medical diagnoses across healthcare providers, with the caveat that they do not directly measure outcomes. EHRs contain rich information, such as clinical notes, images, and lab test values; however, they are often locked within institutional silos on systems that are unique for each provider institution and suffer from bias related to their primary purpose, a clinical and legal record.

The Sentinel initiative extends the pharmacovigilance capabilities of the FDA by leveraging EHR systems and insurance claims data in distributed data networks of partner institutions (*4*).The Sentinel system is used to study specific drug-event outcomes and, more recently, is being used to generate drug safety signals. Analyses can be submitted to the partner network and run independently at each site and results can then be combined to provide comprehensive safety profiles. The integration of these various data sources has allowed for a more comprehensive and synergistic pipeline and capabilities. A general workflow is presented in the top row of **Figure 1.2**. Sentinel required the development and implementation of a common data model and data quality assurance standards to ensure interoperability of data and reliability of analytical findings. Current efforts have been primarily focused on billing and claims data. Several new data partnership networks and consortia have emerged, such as PedsNet and the Open Health Data Science Informatics (OHDSI) network, that are improving and extending the governance, interoperability, and data stewardship frameworks pioneered by Sentinel. For example, the OHDSI network has adopted the OMOP's Common Data Model for standardizing identifiers for diseases, procedures, drugs, and other components of a patient health record and has created a network of hospitals standardized to this data model. This enables an analysis designed at one member institution to be quickly replicated in other healthcare systems within the OHDSI network with minimal need to readjust the analysis. For instance, an analysis designed at Stanford could be run at hospitals in Israel, South Korea, and Australia, quickly finding support for or discrepancies in the findings of a single institution. Patient Centered Outcome Research Institute, PCORI, is establishing data networks, as well as procedures for evaluating and ensuring the relevance and reliability of data. The FDA is piloting demonstration cases for the use of RWE in regulatory decision making.

An example of a new drug approval that relied on RWE, is Avelumab, a monoclonal antibody directed against PD-L1, programmed death ligand 1. Avelumab was approved based on a single arm, Phase II trial where historical controls were identified from electronic health records and were used to characterize the natural history of the disease (*5*). Additionally, ADAPTABLE (Aspirin Dosing: A Patient-Centric Trial Assessing Benefits and Long-Term Effectiveness), a clinical trial evaluating the optimal dose of aspirin in patients with atherosclerotic cardiovascular disease, has utilized PCORnet EHRs and claims data at multiple stages of their study, from identifying patients which meet the inclusion/exclusion criteria to capturing primary and secondary study endpoints (*6*). The ADAPTABLE trial represents the first randomized trial within PCORnet and as such, has also developed new methodologies to take advantage of the data with the PCORnet data infrastructure.

The primary purpose of EHRs is to inform clinical decisions and/or support administrative functions (i.e. documentation to support billing). As a result, issues such as human/coding errors or bias may affect how information is captured prior to analysis. Additionally, the fractionalized nature of the U.S. healthcare system makes it difficult to track patients across different healthcare systems resulting in incomplete data entries.

Clinical definitions, terminology, and note-taking style vary between and within healthcare systems, making the extraction and transformation of clinical information to standardized elements, such as SNOMED codes, technically difficult. The challenging nature of clinical note processing has resulted in the majority of analyses to-date primarily focusing on the billing related ICD10 codes. Lastly, unpredictability about patient compliance (i.e. even if a prescription is written does not mean the patient will pick it up) limits the use and extension of this data. These represent major obstacles to wide-spread pharmacovigilance using EHRs and future work will need to overcome these issues before the benefits of EHR data can be fully realized.

1.5 Experimental Pharmacovigilance Systems

Though Sentinel, PCORI, and OHDSI have greatly improved pharmacovigilance efforts, they rely on a constrained set of information within the healthcare system, that is, information in the

EHR or in billing and claims data (*7*). Outside the healthcare system, data from social media represent another key opportunity for pharmacovigilance. Social media data contains various data streams, potentially enabling us to identify patterns in behavior, environment, drug use, drug-drug interactions, and ADRs. A general workflow for pharmacovigilance in social media data is presented in the bottom row of **Figure 1.2**. The broad usage of social media by the public yields a massive dataset that is continuously growing and has huge potential for generating public health benefits. Individual experiences with a particular drug are often posted directly to social media. These testimonials can be found on both general platforms like Twitter and Reddit, as well as health-oriented websites, such as AskaPatient.com, drugs.com, and iodine.com. Social media data often contain information critical to postmarket pharmacovigilance, such as individual experiences of adverse drug reactions, information about environmental factors, reports of pill diversions, and polypharmacy (both recreational and prescribed) that is often missed by other postmarketing surveillance systems.

There has been progress in developing new methods for postmarketing surveillance in social media data through the use of statistical models, machine learning, and deep neural network architectures. The annual Social Media Mining for Health Applications (SMM4H) workshop has resulted in algorithms capable of identifying drug mentions with high precision and recall, even in situations where these mentions are informal slang terms or misspelled drug names. However, high performance of ADRs continues to present a challenge as text descriptions of a particular ADR might vary greatly in written language, for instance “stomach” may be expressed as “stomach ache”, “stomach pain”, “abdominal pain”, “tummy ache”, etc. Additionally, classifying a particular tweet for first-person vs. secondary reports of medication ingestion presents another challenge and has also been featured as challenges for the community with varying levels of success. Ideally, these efforts will culminate in systems capable actively monitoring social media data and generating real-time statistics relevant to pharmacovigilance efforts.

While social media can provide a large volume of easily accessible data, the nature of social media presents several challenges for the extraction of signals related to pharmacovigilance. The first set of these challenges are that (1) very few social media posts are relevant to pharmacovigilance, ~0.2% of tweets mention a medication (*8*), (2) information is represented in unstructured text, (3) drugs and medical conditions are often misspelled, abbreviated, or discussed using slang (*9*), and (4) mentions of medical events may not be firsthand accounts, (5) social media reports will contain false positives, but often provide less information than clinical case reports and so the reliable identification of true drug side effects from this data will be difficult. Recent work, as mentioned above, indicates that many of these problems may be overcome in the near future. Once these systems can produce robust ADR event statistics, further work may extend their functionality through analysis of the individual testimonies found within social media data. Social media data often contains lifestyle information like exercise patterns, eating habits, socio-economic issues, and/or drug abuse behavior that will be missing from the EHR for the foreseeable future. For example, systems may find indications of relative quality of life improvements given a particular medication, patient preferences, or capture additional demographic information that could be key to protecting at risk populations, such as pregnant women and children.

In a demonstration of the value of general social media, recent efforts using Twitter have focused on vulnerable populations, such as pregnant women, that are often excluded from clinical trials, and as a result, drug safety is not typically established in these groups in the premarket space. Although there are methods to gather this information post-approval, such as pregnancy registries, these databases are often constrained by issues such as attrition, cost, and patient compliance. A recent study using data from Twitter accounts of pregnant women observed a higher medication intake in women who reported birth defects (*10*). Similarly, another study developed a natural language processing method to identify tweets by users whose child had a birth defect (*11*). These preliminary studies demonstrate how social media, such as Twitter, might help supplement existing resources, especially in vulnerable populations. Thus, it represents an exciting source of potentially complementary information for postmarket pharmacovigilance efforts.

A recent effort questioned the overall value proposition of social media data, citing the low prevalence of posts relevant to pharmacovigilance and low coverage for many drugs (*12*). The analysis compared ADR signals from social media to Vigibase report statistics, focusing on FDA drug labeling changes or “validated” safety signals, where there is evidence the drug has a causal relationship with the ADR. However, Vigibase report statistics may not be an appropriate evaluation baseline because FDA labeling changes and/or the “validated” safety signal may have resulted from signals within the spontaneous reporting systems, likely inflating the baseline performance. Additionally, this evaluation effort did not adequately address the noisy nature of social media drug reports, failing to include drug misspellings or slang terms in their search queries, potentially missing a substantial number of reports (*9*). It is likely that more advanced report identification methods would increase the value of social media data. The overall lack of social media discussions surrounding some drugs will continue to pose a challenge. While the authors did not recommend the use of general social media data for pharmacovigilance, they indicated that social media generated in the context of a drug or health-oriented platform (e.g. drugs.com) vs a general platform (e.g. Twitter) may still hold value.

Beyond the technical challenges of working with social media data, its pseudonymous, open, and ephemeral nature creates new challenges in ethics, law, and reproducibility that must be navigated. Many platforms limit the sharing of data collected from their users and require that content be deleted upon user request. Social media posts experience high deletion rates with more than 40% of posts from one study being deleted from the platform after the study was published (*13*). Researchers must preserve their own copies of data used for a particular study to ensure reproducibility. The publishing the contents of social media posts in scientific journals may disclose potentially sensitive information about users such as illicit drug use or mental health issues. Researchers must balance between making research reproducible and the ethical concerns of risk of making research datasets freely available, which might increase the risk of abuse.

Mobile devices are a recent innovation in capturing information about ADRs, again providing another avenue of data collection in an uncontrolled setting. A general workflow for pharmacovigilance using mobile devices is presented in the middle row of **Figure 1.2**. MyHeart Counts is used to do a six minute walk test which can be done daily in an in-home setting. MedWatcher was a mobile application version of the FDA 3500 form for medical devices and is currently undergoing implementation in the European Union. Hugo platform for postmarket surveillance is under development at the Yale-Mayo Center of Excellence in Regulatory Science and Innovation, Yale-Mayo, which can collect electronic patient reported outcomes outside of the hospital (*14*). Next steps include interfacing with connected devices to measure endpoints; however, the strides made in this more recent area of pharmacovigilance are very promising.

These are two modalities among many that researchers are investigating as potential new means of pharmacovigilance. Through the FDA funded Centers of Excellence in Regulatory Science and Innovation (CERSI), other databases and methodologies are being studied as potential pharmacovigilance systems, for examples see https://pharm.ucsf.edu/cersi/research.

1.6 Conclusion

Clearly, the development of these massive sources of data for future pharmacovigilance efforts creates an opportunity for capitalizing on recent advances in deep learning and anomaly detection. A continuously learning AI system could not only learn to integrate these heterogeneous data sources for real-time ADR detection, but could help identify potential cases and interface with members of the pharmacotherapy community to gather more information when needed. The field of pharmacovigilance is rapidly evolving, however the resources we have highlighted are only part of the solution; the FDA and NIH will need to continue their funding of research that focuses on how to effectively analyze these data streams. Ideally, funding mechanisms will ensure interdisciplinary teams of experts from epidemiology, sociology, statistics, and computer science among others. Collaborative interdisciplinary efforts will ensure both institutional buy-in as well as methodological rigor. Ultimately, the combination of various data sources and expertise will result in safer and more effective pharmacotherapy for everyone.

1.7 Statement of Purpose

In this dissertation, we aim to highlight how real world data, specifically electronic health records (EHRs), can complement *in vitro* and clinical studies investigating approved compounds. Although there are shortcomings as highlighted above, the increasing availability of de-identified EHR data for research purposes as well as the richness of information contained in them have made EHRs a valuable resource.

In each of the subsequent chapters, real world data from EHRs are used to complement and potentially validate findings in the laboratory or from clinical trials related to transporter-mediated drug interactions. In Chapter 2, we implement a multifaceted approach by performing a high-throughput *in vitro* primary screen, building an *in silico* model, and leveraging real world data from EHRs to investigate the impact and clinical relevance of drug-induced thiamine deficiency via inhibition of ThTR-2. The EHR data were consistent with a drug-nutrient interaction for several of the drugs that were determined to inhibit ThTR-2 in the *in vitro* screen and predicted to cause a clinical drug-nutrient interaction. Chapter 3 expands on Chapter 2 where we designed and executed a prospective randomized, two-arm drug-nutrient interaction (DNI) clinical study in healthy volunteers to evaluate the inhibition potential of trimethoprim, a potent and predicted clinically relevant ThTR-2 inhibitor identified in Chapter 2. *In vitro* studies and electronic health records were used to complement and investigate our preliminary clinical findings, again providing support for the findings. In Chapter 4, we aimed to characterize the relationship(s) between BCRP p.Q141K, the pharmacokinetics and pharmacodynamics of oxypurinol, and serum uric acid levels. Real world data were used to determine whether clinical inhibitors of BCRP could phenocopy the missense variant in patients. Again, RWD substantiated our findings. Lastly, given the ongoing COVID19 pandemic during which time this dissertation work was performed, Chapter 5 focuses on prediction of the potential of 25 small molecule drugs being evaluated in clinical trials for COVID19 to cause clinically relevant drug-drug interactions. EHRs, from the general population and COVID19 patients, were used to provide preliminary validation of our *in vitro* predictions.

Taken together, these studies demonstrate how mining data from electronic health records complements and extends findings on transporter-mediated drug interactions from the laboratory and from clinical trials.

1.8 FIGURES

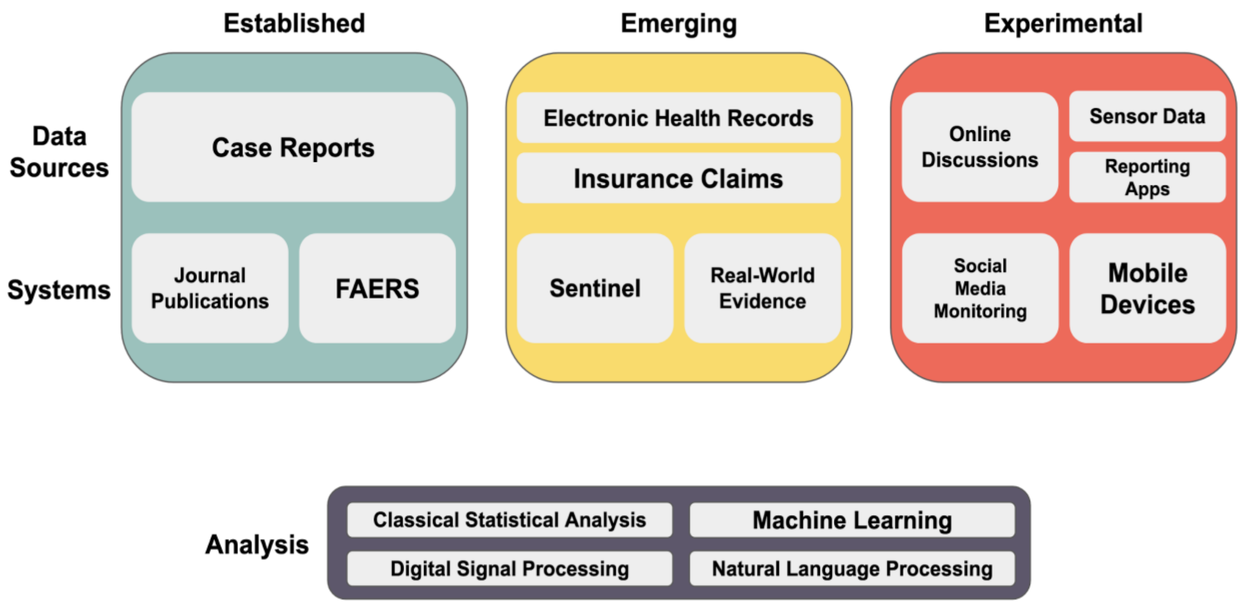

Figure 1.1 Overview of pharmacovigilance methods at varying stages of development. Established (green, left), emerging (yellow, middle), and experimental (red, right) pharmacovigilance data sources and systems are presented. Examples of methodological areas that are currently used and under active development for the analysis of these different data types are included in the bottom box.

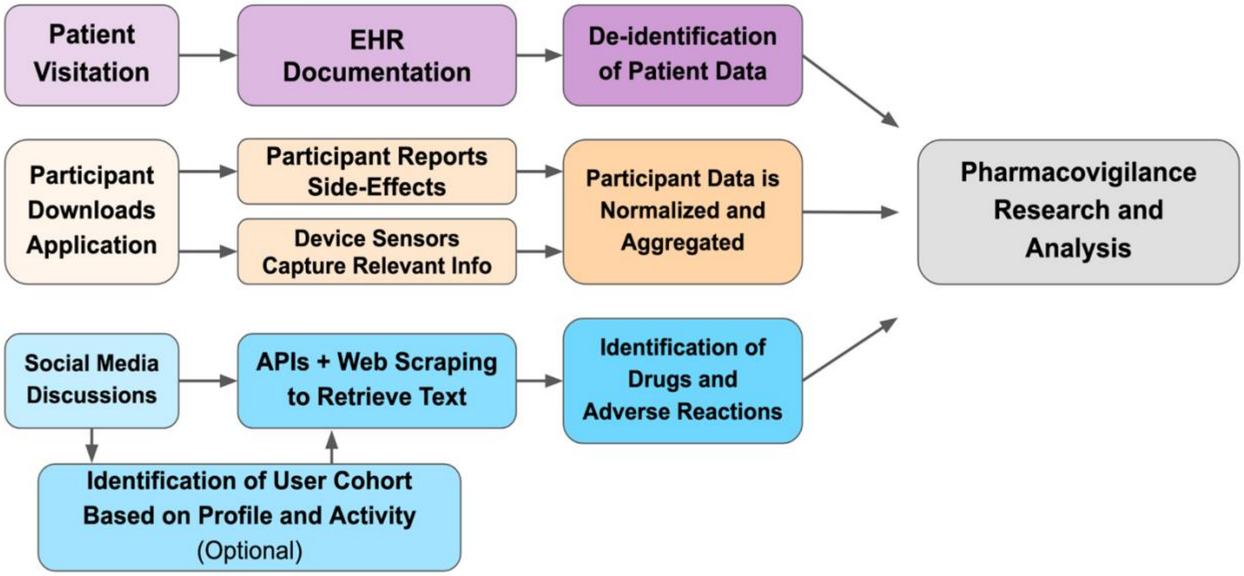

Figure 1.2 General pharmacovigilance workflows for emerging and experimental systems. EHR based pharmacovigilance workflow is shown in the purple top row. A mobile device based pharmacovigilance workflow is shown in the orange middle row. The social media based pharmacovigilance workflow is shown in the blue bottom-row. These data can then be used separately or in combination to perform pharmacovigilance research and analysis.

1.9 TABLES

Table 1.1 Select examples of successful pharmacovigilance studies in which ADR and RWD database studies played a prominent role.

Drug(s)	Effect(s)	Source(s)	Citation
Acetaminophen	Liver injury	EHR	(*15*)
Agomelatine	Liver injury	Lit Review	(*16*)
Gabapentin, Pregabalin	Liver injury, Hematological disorders	ADR database	(*17*)
Apixaban	Liver injury	Case report, ADR database	(*18*)
Ketoconazole	Liver injury	Lit review, ADR database	(*19*)
Methadone	Arrhythmia	Lit review, ADR database	(*20*)
Ranolazine	Seizure	Sentinel	(*21*)
Levetiracetam, Phenytoin	Angioedema	OHDSI	(*22*)
Citalopram	Arrhythmia	EHR	(*23*)
Hydroxyzine	Arrhythmia	Lit review, ADR database	(*24*)

1.10 REFERENCES

1. K. M. Giacomini *et al.*, When good drugs go bad. *Nature* **446**, 975-977 (2007).
2. E. Pinnow *et al.*, Postmarket Safety Outcomes for New Molecular Entity (NME) Drugs Approved by the Food and Drug Administration Between 2002 and 2014. *Clin Pharmacol Ther* **104**, 390-400 (2018).
3. J. Lester *et al.*, Evaluation of FDA safety-related drug label changes in 2010. *Pharmacoepidemiol Drug Saf* **22**, 302-305 (2013).
4. R. Platt *et al.*, The FDA Sentinel Initiative - An Evolving National Resource. *N Engl J Med* **379**, 2091-2093 (2018).
5. US Food and Drug Administration. (https://www.fda.gov/drugs/resources-information-approved-drugs/fda-disco-avelumab-merkel-cell-carcinoma-transcript, 2017).
6. G. Marquis-Gravel *et al.*, Rationale and Design of the Aspirin Dosing-A Patient-Centric Trial Assessing Benefits and Long-term Effectiveness (ADAPTABLE) Trial. *JAMA Cardiol* **5**, 598-607 (2020).
7. C. C. Freifeld, Digital Pharmacovigilance: the medwatcher system for monitoring adverse events through automated processing of internet social media and crowdsourcing. (2014).
8. D. Weissenbacher *et al.*, Deep neural networks ensemble for detecting medication mentions in tweets. *J Am Med Inform Assoc* **26**, 1618-1626 (2019).
9. A. Lavertu, R. B. Altman, RedMed: Extending drug lexicons for social media applications. *J Biomed Inform* **99**, 103307 (2019).

10. S. Golder *et al.*, Pharmacoepidemiologic Evaluation of Birth Defects from Health-Related Postings in Social Media During Pregnancy. *Drug Saf* **42**, 389-400 (2019).

11. A. Z. Klein, A. Sarker, D. Weissenbacher, G. Gonzalez-Hernandez, Towards scaling Twitter for digital epidemiology of birth defects. *NPJ Digit Med* **2**, 96 (2019).

12. J. van Stekelenborg *et al.*, Recommendations for the Use of Social Media in Pharmacovigilance: Lessons from IMI WEB-RADR. *Drug Saf* **42**, 1393-1407 (2019).

13. A. Magge, A. Sarker, A. Nikfarjam, G. Gonzalez-Hernandez, Comment on: "Deep learning for pharmacovigilance: recurrent neural network architectures for labeling adverse drug reactions in Twitter posts". *J Am Med Inform Assoc* **26**, 577-579 (2019).

14. S. S. Dhruva *et al.*, Aggregating multiple real-world data sources using a patient-centered health-data-sharing platform. *NPJ Digit Med* **3**, 60 (2020).

15. H. Y. Tong *et al.*, Hepatotoxicity induced by acute and chronic paracetamol overdose in adults. Where do we stand? *Regul Toxicol Pharmacol* **72**, 370-378 (2015).

16. S. D. Freiesleben, K. Furczyk, A systematic review of agomelatine-induced liver injury. *J Mol Psychiatry* **3**, 4 (2015).

17. R. Fuzier *et al.*, Adverse drug reactions to gabapentin and pregabalin: a review of the French pharmacovigilance database. *Drug Saf* **36**, 55-62 (2013).

18. S. A. Clarke, A. A. Alsaad, A. Mack, M. B. Phillips, Apixaban-induced liver injury. *BMJ Case Rep* **2016**, (2016).

19. E. Raschi, E. Poluzzi, A. Koci, P. Caraceni, F. D. Ponti, Assessing liver injury associated with antimycotics: Concise literature review and clues from data mining of the FAERS database. *World J Hepatol* **6**, 601-612 (2014).

20. D. P. Kao, M. C. Haigney, P. S. Mehler, M. J. Krantz, Arrhythmia associated with buprenorphine and methadone reported to the Food and Drug Administration. *Addiction* **110**, 1468-1475 (2015).

21. E. Eworuke, E. C. Welch, A. Tobenkin, J. C. Maro, Use of FDA's Sentinel System to Quantify Seizure Risk Immediately Following New Ranolazine Exposure. *Drug Saf* **42**, 897-906 (2019).

22. J. D. Duke *et al.*, Risk of angioedema associated with levetiracetam compared with phenytoin: Findings of the observational health data sciences and informatics research network. *Epilepsia* **58**, e101-e106 (2017).

23. V. M. Castro *et al.*, QT interval and antidepressant use: a cross sectional study of electronic health records. *BMJ* **346**, f288 (2013).

24. A. F. Schlit *et al.*, Risk of QT prolongation and torsade de pointes associated with exposure to hydroxyzine: re-evaluation of an established drug. *Pharmacol Res Perspect* **5**, e00309 (2017).

CHAPTER 2

Drug-Nutrient Interactions: Discovering prescription drug inhibitors of the thiamine transporter ThTR-2 (SLC19A3)

2.1 ABSTRACT

Transporter-mediated drug-nutrient interactions have the potential to cause serious adverse events. However, unlike drug-drug interactions, these drug-nutrient interactions receive little attention during drug development. The clinical importance of drug-nutrient interactions was highlighted when a phase III clinical trial was terminated due to severe adverse events resulting from potent inhibition of thiamine transporter 2 (ThTR-2; SLC19A3). In this study, we tested the hypothesis that therapeutic drugs inhibit the intestinal thiamine transporter ThTR-2, which may lead to thiamine deficiency. For this exploration, we took a multifaceted approach, starting with a high-throughput *in vitro* primary screen to identify inhibitors, building *in silico* models to characterize inhibitors, and leveraging real world data from electronic health records to begin to understand the clinical relevance of these inhibitors. Our high-throughput screen of 1360 compounds, including many clinically used drugs, identified 146 potential inhibitors at 200 μM. Inhibition kinetics were determined for 28 drugs with half-maximal inhibitory concentration

*Modified from the publication: Vora B and Green EAE, Khuri N, Bällgren F, Sirota M, Giacomini KM. (2020) "Drug-nutrient interactions: discovering prescription drug inhibitors of the thiamine transporter ThTR-2 (SLC19A3)." *American Journal of Clinical Nutrition*. doi: 10.1093/ajcn/nqz255.

(IC_{50}) values ranging from 1.03 μM to >1 mM. Several oral drugs, including metformin, were predicted to have intestinal concentrations that may result in ThTR-2 mediated drug-nutrient interactions. Complementary analysis using electronic health records suggested that thiamine laboratory values are reduced in individuals receiving prescription drugs found to significantly inhibit ThTR-2, particularly in vulnerable populations (e.g., individuals with alcoholism). Our comprehensive analysis of prescription drugs suggests that several marketed drugs inhibit ThTR-2, which may contribute to thiamine deficiency, especially in at-risk populations.

2.2 Introduction

In 2012, a phase III clinical trial involving the development of the Janus kinase 2 (JAK2) inhibitor fedratinib was terminated when several patients developed Wernicke's encephalopathy (WE) (*1*). WE is a serious, life-threatening neurologic condition which occurs as a result of vitamin B1 (thiamine) deficiency (*2, 3*). Following termination of the fedratinib trial, subsequent studies indicated that fedratinib potently inhibits the primary intestinal absorptive transporter for thiamine, thiamine transporter 2 (ThTR-2; SLC19A3).

Thiamine is a water-soluble vitamin that is obtained from exogenous sources and primarily from the diet (*4, 5*). The vitamin is absorbed in the small intestine via facilitated transport and is rapidly converted via thiamine kinases into thiamine monophosphate, thiamine pyrophosphate (TPP), and thiamine triphosphate (*6*). TPP accounts for approximately 80% of total thiamine stores in the human body and is the active form of the vitamin, acting as a coenzyme for various enzyme complexes (*6*).

Membrane transporters are known sites for drug–drug interactions (DDIs), especially in the small intestine, kidney, and liver (*7-9*). Transporter-mediated DDIs occur when one drug induces or inhibits a transporter, which results in a change in the influx or efflux of another drug and potentially leads to drug toxicities and adverse events (*9, 10*). As a result, DDIs are thoroughly investigated throughout drug development and impact drug dosing and labeling (*8*).

In sharp contrast, transporter-mediated drug–nutrient interactions (DNIs) had been largely ignored during drug development until the fedratinib trial. It was suggested that the toxicity observed in this clinical trial was a result of a DNI in a population vulnerable for thiamine deficiency, patients with myelofibrosis (*11-15*). This incident raised awareness in the drug development and regulatory communities about the potential for transporter-mediated DNIs. Although thiamine deficiency has been primarily associated with alcoholism, malnutrition, and various disease states such as infection with HIV, the catastrophic event brought to light a new mechanism for thiamine deficiency, drug-induced deficiency (*3, 5, 16-18*).

Using a multifaceted approach to determine the impact and clinical relevance of drug-induced thiamine deficiency beyond the fedratinib trial, we were able to do the following: *1)* identify 146 inhibitors of ThTR-2, some of which were predicted to cause a DNI based on current FDA DDI guidelines, by conducting a high-throughput screen of 1360 FDA-approved compounds, *2)* elucidate key descriptors of ThTR-2 inhibition by building a quantitative structure activity relationship (QSAR) model with machine learning methodology which could serve as a tool for drug discovery programs to evaluate the potential for ThTR-2 inhibition for novel compounds, and *3)* identify thiamine deficiency in both a general patient population and in patients who have been diagnosed with malnutrition, alcoholism, or HIV and are taking 1 or more of the clinically relevant inhibitors identified in our prescription drug library screen using real world data from electronic health records (EHRs).

2.3 METHODS

2.3.1 Chemicals and reagents

Radiolabeled thiamine was purchased from American Radiolabeled Chemical Incorporations. The specific activity of the tritium-labeled thiamine hydrochloride was 20 Ci/mmol. Unlabeled chemicals were purchased from Sigma Aldrich. Fedratinib was purchased from Med Chem Express. Cell culture supplies were purchased from the cell culture facility at the University of California, San Francisco (UCSF), and Life Tech. The ThTR-2 stable HEK 293 cell line used was created by the Giacomini laboratory and described in Liang et al. (*13*). Cell lines were obtained from -80°C storage at the UCSF Cell Culture Facility for the purposes of this study. The compound library, the US Drug Collection, was purchased from Microsource Discovery Systems. The starting concentration of each drug was 10 mM in 100% DMSO.

2.3.2 Radiometric cell uptake screen

The ThTR-2 cell line [stably transfected HEK293 cells (*13*)], was maintained in DMEM supplemented with penicillin (100 U/mL), streptomycin (100 mg/mL), puromycin (5 µg/mL), and 10% FBS. Penicillin, streptomycin, and puromycin were included in the growth media and removed prior to the radiometric study. All 3 compounds were tested in our screen and did not induce more than a 10% inhibition of thiamine uptake compared to control. Cells were seeded at 70,000 cells per well and cultured on poly-d-lysine-coated 96-well plates for 24 h to reach 90% confluence. Uptake assay solutions were prepared at 2 times their final assay concentrations. The inhibitor compound solution and the substrate (thiamine) solution were combined at a 1:1 ratio to allow for throughput assay design. The inhibitor compound solution was prepared by transferring 20 µL of the US Drug Collection into 180 µL of HBSS, pH 7.4, in a 96-well plate, producing a stock solution of 1 mM. On the day of the assay, the compound stock solutions were used to make compound assay solutions at a concentration of 400 µM. The thiamine solutions were prepared at a concentration of 500 nM thiamine hydrochloride in HBSS, with 450 nM unlabeled thiamine and 50 nM tritium labeled thiamine. The plates were designed to test 80 compounds in columns 2–11. The negative control, DMSO, and the positive control, fedratinib, were assayed in alternating wells in columns 1 and 12. The results from the negative control on each plate were used to determine hits for that plate. Each compound was tested at 200 µM against a thiamine concentration of 250 nM, except for 2 of the 17 plates, for which the compounds were screened at 500 µM. The exact concentrations of substrate, inhibitor, and the positive control can be found in **Supplemental Table 2.1**. To initiate the assay, the cells were washed once in 80 µL of warm HBSS, and then incubated in 80 µL of the assay buffer at 37°C for 5 min. Following the incubation, the cells were washed twice with 80 µL ice-cold HBSS buffer. MicroScint-20 (Perkin Elmer) was added to the 96-well plates and sealed with an adhesive plastic cover. Following radiometric uptake assays, the plates were placed on a shaker overnight. The plates were read in a MicroBeta2 (Perkin Elmer) using the dual counting mode.

2.3.3 Radiometric cell uptake dose-response curves

The ThTR-2 cell line was cultured in the same manner as for the screen. Compounds selected for potency validation were assessed in dose-response curves with concentrations ranging from 2.5 nM to 200 µM at a substrate concentration of 250 nM thiamine. The compound and substrate buffers were made at 2 times their assay concentration and then combined at a 1:1 ratio to reach the final assay concentrations as in the primary screen. The compound buffer was made by serial dilutions in HBSS. The substrate buffer was made with 450 nM unlabeled thiamine and 50 nM tritium-labeled thiamine, which was subsequently diluted to reach final thiamine concentrations of 225 nm unlabeled thiamine and 25 nM tritium-labeled thiamine. Each plate contained control wells with no inhibitor which were used for normalization in data analysis. To initiate the assay, the cells were washed once in 80 µL warm HBSS, and then incubated in 80 µL of the assay buffer at 37°C for 5 min. Following the incubation, the cells were washed twice with 80 µL ice-cold HBSS buffer. MicroScint-20 (Perkin Elmer) was added to the 96-well plates and sealed with an adhesive plastic cover. Following radiometric uptake assays, the plates were placed on a shaker overnight. The plates were read in a MicroBeta2 (Perkin Elmer) using the dual counting mode.

2.3.4 Data analysis for radiometric cell uptake assays

Hit calling for the primary screen was conducted and Z-prime scores were calculated within each plate using the positive and negative controls (*19*). The mean ± SD of the vehicle negative control for each plate was determined and all compounds were normalized to this control. A hit threshold was set as 3 SDs below the average of the negative control respective to each plate. Compounds were classified as hits if they were below this cutoff. All the hits and nonhits from each plate were compiled together and the normalized values were plotted (with respect to plate) using ggplot. Data from half-maximal inhibitory concentration (IC_{50}) curves were exported to Excel for normalization and entered into GraphPad Prism 8.0 for graphing and nonlinear fitting.

2.3.5 Clinical relevance ratios

One-point thiamine inhibition values for each compound from the primary screen were used in combination to determine the predicted IC_{50} ($prIC_{50}$) (*20*) with the equation $V = V0/\{1 + [(I)/prIC_{50}]\}$, where V and V0 are the activity with and without inhibitor, respectively, and I is the inhibitor concentration of 200 μM. Dosing information for each of the primary screen hit compounds was reviewed from the clinical databases IBM Micromedex and Lexicomp, and a maximal reported single dose was documented. The maximal intestinal concentration for each drug was determined by dividing the maximal dose by 250 mL (*21*). A ratio was calculated using the $prIC_{50}$ and the maximal intestinal concentration.

2.3.6 Data preparation for the QSAR model

Compound names (n = 1360) were used as queries to the PubChem database (*22*) to retrieve compound identification numbers and structure data files (SDFs). Four compounds were removed due to failure to compute SDF files. SDF files were processed with PaDEL software (*23*) to compute 770 molecular descriptors for each screened compound. Molecular descriptors were filtered to remove descriptors with missing values (n = 595) and descriptors with zero variance (n = 60). To identify highly correlated features (correlation coefficient > 0.95), pairwise descriptor correlations were computed and, from each highly correlated pair, 1 randomly chosen feature was removed (n = 41), leaving 74 molecular descriptors for 1356 compounds. Feature selection was implemented using the *caret* R package (*24*). Correlation-based feature selection was performed, in which a greedy heuristic is employed to pick a subset of features that are independent of each other but are correlated with a class label (*25*). *In vitro* screening data were used to label 144 compounds as hits (label = 1) and 1212 as nonhits (label = 0).

2.3.7 Analysis of physicochemical properties for QSAR model

MayaChemTools package (*26*) was used to compute 8 physico-chemical descriptors, namely, molecular weight, molecular volume, number of rotatable bonds, number of heavy atoms, number of hydrogen bond donors and acceptors, octanol-water partition coefficient (SLogP), and total polar surface area. Distributions of physicochemical properties for hit and nonhit compounds were analyzed in the R statistical package. Pairwise Student's t-test was performed, using t.test in R, for the 8 physicochemical properties to identify those that differed significantly. Results were plotted using the boxplot function in R.

2.3.8 QSAR model development with machine learning

Four machine learning algorithms from the caret package in R (k-nearest neighbors, partial least squares regression discriminant analysis, support vector machine, and random forest), were employed to build binary classifiers. A double loop cross-validation (*20*) was used to assess the predictive power of each algorithm. First, the train function in the caret R package was used to fit predictive models for the 4 algorithms for 75% of the original data (training data set; n = 1017). Parameter tuning was done with 10-fold cross-validation as follows. The training set was divided into 10 subsets with each subset comprising the same ratio of hits (~90%) and nonhits (~10%) as the original data set. Model parameters were optimized by fitting classifiers to 9 out of 10 subsets and assessing them with the 1 out of 10 subsets. Next, the performance of each tuned model was assessed on 25% of the data (holdout set; n = 340) using the area under the receiver operating characteristic curve (auROC) (*27*) as the performance measure. Double-loop cross-validation was repeated 10 times for both full and reduced feature sets. First, classifiers were built with 74 molecular descriptors (full feature set). Second, feature reduction was performed with the cfs filtering algorithm in the FSelector R package for each of the training data sets. We identified a subset of 18 features that overlapped between different training sets to create a reduced feature set. Finally, cross-validation of models trained with these 18 features was performed. ROC curves were plotted with the ROCR package in R (*28*).

2.3.9 Substructure similarity search

The ChemBioServer web service (*29*) was used to search for compounds containing fragments similar to the 2,4-diaminopyrimidine fragment. To that end, the structure of 2,4-diaminopyrimidine in SDF format was queried against the 1356 SDF files using an online interface with default settings.

2.3.10 EHR data and analysis

We used the UCSF Research Data Browser to search for patients who had a reported numeric thiamine pyrophosphate laboratory (measured in whole blood by the UCSF Health Clinical Laboratories) test value < 1200 nM, which gave us a total of 1433 patients and 2016 laboratory values. Thiamine laboratory values reported as < 7 nM were assigned the value of 0 nM. Only patients with 1 thiamine laboratory value were included in the analysis, which reduced our sample size to 1133 individuals.

Patients were divided into 2 groups depending on their medication use. Patients prescribed 1 or more of the orally dosed drugs that were identified as potentially clinically relevant hits in the primary screen and analysis (metformin, verapamil, amitriptyline, sertraline, amoxapine, penicillamine, quinidine, quinapril, and/or hydroxychloroquine) were grouped into the “on” drug group, which resulted in 236 patients. In addition, sulfamethoxazole-trimethoprim was an inclusion criterion for the on group only in the HIV analysis since this drug is not chronically taken among the general population but can be chronically used in HIV patients as a prophylaxis for pneumonia. Fedratinib was not included in any of the analyses since it was not an approved therapeutic agent. The 897 remaining patients (i.e. individuals who were never prescribed any of the clinical hits mentioned above) were grouped into the “off” drug group. Patients in the on group were further filtered based on their laboratory collection date relative to their first medication order start date. Thiamine laboratory values measured before the on group patient's first medication order start date or within 30 days after their first medication order start date were excluded. A minimum of 30 days between medication start date and the thiamine laboratory value measurement was chosen since it can take a few weeks for thiamine stores to deplete. In total, 155 patients met this criterion and were in the on group.

For patient population-specific analyses, patients were further assigned to subgroups based on a diagnosis of malnutrition, alcoholism, or HIV. Malnutrition diagnosis was defined using the International Classification of Diseases (ICD) as ICD10 level 1 “endocrine, nutritional and metabolic diseases” (E00-E89) and ICD10 level 2 “malnutrition” (E40-E46). Alcoholism diagnosis was defined as ICD10 level 3 “alcohol related disorders,” “alcoholic liver disease,” “evidence of alcohol involvement determined by blood alcohol level,” and “toxic effect of alcohol.” HIV diagnosis was defined as ICD10 level 1 “certain infectious and parasitic diseases (A00-B99)” and ICD10 level 2 “human immunodeficiency virus [HIV] disease.” There were 221, 121, and 19 patients with 1 reported thiamine laboratory value and a malnutrition, alcoholism, and HIV diagnosis, respectively, without any regard to medication use. Patients which met the inclusion criteria for 2 or more diagnoses were included in both patient population-specific analyses.

We further subdivided the patient groups in each respective patient population based on their laboratory collection date relative to their first diagnosis date. Laboratory values taken any time before diagnosis were considered for patients diagnosed with malnutrition. For patients with alcoholism, laboratory values taken within 1 year of diagnosis were used. Lastly, for patients diagnosed with HIV, laboratory values taken 1 year prior to or any time after diagnosis were considered. This resulted in 45 patients with malnutrition, 76 patients with alcoholism, and 16 patients with HIV before filtering for medication use/prescriptions was performed. The total number of patients in the on and off groups after filtering based on medication order start date and prescriptions is listed in the Results section. All analyses were performed relative to only the date of initial diagnosis, laboratory value collection dates, and medication start dates; no other covariates were included in the analysis.

Welch's 2-sample t-test was performed to evaluate if there was a significant difference in laboratory values when comparing both groups and ggplot was used to plot the data using R (version 3.4.0).

2.4 RESULTS

2.4.1 Overview

The overview of our study design is presented in **Figure 2.1**. Our first goal was to perform a cell-based high-throughput screen to identify prescription drugs and other bioactive compounds that inhibit ThTR-2. Using the data from the primary screen, we validated a subset of the most potent compounds as well as investigated several drugs to assess their potential to cause clinically relevant DNIs at ThTR-2 (**Figure 2.1**). Additionally, we leveraged computational methods to identify features specific to hits and nonhits from our screen. To complement our screen and model, we investigated and compared thiamine laboratory values in patient populations that are prone to thiamine deficiency. Specifically, we compared thiamine pyrophosphate plasma concentrations from patients taking 1 or more of the clinically relevant inhibitors that had been identified in our high-throughput screen with concentrations from patients who were not on any of those inhibitors. Our goal here was to explore the hypothesis that these inhibitors may exacerbate thiamine deficiency in vulnerable populations.

2.4.2 In vitro radiometric thiamine inhibition screen identified 146 potential thiamine inhibitors

A radiometric screen to identify marketed drugs that inhibit ThTR-2-mediated thiamine uptake was performed using tritium-labeled thiamine hydrochloride. Prior to the screen, the optimal conditions for thiamine uptake in cells overexpressing ThTR-2 were determined (i.e. duration of uptake, concentration of thiamine, and plating density of cells, see the Methods section). Most compounds were screened once in a 96-well plate using a 5-minute uptake assay. To determine the inhibitor concentration to use for the screen, the single maximum doses for commonly prescribed drugs were collected and used to predict intestinal concentrations (**Supplemental Figure 2.1**). This informal *in silico* review guided the selection of the final drug concentration of prescription drugs and other compounds in the library (200 μM) used in the primary screen.

The drug library used for the primary screen comprised 1360 diverse compounds with various mechanisms of action and from many therapeutic classes (**Figure 2.2**). Inhibitors, or hits, were defined by a decrease in thiamine uptake greater than 3 SDs from the thiamine only (no inhibitor) control (**Supplemental Figure 2.2**). Slight enrichment of hits was seen in certain therapeutic classes, including drugs used in the treatment of gastrointestinal and central nervous system disorders (**Figure 2.3**). Out of the 1360 compounds screened, 146 were determined to be ThTR-2 inhibitors (z-prime: 0.44-0.81) (**Supplemental Table 2.1**) (*19*).

2.4.3 Potency studies of top inhibition hits validate primary screen

As the primary screen was conducted with single point determinations, the top 11 compounds, based on percentage inhibition of ^{3}H-thiamine uptake, were selected to test in 8-point dose response curves to validate the accuracy of the primary screen. Ten of the 11 compounds were validated as hit compounds (**Supplemental Table 2.2**). Citric acid was determined to be a false positive. In general, the 10 validated hits have IC_{50} values, the half-maximal inhibitory concentration, < 100 μM (**Figure 2.4** and **Supplemental Figure 2.3**). Additionally, randomly selected compounds that were identified as noninhibitor compounds were also tested and confirmed to not inhibit the transporter.

2.4.4 Selected clinically relevant screen hits maintain predicted potency

As screening of the top hit compounds validated the primary screen, a clinical relevance ratio, calculated using the predicted intestinal concentration following a single dose divided by the IC_{50}, was employed to identify which of the 146 hits from the primary screen would be clinically relevant. These compounds were chosen based on their clinical relevance ratios (≥ 10), availability in oral dosage forms, chronic dosing schedules, which could result in prolonged inhibition of intestinal ThTR-2, and use in patient populations at-risk for thiamine deficiency. Of the 146 hits, 88 were orally administered drugs. Out of the 88 orally administered compounds, 10 compounds were selected for further validation by utilizing the additional selection criteria, noted above (**Supplemental Table 2.3**). Of the 10 compounds, 5 were identified as potent inhibitors of ThTR-2 with low nanomoles per liter IC_{50} (**Figure 2.4** and **Supplemental Figure 2.4**). Five inhibitors with predicted clinical relevance, and 3 of the other selected inhibitors, despite higher IC_{50} values, were estimated to reach intestinal concentrations 10 times greater than their IC_{50} values, suggesting the potential to cause a DNI at ThTR-2 (**Table 2.1** and **Figure 2.1**).

2.4.5 Computational characterization of properties of hit compounds

We used several methods to characterize and differentiate properties of hit and nonhit compounds identified by high-throughput screening.

First, we computed and analyzed 8 physicochemical properties of hits and nonhits, such as molecular weight, molecular volume, number of heavy atoms, number of rotatable bonds, number of hydrogen bond donors and acceptors, SLogP, and topological polar surface area (**Table 2.2** and **Supplemental Figure 2.5**). No statistical differences were observed in molecular weight, volume, number of heavy atoms, or number of rotatable bonds. The values for the number of hydrogen bond donors and acceptors and total polar surface area were significantly lower among hit compared to nonhit compounds ($P < 0.0001$). Moreover, hit compounds were more lipophilic as evidenced by significantly higher SLogP values ($P < 0.0001$) compared to those of nonhits.

Second, we developed machine learning classifiers to differentiate between hit and nonhit compounds from the high-throughput screen. The performance of 4 machine learning algorithms was estimated by means of double-loop cross-validation, consisting of internal 10-fold cross-validation and external validation using 10 test sets consisting of 25% of samples (see Methods section). We evaluated 4 machine learning algorithms, namely k-nearest neighbors, partial least squares regression discriminant analysis, support vector machines, and random forest (RF). For each algorithm, we trained each classifier with 770 and 18 molecular descriptors, respectively. The 18 descriptors were identified via a recursive feature selection method (**Supplemental Table 2.4**). These descriptors represent a common subset of features selected from different training sets during the cross-validation. The receiver operating characteristic (ROC) curves for external validation experiments of 4 algorithms are shown in **Supplemental Figure 2.6** for 18 features and for 770 features. The RF classifier outperformed the other 3 models as assessed by the average auROC for the 10 external validation tests. Performance of all models was considered better than random. Notably, the auROC of RF classifier with 770 features was 0.71 ± 0.03 and with 18 features 0.74 ± 0.05, respectively. The performances of the other models, though slightly worse than that of the RF model (**Supplemental Figure 2.6**), improved with use of the 18 descriptors over the full 770 features (**Supplemental Figure 2.6**). Analysis of the 18 selected features revealed that the lipophilicity, descriptors of topological and chemical diversity, and descriptors of hydrogen bond counts were important for the accuracy of differentiating between hit and nonhit compounds. More specifically, the number of nitrogen atoms and number of CrippenLogP descriptors were ranked as the 2 most important descriptors for the RF classifier (**Supplemental Table 2.4**). Four discrepancies in hit calling between screen and the RF QSAR model were observed (**Supplemental Tables 2.5** and **2.6**). To analyze the tradeoff between the precision and recall of the RF classifier with 18 features, we computed the average F1 measure, which was 0.58. The average precision and recall were 0.7 and 0.5, respectively. The lower recall indicates that the model is less successful at filtering out false negatives than false positives.

2.4.6 EHRs validate identified clinically relevant inhibitors

To investigate the clinical relevance of the inhibitors identified, we mined EHRs from UCSF and identified drug-induced decreases in thiamine laboratory values associated with the use of the drugs identified in our screen in both the general population and distinct patient populations. Specifically, we compared thiamine laboratory values in patients prescribed 1 or more of the 9 (10 for HIV patients) clinically relevant inhibitors identified in the primary screen (**Table 2.1**) with thiamine laboratory values in patients who were never prescribed any of the respective inhibitors. Based on the inclusion and exclusion criteria described in the Methods, we were able to classify patients as “on” drug (i.e. on 1 or more of the clinically relevant inhibitors) or “off” drug.

In the general population, we observed a significant difference in thiamine laboratory values between the 2 groups (P = 0.02; n = 154 on drug; n = 878 off drug). If we add thiamine medication orders as an exclusion criterion, we still observed a significant difference (P = 0.003) in thiamine laboratory values between the on drug (n = 36) and off drug (n = 215) groups, demonstrating the robustness and sensitivity of our analysis. Population demographics, such as age and sex, as well as number of medication orders based on unique pharmaceutical class (i.e. each pharmaceutical class is counted only once per patient irrespective of number of prescriptions), were comparable between both groups (**Supplemental Table 2.7**).

Three distinct patient populations: malnourished, alcoholic, and HIV patients, which have been associated with thiamine deficiency (*3*, *5*, *16*-*18*), were used to further investigate and elucidate drug-induced decreases in thiamine laboratory values. In all 3 patient populations, patients in the on drug group had lower thiamine pyrophosphate blood concentrations than those in the off drug group (**Figure 2.5**). In malnourished patients, when comparing thiamine laboratory values from samples taken any time before diagnosis, we observed lower concentrations of thiamine pyrophosphate for individuals on drug (n = 8) than individuals off drug (n = 30) at a statistically significant level (P = 0.015) (**Figure 2.5**). In patients diagnosed with alcoholism, there were significantly lower concentrations (P = 0.000002) in the on than the off drug groups when we compared thiamine laboratory values taken within 1 year of diagnosis (n = 2 on drug; n = 68 off drug) (**Figure 2.5**). Lastly, although we did not observe a significant difference between the 2 groups in HIV patients when including thiamine laboratory values taken within 1 year before diagnosis or any time after diagnosis (P = 0.20; n = 9 on drug; n = 4 off drug), we still observed lower thiamine laboratory values in on patients compared to off patients, which was consistent with our other patient populations (**Figure 2.5**). If we combine all 3 patient populations with the same inclusion and exclusion criteria used in the individual analyses, we observe a statistically significant difference, as previously observed ($P = 0.0004$; $n = 18$ on drug; $n = 96$ off drug) (**Figure 2.5**).

Finally, if we added thiamine medication orders (i.e. prescribed thiamine or vitamin B1 supplements and/or given thiamine intravenously) as an exclusion criterion, we still observed a significant difference between the 2 groups (on drug and off drug) in the alcoholic patient population ($P = 0.00008$ for laboratory values within 1 year of diagnosis, $n = 2$ on drug, $n = 24$ off drug) and we still observed a downward trend in malnourished and HIV patients; that is, thiamine laboratory values were lower in malnourished and HIV patients on a ThTR-2 inhibitor than in those not on a ThTR-2 inhibitor ($P = 0.056$ and $P = 0.27$ respectively).

2.5 DISCUSSION

DDI studies are a routine and necessary component of clinical drug development. In contrast, DNI studies are rarely performed. The clinical trial of fedratinib, with the development of WE in a handful of patients, underscored the importance of DNIs and the effect of drugs on transporter-mediated nutrient absorption in clinical drug development (*1, 30, 31*). The current study explored the idea that DNIs mediated by intestinal ThTR-2 occur with clinically used drugs and that such interactions may contribute to thiamine deficiency, especially in vulnerable populations.

This study resulted in 4 major findings and highlighted the potential for commonly prescribed drugs to contribute to thiamine deficiency. First, we identified many prescription drug inhibitors of ThTR-2-mediated thiamine uptake, representing a surprising fraction (approximately 10%) of the prescription drug library that was screened. Second, 4 key molecular descriptors were identified that can aid in distinguishing ThTR-2 inhibitors from noninhibitors, including increased hydrophobicity, lower polar surface area, and reduced ability to form hydrogen bonding as acceptors or donors. Third, many of the prescription drug ThTR-2 inhibitors are predicted to inhibit intestinal ThTR-2-mediated thiamine absorption at clinically relevant intestinal concentrations. Finally, a thiamine deficient signature was observed in patients diagnosed with HIV, malnutrition, and alcoholism taking 1 or more of the drugs predicted to inhibit intestinal ThTR-2-mediated thiamine uptake. The results suggest the potential of these drugs to cause DNIs and contribute to thiamine deficiency and WE in susceptible patient populations.

Thiamine deficiency has been repeatedly associated with a cascade of events linked to cognitive decline, many of which are commonly observed in Alzheimer disease and Parkinson disease, where thiamine has been suggested as a potential therapeutic modality (*32-36*). Thiamine deficiency is a treatable condition when recognized, as seen in global populations where malnutrition is a major concern (*37-40*). Additionally, the dire consequences of thiamine deficiency have repeatedly been observed in children of developing countries where thiamine deficiency disorders, often triggered by infectious diseases, are a major cause of infant mortality (*41-46*). Though severe outcomes of thiamine deficiency can lead to a clear diagnosis, mild to moderate thiamine deficiency symptoms are frequently overlooked or misdiagnosed (*3, 18, 47-*

51). Furthermore, even in conditions known to predispose patients to thiamine deficiency, the variability in the presentation of the disorder suggests that unknown confounding factors may also contribute to the deficiency syndrome. Unfortunately, recent studies echo the complexity of recognizing thiamine deficiency and suggest that thiamine deficiency even in developed countries is underdiagnosed and undertreated (*52-54*). Unrecognized thiamine deficiency is a real problem as the neurologic sequelae may increase the burden on healthcare systems and reduce the general health of world populations.

This study represents one of the first studies to evaluate the broad potential of approved drugs to contribute to nutrient deficiency syndromes, and to our knowledge, is one of the first high-throughput *in vitro* screens for ThTR-2. Hit compounds from our primary screen did not show enrichment for any 1 therapeutic class, suggesting that drug-thiamine interactions may occur across drug classes. The broad inhibitor specificity identified in this study is consistent with recent studies from our laboratory, which have indicated that human ThTR-2 may be more promiscuous in terms of its substrate selectivity than rodent orthologs, which narrowly transport thiamine (*13*).

Previous studies have indicated that ThTR-2 inhibitors share a common structural feature, a 2,4-diaminopyrimidine, specifically within the Janus kinase inhibitor class (*11*, *12*). To assess if ThTR-2 inhibition could be caused by compounds without this structure, we utilized a diverse compound library. Preliminary computational analysis of our screen results revealed that inhibitors were significantly smaller, less polar, and more hydrophobic. Prediction of a compound's inhibitory potential based on these broad molecular descriptors alone would be difficult given the large molecular and structural diversity of our library and would likely result in many false positives. Therefore, we attempted to use machine learning and the identified descriptors to build models that may more reliably predict compounds that may inhibit the transporter. The models built with the RF algorithm performed better than random, as determined by the cross-validated auROC of about 0.7. Our RF model differs from published computational models that predict drug-food interactions and/or food bioactivities in that it aims to identify properties of molecules that inhibit ThTR-2 and may lead to thiamine deficiency (*55*).

The aim of this study was not only to assess the extent to which ThTR-2 may be inhibited by marketed prescription drugs but to also determine their potential to contribute to thiamine deficiency clinically. Current FDA DDI guidelines provide a ratio, previously described in the Methods sections, for which > 10 indicates a dedicated healthy volunteer DDI study may be warranted (*21*). Eleven of the 14 selected orally prescribed drugs were predicted to reach this benchmark, by estimating the ratio of predicted intestinal concentration following maximum single dose to experimental IC_{50}, suggesting that they may result in clinically relevant inhibition of ThTR-2. Metformin was among the drugs deemed clinically relevant and mirrored previous suggestions about its ability to cause DNI at ThTR-2 (*13*). Additionally, some of the clinically relevant drugs identified in our study are used chronically in patients who may already be at risk for thiamine deficiency (*56-64*).

By examining the EHRs for patients at risk for thiamine deficiency, we were able to use real world data to support the idea that prescription drugs may contribute to thiamine deficiency, and indeed may be major risk factors for WE or beriberi in vulnerable populations. Additionally, inhibition of ThTR-2 may contribute to adverse events associated with some of the therapeutics. For example, a common adverse event associated with metformin use is lactic acidosis (*65*), a potentially fatal adverse event also associated with thiamine deficiency. If, as our results suggest, metformin inhibits intestinal ThTR-2-mediated thiamine transport, the resulting low concentrations of thiamine and TPP could contribute to metformin-induced lactic acidosis (*18, 50, 66-68*).

The limitations of this study include the high concentrations used in the initial screen, which were much higher than concentrations used in typical drug discovery screens (*69-71*). A high screening concentration was used to reflect the concentrations predicted to be achieved in the intestine after therapeutic doses of drugs. Another limitation of the high-throughput screen was that each compound was evaluated in a single well. This approach was taken due to the fact that no fluorescent probe was available and may have resulted in false negatives. Another limitation was the performance of the machine learning classifier, which was constrained due to the large structural diversity of the compound library, limited number of compounds (< 2000), and lack of novel molecular structures currently in development. Screening a larger library with many molecules having particular structural backbones may help refine the structure-activity relationships as well as improve the prediction capability of the model. Furthermore, although we used FDA guidance as a benchmark to select compounds which have the potential to cause clinically relevant DNIs, this guidance is meant for drugs and not nutrients and for efflux transporters (and not influx transporters) that are targets for DDIs. Since inhibition of efflux transporters requires inhibitors to access the intracellular compartment, which is not required for inhibition of an influx transporter, the guidelines may have been overly stringent for our study.

In addition, our EHR analysis was limited by small sample sizes. Finally, the use of publicly available data rather than a designated clinical trial allowed us to show an association between these drugs and low thiamine laboratory values but prevented us from differentiating between the role of disease and role of the drug, assessing the effect of nutritional status on thiamine laboratory values, and determining whether these drugs inhibit intestinal ThTR-2-mediated thiamine uptake. Additional samples or designated clinical studies powered to detect drug-related differences as well as assess nutritional status are needed to make broader conclusions.

Overall, our comprehensive study was able to identify 146 inhibitors of ThTR-2, most of which were not previously known. These compounds aided in elucidating structural and chemical features of ThTR-2 inhibitors and, though further screens are needed, provided a preliminary *in silico* model for identifying compounds that inhibit ThTR-2. Compounds that may cause clinically relevant drug-nutrient interactions were predicted, and real world data from the EHR in vulnerable patient populations were consistent with our predictions. Future work includes investigating the effects of ThTR-2 genetic variants on the plasma concentrations of both thiamine as well as prescription drugs and conducting prospective DNI studies of prescription drugs and thiamine. This study has led to the largest available dataset of ThTR-2 inhibitors and underscores the potential importance of transporter-mediated drug-nutrient interactions at ThTR-2 as well as other vitamin transporters.

2.6 FIGURES

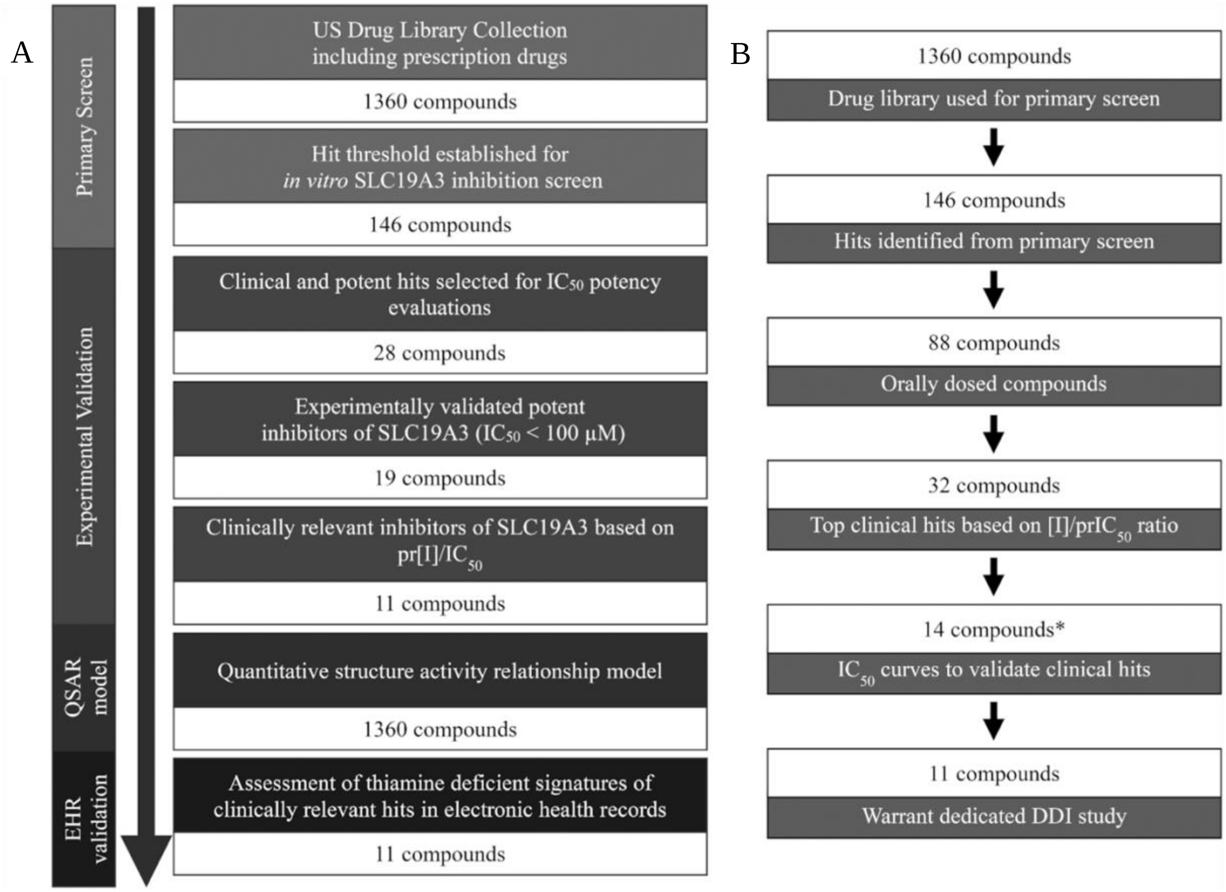

Figure 2.1 Workflow of experimental and computational methods for primary screen and identification of clinically relevant hits. Schematic of workflow used to identify, validate, and determine the potential clinical relevance of ThTR-2 inhibitors (A). Shown on the left are the 4 major stages to identify marketed drug inhibitors of ThTR-2. These major stages are accompanied by substages of each effort (on the right) with the selection criteria in the colored box and the number of compounds selected for progression to the next stage below each colored box. Detailed methods used to select compounds at each stage can be found in the Methods section. Detailed workflow used to identify and validate clinically relevant hits (B). Parallel steps were applied to the hits identified from the primary screen to determine the clinical relevance and potential to cause a drug-nutrient interaction. The number of compounds entering each step is noted above and the criteria that filtered that collection of compounds is summarized in the box below it. *12 compounds were validated using experimental IC_{50} values and 2 compounds (metformin hydrochloride and trimethoprim) were validated using literature derived IC_{50} values (*12*, *13*). IC_{50}, concentration which causes 50% inhibition of uptake; pr[I], predicted inhibitor concentration in the small intestine following maximum single dose; ThTR-2, thiamine transporter 2.

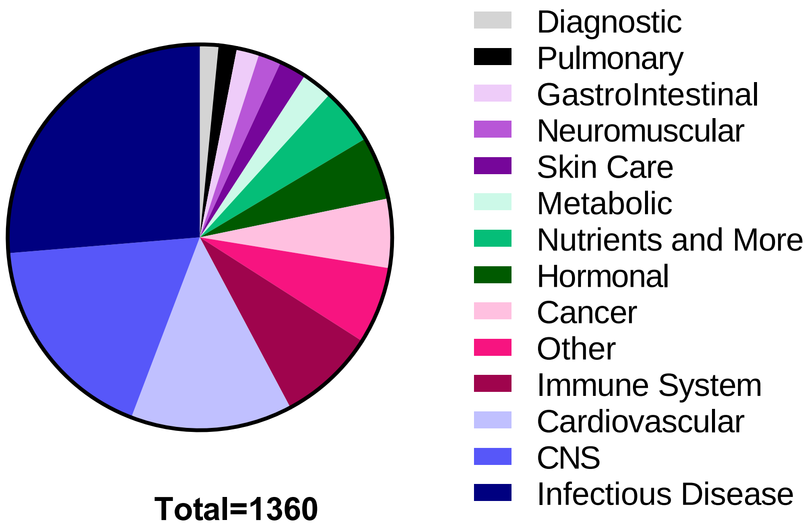

Figure 2.2 Classification of drug library by therapeutic class. The US drug collection library used for the high-throughput screen comprised a diverse set of compounds which ranged across various pharmacological classes. CNS, central nervous system.

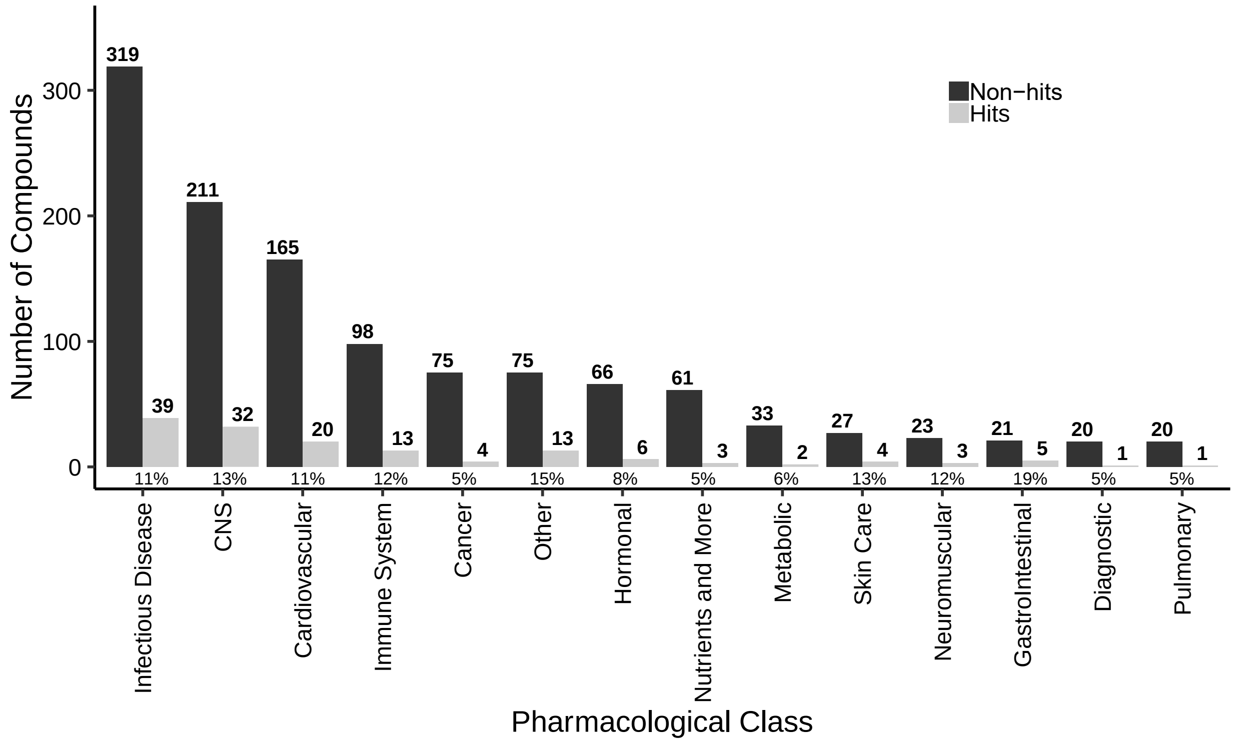

Figure 2.3 Total number of hits and nonhits in each therapeutic class. Although the diversity of the hits trended similarly to the diversity of the prescription drug library, there was enrichment of certain pharmacological classes such as drugs used in the treatment of gastrointestinal and CNS disorders. Numbers above bars represent raw count of hits and non-hits in each therapeutic class respectively. Percent represents enrichment of hits in a therapeutic class (i.e. hits which fall in a class/total number of compounds in that same class). CNS, central nervous system.

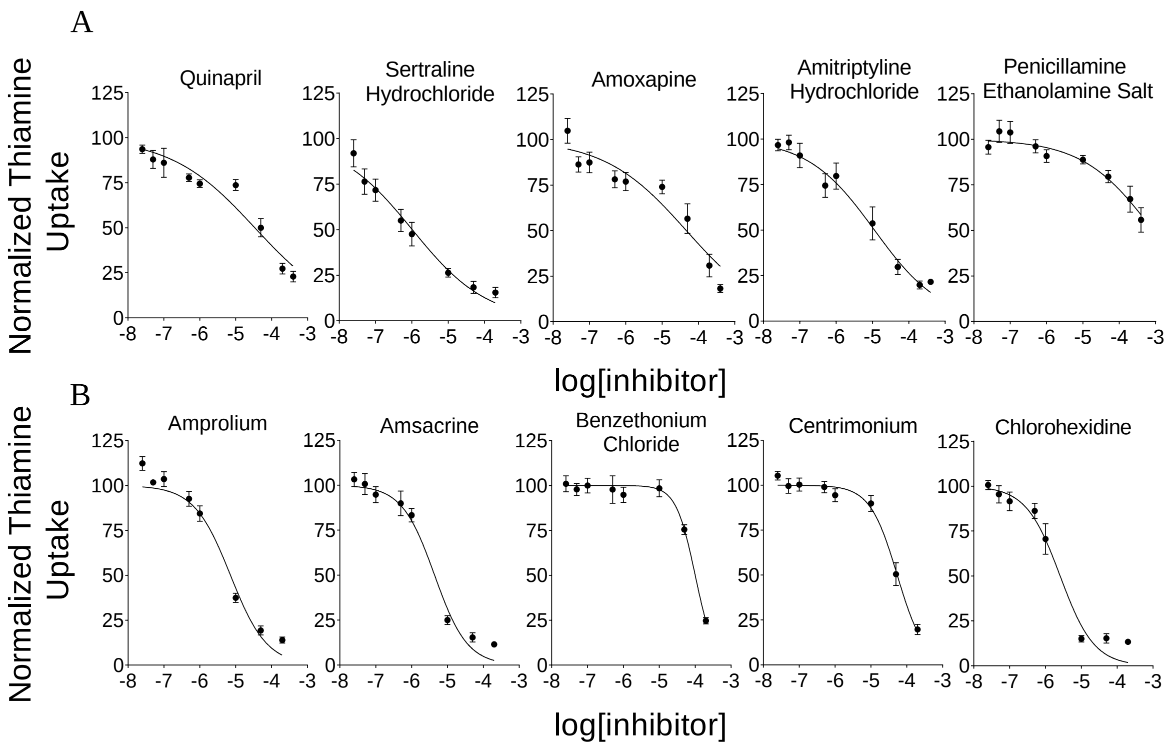

Figure 2.4 IC_{50} curves of a subset of (A) potent and (B) clinically relevant hits. IC_{50} values were determined for selected drugs in HEK293 cells stably overexpressing ThTR-2. Eight-point curves were conducted on 96-well plates with inhibitor concentrations ranging from 200 µM to 2.5 nM and 250 nM thiamine. Data points and error bars are presented as means ± SEMs, respectively. Each curve is representative of 3 experiments and each concentration was tested in duplicate within each experiment. IC_{50} values range from 2.56 to 100 µM in panel A and 1.03 to 4.04 mM in panel B and are listed in detail in **Supplemental Tables 2.2** and **2.3**. IC_{50}, concentration which causes 50% inhibition of uptake; ThTR-2, thiamine transporter 2.

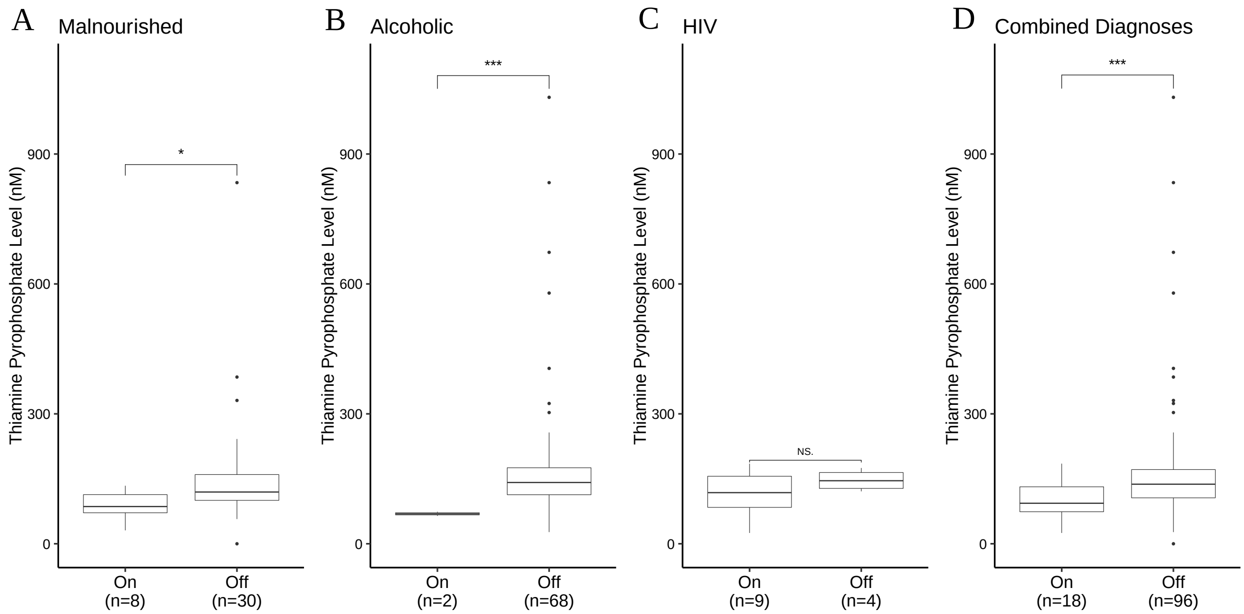

Figure 2.5 Thiamine laboratory values in patients on 1 or more clinically relevant inhibitors compared with concentrations in patients in vulnerable populations but not on a clinically relevant inhibitor. Boxplots of thiamine laboratory values in malnourished, P = 0.015 (A); alcoholic, P = 0.000002 (B); and HIV, P = 0.20 (C) patients, as well as all 3 patient populations combined, P = 0.0004 (D), comparing laboratory values of individuals on 1 or more of the clinically relevant inhibitors identified in the primary screen with patients who were not. Inhibitors are noted in **Table 2.1** (based on the DDI recommended column). *$P \leq 0.05$, ***$P \leq 0.001$ following a Welch's 2-sample t-test. Sulfamethoxazole-trimethoprim was an inclusion criterion for the on group only in the HIV analysis since this drug is not chronically taken among the general population but can be chronically used in HIV patients as a prophylaxis for pneumonia. DDI, drug-drug interaction.

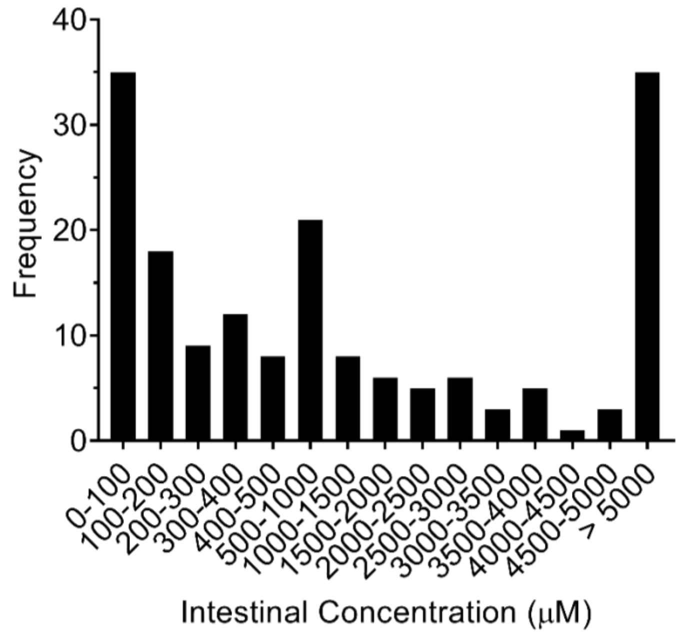

Supplemental Figure 2.1 Frequency distribution of predicted intestinal concentrations for 175 commonly used drugs. Histogram of the predicted intestinal concentration of 175 drugs. Predicted intestinal concentration was calculated using the maximum single dose for each given drug and 250 mL as recommended by the FDA (*21*).

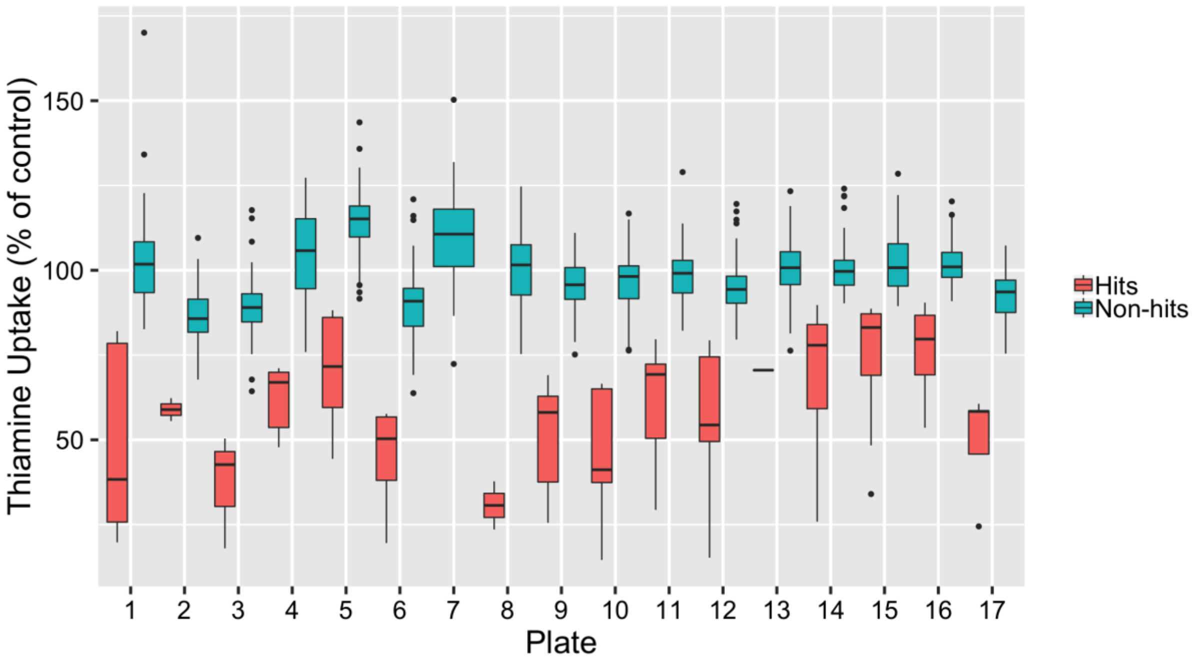

Supplemental Figure 2.2 Distribution of inhibition of thiamine uptake across all plates in primary screen. Boxplot of percent uptake of all hits and non-hits by plate. All uptake values are represented as percentages normalized to thiamine only negative control respective to each plate. Compounds were classified as hits if they caused a decrease in thiamine uptake greater than three standard deviations from the thiamine only negative control. All other compounds were considered non-hits at the screening concentration of 200 µM. Hits are colored in pink and non-hits are colored in blue.

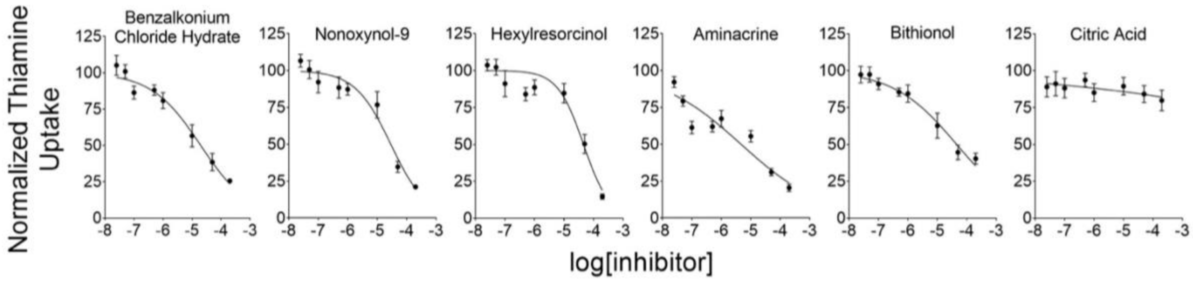

Supplemental Figure 2.3 Additional dose response curves of top hits from primary screen. IC_{50} values were determined for selected drugs in HEK293 cells stably overexpressing ThTR-2. Eight-point curves were conducted on 96 well plates with inhibitor concentrations ranging from 200 µM to 2.5 nM and 250 nM thiamine. Data points and error bars are presented as mean ± SEM respectively. Each curve is representative of three experiments and each concentration was tested in duplicate within each experiment. IC_{50} values ranged from 2.56 to 100 µM and are listed in detail in **Supplemental Table 2.2**.

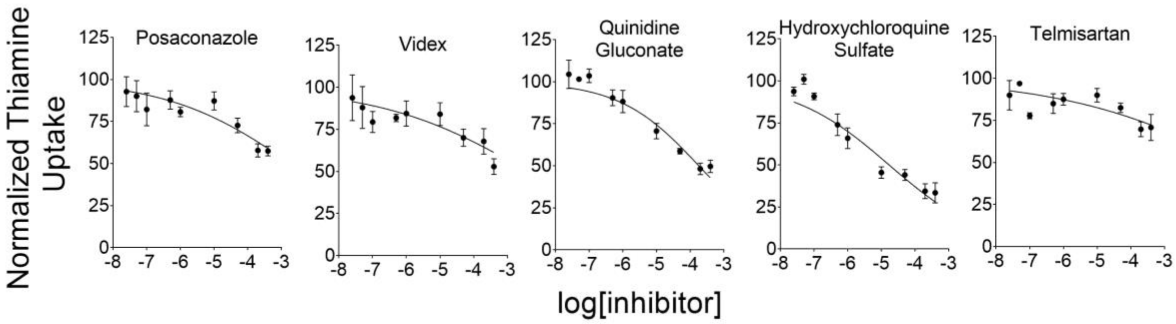

Supplemental Figure 2.4 Additional dose response curves of top hits with high clinical interaction ratios. IC_{50} values were determined for selected drugs in HEK293 cells stably overexpressing ThTR-2. Eight-point curves were conducted on 96 well plates with inhibitor concentrations ranging from 200 µM to 2.5 nM and 250 nM thiamine. Data points and error bars are presented as mean ± SEM respectively. Each curve is representative of three experiments and each concentration was tested in duplicate within each experiment. IC_{50} values ranged from 1.03 µM to 4.04 mM and are listed in detail in **Supplemental Table 2.3**.

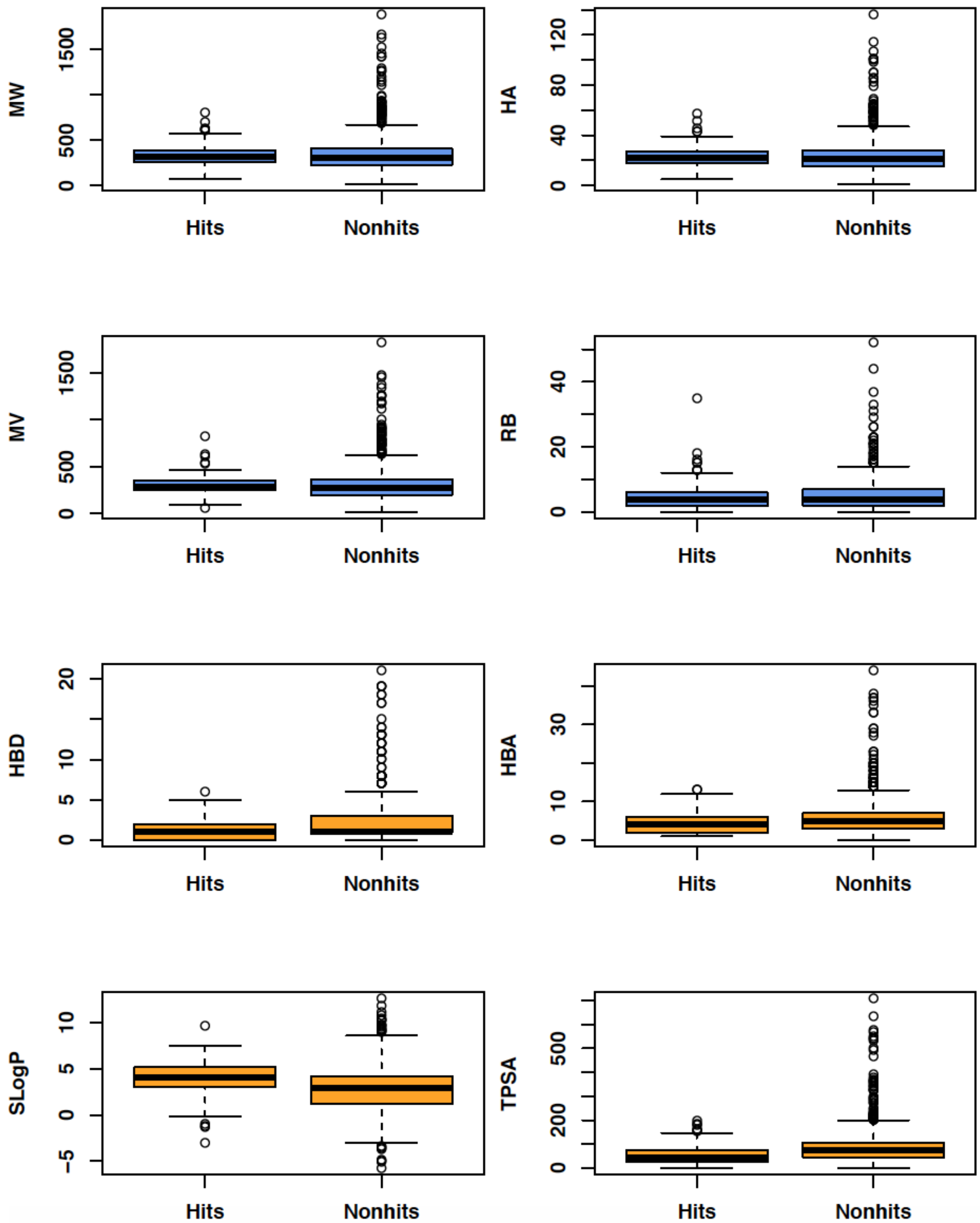

Supplemental Figure 2.5 Differences in physicochemical properties between hits and nonhits. Boxplots of physicochemical properties are shown: molecular weight (MW), number of heavy atoms (HA), number of rotatable bonds (RB), molecular volume (MV), number of hydrogen bond donors (HBD), number of hydrogen bond acceptors (HBA), Crippen's log of the octanol/water partition coefficient, including implicit hydrogens (SLogP) and total polar surface area (TPSA). Statistically significant differences (p-value < 0.005, pairwise Student's t-test) between inhibitor and noninhibitor properties are denoted by blue boxplots and non-significant differences are denoted by orange boxplots.

A

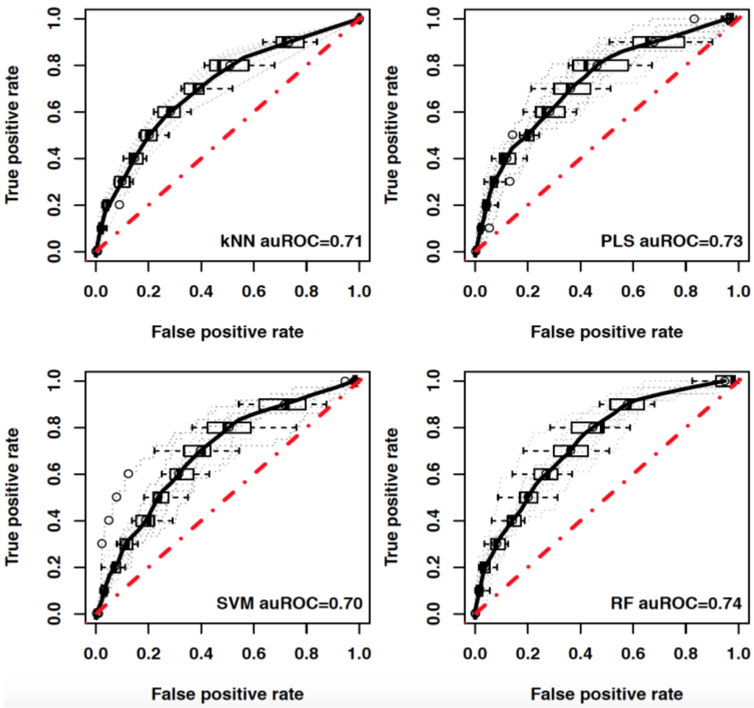

B

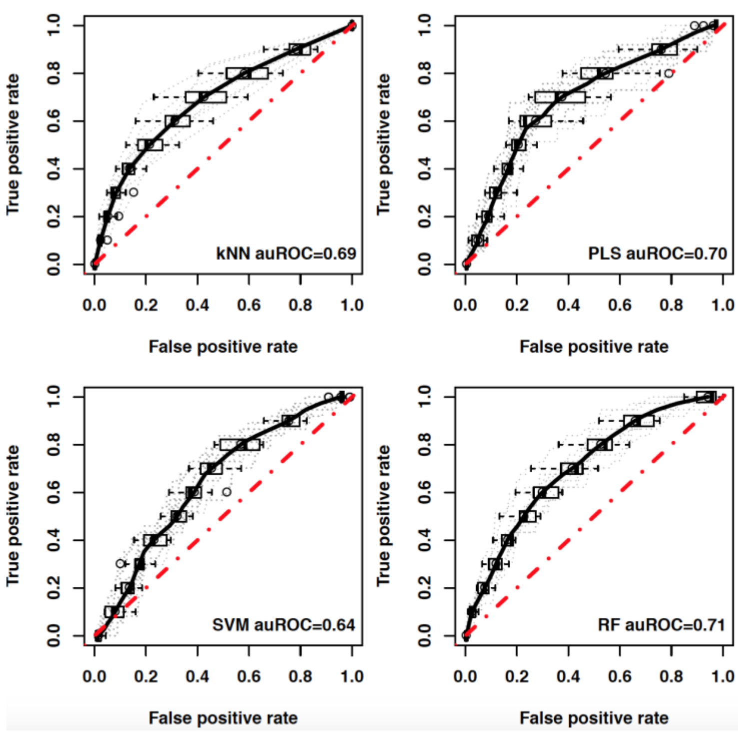

Supplemental Figure 2.6 Receiver Characteristic Operating (ROC) curves of double-loop cross-validation experiments using (A) 18 features and (B) 770 molecular descriptors. Four machine learning classifiers, namely k-Nearest Neighbor (kNN, top left quadrant), Partial Least Squares Regression Discriminant Analysis (PLS, top right quadrant), Support Vector Machines (SVM) and Random forest (RF) were validated with A) 18 features and B) 770 molecular descriptors. Boxplots show the spread of auROC (area under ROC curve) values computed for ten repeated validation experiments on withheld data (25% of samples). Red diagonal line in each plot denotes the performance of a classifier with auROC of 0.50.

2.7 TABLES

Table 2.1 Prescription drug inhibitors predicted to be clinically relevant based on experimental and computational methods.

Drug Name	Max Single Dose (mg)	IC_{50} (μM)	[Predicted Intestinal]/IC_{50}	DDI study recommended?[1]
Trimethoprim[2]	320	5.6 ± 0.59	793	Yes
Fedratinib	500	7.50 ± 0.883	600	Yes
Hydroxychloroquine Sulfate	400	17.0 ± 5.24	217	Yes
Sertraline Hydrochloride	200	1.03 ± 0.255	201	Yes
Amitriptyline Hydrochloride	100	11.3 ± 2.85	116	Yes
Metformin Hydrochloride[2]	2500	680 ± 372	88.8	Yes
Amoxapine	300	46.6 ± 14.7	81.4	Yes
Penicillamine Ethanolamine Salt	2000	857 ± 372	62.6	Yes
Verapamil	480	141 ± 46	27.7	Yes
Quinidine Gluconate	648	181 ± 52.8	27.5	Yes
Quinapril	80	34.0 ± 7.36	19.8	Yes
Didanosine	400	4040 ± 5740	8.29	No
Posaconazole	400	1896 ± 1767	1.80	No
Telmisartan	160	Not Convergent	-	No

Based on the workflow detailed in **Figure 2.1**, 14 compounds were predicted to be clinically relevant hits and selected for further validation. Hit inhibitors were defined as clinically relevant if the ratio of the compound's predicted intestinal concentration (following maximum single dose given at one time) divided by its IC_{50} was > 10. DDI, drug-drug interaction; IC_{50}, half maximal inhibitory concentration; [Predicted Intestinal], predicted intestinal concentration.

[1]A subset of these compounds would be recommended for a DDI trial based on current FDA guidelines.
[2]Trimethoprim and metformin hydrochloride IC_{50} values were obtained from published literature (*12*, *13*).

Table 2.2 Physicochemical descriptors of hit and nonhit compounds identified in a screen of ThTR-2.

Descriptors	Hits	Non-hits	P-Value
Molecular Weight (Da)	330 ± 116	343 ± 194	2.24E-01
Molecular Volume (Å^3)	304 ± 105	309 ± 180	6.14E-01
Heavy Atoms (*n*)	23.0 ± 8.02	23.5 ± 13.3	4.51E-01
Rotatable Bonds (*n*)	5.07 ± 4.35	5.05 ± 4.50	9.60E-01
Hydrogen Bond Donors (*n*)	1.06 ± 1.13	2.04 ± 2.42	1.04E-15
Hydrogen Bond Acceptors (*n*)	4.32 ± 2.70	5.96 ± 4.60	1.19E-09
SLogP	4.02 ± 1.90	2.90 ± 2.44	6.48E-10
Total Polar Surface Area (Å^2)	56.1 ± 42.2	88.5 ± 74.3	7.57E-14

Mean ± SD values for 8 physicochemical descriptors are shown for 144 hits and 1213 nonhits. $P < 0.005$ for differences in distributions of physicochemical properties of hits compared with those of nonhits, estimated with the Student's pairwise t-test. SLogP, log of the octanol-water partition coefficient, including implicit hydrogens; ThTR-2, thiamine transporter 2.

Supplemental Table 2.1 Z-prime and number of hits for each plate.

Plate	Thiamine (µM)	Fedratinib (µM)	Z-prime (100µM)	Z-prime (250µM)	Z-prime (500µM)	# of Hits
1	250	100 & 250	0.705	0.666	-	11
2	250	100 & 250	0.563	0.611	-	2
3	250	100 & 250	0.479	0.521	-	3
4	250	100 & 250	0.474	0.556	-	6
5	250	500	-	-	0.469	16
6	250	100 & 250	0.497	0.517	-	4
7	250	100 & 250	0.415	0.437	-	0
8	250	100 & 250	0.587	0.395	-	2
9	250	100 & 250	0.569	0.512	-	6
10	250	100 & 250	0.502	0.576	-	5
11	250	100 & 250	0.781	0.714	-	7
12	250	100 & 250	0.675	0.684	-	13
13	250	100 & 250	0.606	0.673	-	1
14	250	500	-	-	0.669	27
15	250	100 & 250	0.676	0.812	-	13
16	250	100 & 250	0.755	0.806	-	25
17	250	100 & 250	0.633	0.630	-	5

Hit calling for the primary screen was conducted and Z-prime scores were calculated within each plate using the positive and negative controls (*19*). The average and standard deviation of the vehicle negative control for each plate was determined and all compounds were normalized to this control. A hit threshold was set as three standard deviations below the average of the negative control respective to each plate. Hits were defined by a decrease in thiamine uptake greater than three standard deviations from the thiamine only negative control.

Supplemental Table 2.2 Detailed dose response curve parameters for a subset of top hits from primary screen.

	IC_{50} (µM)		
	Value	SEM	95% CI
Benzalkonium Chloride Hydrate	19.9	4.79	12.3, 32.9
Nonoxynol-9	29.0	6.23	18.7, 44.6
Hexylresorcinol	45.9	8.07	31.1, 65.0
Aminacrine	4.69	1.34	2.69, 8.51
Benzethonium Chloride	100	9.87	82.3, 123
Chlorohexidine Dihydrochloride	2.56	0.439	1.81, 3.69
Bithionol	45.1	13.4	25.5, 88.9
Amprolium	7.17	1.04	5.32, 9.67
Centrimonium Bromide	54.1	5.94	43.3, 67.4
Amsacine*	4.37	0.703	3.14, 6.10
Citric Acid*	NA	NA	17840, infinity

IC_{50} were conducted on 96 well plates with inhibitor concentrations ranging from 200 µM to 2.5 nM and a thiamine substrate concentration of 250 nM. Each inhibitor concentration was tested in duplicate in each experiment. Each IC_{50} curve was repeated 3 times except where an asterisks (*) notes only two experiments were conducted. All values are derived from Graph Pad Prism 8.0 analysis setting of log(inhibitor) vs. normalized response -- Variable slope. IC_{50}, half maximal inhibitory concentration; SEM, standard error of the mean; CI, confidence interval.

Supplemental Table 2.3 Detailed dose response curve parameters for selected hits with high clinical interaction ratios.

	IC_{50} (µM)		
	Value	SEM	95% CI
Sertraline Hydrochloride	1.03	0.255	0.627, 1.73
Posaconazole	1900	1770	450, 38300
Videx	4040	5740	545, 1230000
Quinapril	34.0	7.36	22.4, 52.8
Penicillamine Ethanolamine Salt	857	372	428, 2900
Quinidine Gluconate	181	52.8	106, 359
Amitriptyline Hydrochloride	11.3	2.85	6.82, 18.8
Amoxapine	46.6	14.7	25.7. 90.7
Hydroxychloroquine Sulfate	17.0	5.24	9.17, 33.1
Telmisartan	NA	NA	4160, infinity

All values are derived from Graph Pad Prism 8.0 analysis setting of log(inhibitor) vs. normalized response -- Variable slope. IC_{50}, half maximal inhibitory concentration; SEM, standard error of the mean; CI, confidence interval; NA, > 1 mM and considered relevant inhibition.

Supplemental Table 2.4 Molecular descriptors used to train QSAR models.

Descriptor	Name	Description	RF Variable Importance
1	BCUTp.1l	Burden eigenvalue descriptor	20.84
2	CrippenLogP	Crippen octanol/water partition coefficient	73.99
3	nHBint5	Hydrogen bonding descriptor	9.35
4	SHssNH	Atom type electrotopological state index	25.86
5	SdssC	Atom type electrotopological state index	61.81
6	mindsCH	Minimum atom-type E-State descriptor	39.28
7	mindssC	Minimum atom-type E-State descriptor	22.79
8	mindsN	Minimum atom-type E-State descriptor	100.00
9	mindO	Minimum atom-type E-State descriptor	0.00
10	maxHBint3	Maximum E-State *descriptors* of strength for potential hydrogen bonding	36.92
11	maxHBint7	Maximum E-State *descriptors* of strength for potential hydrogen bonding	24.92
12	maxsCl	Maximum E-State *descriptors* of strength for potential hydrogen bonding	0.00
13	hmin	Minimum hydrogen Estate value for all the atoms in the molecule	53.78
14	gmin	Minimum Estate value for all the atoms in the molecule	0.00
15	ETA_Shape_P	Extended topochemical atom descriptor	20.84
16	ETA_EtaP_B	Extended topochemical atom descriptor	52.85
17	MDEC.22	Molecular distance edge descriptor	43.96
18	MDEO.11	Molecular distance edge descriptor	0.00

Eighteen molecular descriptors selected by feature selection algorithm that were used to train four machine learning classifiers. SDF files were processed with PaDEL software (*23*) to compute molecular descriptors for each screened compound.

Supplemental Table 2.5 Detailed dose response curve parameters for selected compounds from QSAR.

	IC50		
	Value	SEM	95% CI
Loxapine	38400	89100	1570, infinity
Cinchonidine	19.7	6.40	10.3, 41.5
Tetramizole HCl	44.4	13.8	24.6, 90.0
Pyrantel Pamoate	76.1	8.02	61.6, 95.1
Levomilnacipran*	NA	NA	infinity, infinity
Clozapine*	NA	NA	NA
Cinchonine*	98.6	37.6	48.4, 269

Drugs with a * represent values from two experiments. All values are derived from Graph Pad Prism 8.0 analysis setting of log(inhibitor) vs. normalized response -- Variable slope. IC_{50}, half maximal inhibitory concentration; SEM, standard error of the mean; CI, confidence interval.

Supplemental Table 2.6 Analysis of discrepancies between *in vitro* screen and QSAR model.

	IC_{50} (μM)		Results	
	Average	SEM	Screen	QSAR
Tetramizole HCl	44.4	13.8	Hit	Non-Hit
Pyrantel Pamoate	76.1	8.02	Hit	Non-Hit
Levomilnacipran*	NC	NC	Hit	Non-Hit
Cinchonine*	98.6	37.6	Non-Hit	Hit

There were four discrepancies in hit calling between screen and the random forest QSAR model. Dose response curves were conducted for those compounds. Two of the four compounds were false negatives in the model, levomilnacipran was a false positive in the screen, and cinchonine was a false negative in the screen. NC = not convergent due to lack of inhibition; IC_{50}, half maximal inhibitory concentration; SEM, standard error of the mean. *Represents compounds tested in two replicates instead of three.

Supplemental Table 2.7 Demographics for on and off groups used in EHR analysis.

	On	**Off**
Gender		
% Female	69	59
% Male	31	41
Age		
Median (range)	54 (16 - 90)	57 (0 - 90)
Medication Orders based on unique Pharmaceutical Class		
Median (range)	56.5 (4 - 113)	32 (1 - 132)

Percent female and male as well as median age and range were computed for each group. Medication orders based on unique pharmaceutical classes (i.e. each pharmaceutical class is only counted once per patient irrespective of number of prescriptions) was also counted for both groups.

2.8 REFERENCES

1. A. Pardanani *et al.*, Safety and Efficacy of Fedratinib in Patients With Primary or Secondary Myelofibrosis: A Randomized Clinical Trial. *JAMA Oncol* **1**, 643-651 (2015).
2. A. Welsh, P. Rogers, F. Clift, Nonalcoholic Wernicke's encephalopathy. *CJEM* **18**, 309-312 (2016).
3. G. Sechi, A. Serra, Wernicke's encephalopathy: new clinical settings and recent advances in diagnosis and management. *Lancet Neurol* **6**, 442-455 (2007).
4. L. Bettendorff, Thiamin. *Present Knowledge in Nutrition*, (2012).
5. H. M. Said, Water-soluble vitamins. *World Rev Nutr Diet* **111**, 30-37 (2015).
6. H. Said, in *Encyclopedia of Dietary Supplements,* P. Coates *et al.*, Eds. (Informa Healthcare, London and New York, 2010), pp. 748-753.
7. J. König, F. Müller, M. F. Fromm, Transporters and drug-drug interactions: important determinants of drug disposition and effects. *Pharmacol Rev* **65**, 944-966 (2013).
8. K. M. Giacomini *et al.*, Membrane transporters in drug development. *Nat Rev Drug Discov* **9**, 215-236 (2010).
9. F. Müller, M. F. Fromm, Transporter-mediated drug-drug interactions. *Pharmacogenomics* **12**, 1017-1037 (2011).
10. L. Zhang, S. M. Huang, L. J. Lesko, Transporter-mediated drug-drug interactions. *Clin Pharmacol Ther* **89**, 481-484 (2011).
11. Q. Zhang *et al.*, The Janus kinase 2 inhibitor fedratinib inhibits thiamine uptake: a putative mechanism for the onset of Wernicke's encephalopathy. *Drug Metab Dispos* **42**, 1656-1662 (2014).

12. M. M. Giacomini *et al.*, Interaction of 2,4-Diaminopyrimidine-Containing Drugs Including Fedratinib and Trimethoprim with Thiamine Transporters. *Drug Metab Dispos* **45**, 76-85 (2017).

13. X. Liang *et al.*, Metformin Is a Substrate and Inhibitor of the Human Thiamine Transporter, THTR-2 (SLC19A3). *Mol Pharm* **12**, 4301-4310 (2015).

14. J. D. Eudy *et al.*, Identification and characterization of the human and mouse SLC19A3 gene: a novel member of the reduced folate family of micronutrient transporter genes. *Mol Genet Metab* **71**, 581-590 (2000).

15. V. Ganapathy, S. B. Smith, P. D. Prasad, SLC19: the folate/thiamine transporter family. *Pflugers Arch* **447**, 641-646 (2004).

16. R. M. Müri, J. Von Overbeck, J. Furrer, P. E. Ballmer, Thiamin deficiency in HIV-positive patients: evaluation by erythrocyte transketolase activity and thiamin pyrophosphate effect. *Clin Nutr* **18**, 375-378 (1999).

17. S. J. Scalzo, S. C. Bowden, M. L. Ambrose, G. Whelan, M. J. Cook, Wernicke-Korsakoff syndrome not related to alcohol use: a systematic review. *J Neurol Neurosurg Psychiatry* **86**, 1362-1368 (2015).

18. P. Attaluri, A. Castillo, H. Edriss, K. Nugent, Thiamine Deficiency: An Important Consideration in Critically Ill Patients. *Am J Med Sci* **356**, 382-390 (2018).

19. J. H. Zhang, T. D. Chung, K. R. Oldenburg, A Simple Statistical Parameter for Use in Evaluation and Validation of High Throughput Screening Assays. *J Biomol Screen* **4**, 67-73 (1999).

20. Y. Kido, P. Matsson, K. M. Giacomini, Profiling of a prescription drug library for potential renal drug-drug interactions mediated by the organic cation transporter 2. *J Med Chem* **54**, 4548-4558 (2011).

21. US Food and Drug Administration, *In Vitro Metabolism and Transporter Mediated Drug-Drug Interaction Studies Guidance for Industry*. (US FDA website, 2017).

22. S. Kim *et al.*, PubChem Substance and Compound databases. *Nucleic Acids Res* **44**, D1202-1213 (2016).

23. C. W. Yap, PaDEL-descriptor: an open source software to calculate molecular descriptors and fingerprints. *J Comput Chem* **32**, 1466-1474 (2011).

24. M. Kuhn, Building Predictive Models in R Using the caret Package. *2008* **28**, 26 (2008).

25. M. A. Hall, L. A. Smith, paper presented at the Proceedings of the Twelfth International Florida Artificial Intelligence Research Society Conference, 1999.

26. M. Sud, MayaChemTools: An Open Source Package for Computational Drug Discovery. *J Chem Inf Model* **56**, 2292-2297 (2016).

27. J. A. Hanley, B. J. McNeil, The meaning and use of the area under a receiver operating characteristic (ROC) curve. *Radiology* **143**, 29-36 (1982).

28. T. Sing, O. Sander, N. Beerenwinkel, T. Lengauer, ROCR: visualizing classifier performance in R. *Bioinformatics* **21**, 3940-3941 (2005).

29. E. Athanasiadis, Z. Cournia, G. Spyrou, ChemBioServer: a web-based pipeline for filtering, clustering and visualization of chemical compounds used in drug discovery. *Bioinformatics* **28**, 3002-3003 (2012).

30. J. I. Boullata, Drug and nutrition interactions: not just food for thought. *J Clin Pharm Ther* **38**, 269-271 (2013).

31. H. M. Said, R. Redha, W. Nylander, Biotin transport in the human intestine: inhibition by anticonvulsant drugs. *Am J Clin Nutr* **49**, 127-131 (1989).

32. A. Costantini, R. Fancellu, An open-label pilot study with high-dose thiamine in Parkinson's disease. *Neural Regen Res* **11**, 406-407 (2016).

33. D. Liu, Z. Ke, J. Luo, Thiamine Deficiency and Neurodegeneration: the Interplay Among Oxidative Stress, Endoplasmic Reticulum Stress, and Autophagy. *Mol Neurobiol* **54**, 5440-5448 (2017).

34. X. Pan *et al.*, Long-Term Cognitive Improvement After Benfotiamine Administration in Patients with Alzheimer's Disease. *Neurosci Bull* **32**, 591-596 (2016).

35. Z. Chen, C. Zhong, Decoding Alzheimer's disease from perturbed cerebral glucose metabolism: implications for diagnostic and therapeutic strategies. *Prog Neurobiol* **108**, 21-43 (2013).

36. G. E. Gibson *et al.*, Vitamin B1 (thiamine) and dementia. *Ann N Y Acad Sci* **1367**, 21-30 (2016).

37. K. C. Whitfield *et al.*, Thiamine deficiency disorders: diagnosis, prevalence, and a roadmap for global control programs. *Ann N Y Acad Sci* **1430**, 3-43 (2018).

38. A. Goyer, Thiamin biofortification of crops. *Curr Opin Biotechnol* **44**, 1-7 (2017).

39. K. C. Whitfield *et al.*, Poor thiamin and riboflavin status is common among women of childbearing age in rural and urban Cambodia. *J Nutr* **145**, 628-633 (2015).

40. World Health Organization, Office of the United Nations High Commissioner for Refugees, *Thiamine Deficiency and Its Prevention and Control in Major Emergencies*. (World Health Organization, 1999).

41. D. Soukaloun *et al.*, Dietary and socio-economic factors associated with beriberi in breastfed Lao infants. *Ann Trop Paediatr* **23**, 181-186 (2003).

42. H. Barennes, K. Sengkhamyong, J. P. René, M. Phimmasane, Beriberi (thiamine deficiency) and high infant mortality in northern Laos. *PLoS Negl Trop Dis* **9**, e0003581 (2015).

43. B. Adamolekun, L. Hiffler, A diagnosis and treatment gap for thiamine deficiency disorders in sub-Saharan Africa? *Ann N Y Acad Sci* **1408**, 15-19 (2017).

44. N. A. Wani, U. A. Qureshi, M. Jehangir, K. Ahmad, W. Ahmad, Infantile encephalitic beriberi: magnetic resonance imaging findings. *Pediatr Radiol* **46**, 96-103 (2016).

45. F. Nosten, Beriberi in Cambodia. *Paediatr Int Child Health* **35**, 283-284 (2015).

46. U. A. Qureshi *et al.*, Thiamine responsive acute life threatening metabolic acidosis in exclusively breast-fed infants. *Nutrition* **32**, 213-216 (2016).

47. J. C. Kerns, C. Arundel, L. S. Chawla, Thiamin deficiency in people with obesity. *Adv Nutr* **6**, 147-153 (2015).

48. E. S. Eshak, A. E. Arafa, Thiamine deficiency and cardiovascular disorders. *Nutr Metab Cardiovasc Dis* **28**, 965-972 (2018).

49. A. Jain, R. Mehta, M. Al-Ani, J. A. Hill, D. E. Winchester, Determining the Role of Thiamine Deficiency in Systolic Heart Failure: A Meta-Analysis and Systematic Review. *J Card Fail* **21**, 1000-1007 (2015).

50. K. Amrein, W. Ribitsch, R. Otto, H. C. Worm, R. E. Stauber, Severe lactic acidosis reversed by thiamine within 24 hours. *Crit Care* **15**, 457 (2011).

51. R. K. Dean, R. Subedi, D. Gill, A. Nat, Consideration of alternative causes of lactic acidosis: Thiamine deficiency in malignancy. *Am J Emerg Med* **35**, 1214.e1215-1214.e1216 (2017).

52. L. M. Linder, S. Robert, K. Mullinax, G. Hayes, Thiamine Prescribing and Wernicke's Encephalopathy Risk Factors in Patients With Alcohol Use Disorders at a Psychiatric Hospital. *J Psychiatr Pract* **24**, 317-322 (2018).

53. L. Hiffler, B. Rakotoambinina, N. Lafferty, D. Martinez Garcia, Thiamine Deficiency in Tropical Pediatrics: New Insights into a Neglected but Vital Metabolic Challenge. *Front Nutr* **3**, 16 (2016).

54. H. Seligmann, R. Levi, A. M. Konijn, M. Prokocimer, Thiamine deficiency in patients with B-chronic lymphocytic leukaemia: a pilot study. *Postgrad Med J* **77**, 582-585 (2001).

55. J. Y. Ryu, H. U. Kim, S. Y. Lee, Deep learning improves prediction of drug-drug and drug-food interactions. *Proc Natl Acad Sci U S A* **115**, E4304-E4311 (2018).

56. F. Rico-Villademoros, M. Slim, E. P. Calandre, Amitriptyline for the treatment of fibromyalgia: a comprehensive review. *Expert Rev Neurother* **15**, 1123-1150 (2015).

57. R. Kwiatek, Treatment of fibromyalgia. *Aust Prescr* **40**, 179-183 (2017).

58. M. J. Snyder, L. M. Gibbs, T. J. Lindsay, Treating Painful Diabetic Peripheral Neuropathy: An Update. *Am Fam Physician* **94**, 227-234 (2016).

59. L. M. Koran *et al.*, Practice guideline for the treatment of patients with obsessive-compulsive disorder. *Am J Psychiatry* **164**, 5-53 (2007).

60. O. Brawman-Mintzer, R. G. Knapp, M. Rynn, R. E. Carter, K. Rickels, Sertraline treatment for generalized anxiety disorder: a randomized, double-blind, placebo-controlled study. *J Clin Psychiatry* **67**, 874-881 (2006).

61. A. V. Ravindran, J. D. Guelfi, R. M. Lane, G. B. Cassano, Treatment of dysthymia with sertraline: a double-blind, placebo-controlled trial in dysthymic patients without major depression. *J Clin Psychiatry* **61**, 821-827 (2000).

62. D. P. P. R. Group, Long-term safety, tolerability, and weight loss associated with metformin in the Diabetes Prevention Program Outcomes Study. *Diabetes Care* **35**, 731-737 (2012).

63. A. C. o. P. Bulletins--Gynecology, ACOG Practice Bulletin No. 108: Polycystic ovary syndrome. *Obstet Gynecol* **114**, 936-949 (2009).

64. C. McGarvey, C. Franconi, D. Prentice, M. Bynevelt, Metformin-induced encephalopathy: the role of thiamine. *Intern Med J* **48**, 194-197 (2018).

65. R. I. Misbin, The phantom of lactic acidosis due to metformin in patients with diabetes. *Diabetes Care* **27**, 1791-1793 (2004).

66. T. A. Alston, Does metformin interfere with thiamine? *Arch Intern Med* **163**, 983; author reply 983 (2003).

67. S. A. Romanski, M. M. McMahon, Metabolic acidosis and thiamine deficiency. *Mayo Clin Proc* **74**, 259-263 (1999).

68. L. L. Frank, Thiamin in Clinical Practice. *JPEN J Parenter Enteral Nutr* **39**, 503-520 (2015).

69. A. M. Ruggiero *et al.*, Nonoisotopic assay for the presynaptic choline transporter reveals capacity for allosteric modulation of choline uptake. *ACS Chem Neurosci* **3**, 767-781 (2012).

70. L. C. Morris *et al.*, A Duplexed High-Throughput Screen to Identify Allosteric Modulators of the Glucagon-Like Peptide 1 and Glucagon Receptors. *J Biomol Screen* **19**, 847-858 (2014).

71. K. J. Filipski *et al.*, Discovery of Orally Bioavailable Selective Inhibitors of the Sodium-Phosphate Cotransporter NaPi2a (SLC34A1). *ACS Med Chem Lett* **9**, 440-445 (2018).

CHAPTER 3

Intersection of Pre-Clinical, Clinical, and Real World Data: A multi-faceted approach to understand complex transporter-mediated drug-nutrient interactions

3.1 ABSTRACT

In studies described in Chapter 2, trimethoprim, an antimicrobial agent, was predicted to be a potent, clinical inhibitor of thiamine transporter 2 (ThTR-2), the primary intestinal absorptive transporter of thiamine. Employing a multi-faceted approach using *in vitro*, clinical trial, and real world data, we aimed to determine the effect of trimethoprim on thiamine concentrations in healthy volunteers. A prospective randomized crossover clinical study was conducted where healthy volunteers were given a single oral dose of thiamine or thiamine + trimethoprim followed by intensive blood sampling. Because of the pandemic caused by COVID19, the clinical trial had to be curtailed, limiting the planned recruitment of 18 volunteers. However, 7 healthy volunteers completed the study, and the results here represent our findings (termed preliminary) in 6 of these individuals. Our results in the 6 individuals showed that thiamine plasma concentrations increased following co-administration with trimethoprim. Thiamine maximum concentration achieved (C_{max}) and area under the curve (AUC) were significantly higher when thiamine was co-administered with trimethoprim (paired t-test p-value: 0.015 and

0.017, respectively). *In vitro* transporter assays demonstrated that trimethoprim is a potent inhibitor of OCT1 (IC_{50}: 4.2 ± 0.6 μM), suggesting that *in vivo*, trimethoprim may inhibit thiamine uptake into the liver, resulting in reduced hepatic metabolism and higher thiamine levels. From the EHR data, we observed that HIV patients prescribed trimethoprim had significantly higher triglyceride, LDL cholesterol, and total cholesterol levels, a known consequence of OCT1 inhibition (p-values: $< 2.2 \times 10^{-16}$, 5.75×10^{-7}, 5.82×10^{-7}, respectively). Our preliminary findings in six volunteers suggest that in addition to OCT1 being an important target for drug-drug interactions, OCT1 may be a target for drug-nutrient interactions.

3.2 Introduction

In 2012, a clinical trial investigating fedratinib, a Janus Kinase 2 (JAK2) inhibitor, for the treatment of myelofibrosis was placed on clinical hold by the Food and Drug Administration (FDA) when several patients developed symptoms similar to Wernicke's encephalopathy (WE), a life-threatening disease caused by Vitamin B1 (thiamine) deficiency (*1-4*). Since then, fedratinib has been approved; however, its package insert includes a boxed warning about serious and fatal encephalopathy, including Wernicke's, and advises assessing thiamine levels prior and during treatment (*5*).

Thiamine is a water-soluble vitamin which is obtained exclusively from our diet and is rapidly converted into thiamine monophosphate, thiamine pyrophosphate (TPP), and thiamine triphosphate (*6-8*). Thiamine is metabolized to TPP (thiamine + ATP ↔ TPP + AMP) by thiamine pyrophosphokinase (TPK1). TPP accounts for approximately 80% of total thiamine stores in the human body and is the active form of the vitamin, acting as a coenzyme for various enzyme complexes (*6*).

In vitro studies have shown that fedratinib is a potent inhibitor of thiamine transporter 2 (ThTR-2; SLC19A3), the primary intestinal absorptive transporter of thiamine (*9, 10*). Subsequent studies have shown that other commonly prescribed drugs can also inhibit ThTR-2 (*10-12*). A recent highthroughput screen from our laboratory (Chapter 2) found that 146 prescription drugs (out of 1360 compounds screened) could inhibit ThTR-2 *in vitro*, several of which were predicted to inhibit ThTR-2 at clinically relevant intestinal concentrations (*12*). One of the drugs which was predicted to be a potent, clinical inhibitor was trimethoprim.

Trimethoprim is an antibiotic, commonly combined with sulfamethoxazole, used in the treatment and prevention of various bacterial infections including but not limited to urinary tract infections, traveler's diarrhea, pediatric otitis media, and shigellosis (*13-15*). Although it is given short term for many indications, trimethoprim (with sulfamethoxazole) can be taken chronically for certain indications including prevention of opportunistic infections such as *Pneumocystis carinii* pneumonia in patients diagnosed with human immunodeficiency virus (HIV) (*13, 16-18*).

The goal of this study was to determine the effect of trimethoprim on thiamine concentrations in healthy volunteers and employ a multi-faceted approach using *in vitro*, clinical trial, and real world data to investigate our findings. More specifically, we designed and executed a prospective randomized, two-arm drug-nutrient interaction (DNI) clinical study in healthy volunteers to evaluate the inhibition potential of trimethoprim clinically and 1) performed *in* *vitro* studies and 2) mined electronic health records to complement our clinical findings. As noted, because of the pandemic, only 7 individuals completed the trial, rendering the information presented here "preliminary."

3.3 METHODS

3.3.1 Clinical study design

This was a randomized, two-arm crossover study conducted in healthy volunteers. To be eligible, subjects had to provide written informed consent, be between the ages of 18 and 65 years, be in good health (determined by a screening questionnaires, physical examination, and clinical laboratory evaluations), and be willing to consume the study diet. Subjects who were excluded included those who were pregnant, breastfeeding, or unwilling to practice birth control during participation in the study; with self-reported severe food allergies or diet restrictions that would prevent consumption of study diets; with extreme obesity (BMI > 35); who were smokers or had smoked in the past year and/or had smoked or ingested THC/marijuana in the past week, or who were unwilling to comply with a 1-week washout; with alcohol use of > 2 servings/day or > 14 servings/wk (on average) or self-reported binge drinking; on vitamin B supplements or multi-vitamins or who had taken vitamin B supplements or multi-vitamins in the past 30 days and were not willing to comply with a 30 day washout of vitamin B supplements; with a possible folate deficiency; taking any other clinically significant drugs as judged by the investigator; undergoing treatment for infertility or hormone replacement therapy; who had taken antimalarials in the past 60 days; who were participating in another research study while participating in this study; and who were Non-English speaking.

This study protocol was approved by the Health Sciences Campus Institutional Review Board at Tufts University and was registered on clinicaltrials.gov (NCT03746106). Subjects who meet all inclusion criteria and none of the exclusion criteria were enrolled into the study.

The clinical study was performed at the Jean Mayer USDA Human Nutrition Research Center on Aging at Tufts University. There were two cycles in this study, each separated by at least 5 days but no more than two weeks. Subjects arrived on Day 0 of each cycle to pick-up three thiamine deficient meals (prepared by the site) which they were asked to consume throughout the day without any other food intake. Female subjects were asked to provide a urine sample to ensure non-pregnant status. On Day 1, subjects arrived at the site following an overnight fast and weight, vitals, and a health history questionnaire were used to review any change in medications or health status. Baseline blood and urine samples were taken before administration of vitamin/drug. A dose of either a) 5 mg thiamine or b) 5 mg thiamine and 300 mg trimethoprim were administered with 500mL of water. No food or additional water was provided for up to 4 hours post-dose to avoid dilution of the dose or a food-drug interaction. After the 4-hour period, subjects were provided their first meal and water ad libitum. Subjects were provided three thiamine deficient meals during their visit on Day 1. Subjects were permitted to leave after the 12-hour post-dose sample collection and were asked to fast overnight. On Day 2 of each cycle, subjects arrived at the site, submitted their urine collection kit, and had one more blood collection.

Plasma and red blood cell samples were collected at pre-dose and 0.25, 0.5, 1, 1.5, 2, 2.5, 3, 3.5, 4, 6, 8, 10, 12, and 24 hours post-dose and urine samples were collected in intervals at 0-4, 4-8, 8-12, and 12-24 hours post-dose. Plasma was immediately separated from red blood cells upon collection to avoid contamination from red blood cells.

3.3.2 Bioanalytical methods

Plasma thiamine was measured by the Newman lab at the Western Human Nutrition Research Center by ultra-performance liquid chromatography tandem mass spectrometry (UPLC-MS/MS). Briefly, plasma aliquots (10 µL) were transferred to 96 well plates and enriched with 10 µL of thiamine-d3 and trimethoprim-d9. Plasma proteins were then precipitated by mixing with 80 µL of chilled 0.1% acetic acid with 0.55 mM ammonium acetate, and plates were agitated for 1 min and centrifuged for 15 min at 2247 g and 4°C. Supernatants were then filtered through 0.2 µm PVDF filters plates (Agilent Technologies, Santa Clara CA) for 2 min under the same centrifugal conditions. Samples (10 µL) were injected on an H-class Acquity UPLC (Waters Corp, Milford MA) interfaced with an API Sciex 4000 QTRAP (Sciex, Framingham MA) mass spectrometer. Thiamine and trimethoprim were separated on a 2 x 150 mm, 3 µm Luna Silica column attached to a 0.5 µm depth x 0.004 in i.d. in-line KrudKatcher filter (Phenomenex, Torrance CA) at 35ºC. Mobile phases consisting of 0.1% acetic acid in water (solvent A) and 0.1% acetic acid in acetonitrile (solvent B) were used to create the following gradient at 0.4 mL/min: 2%B from 0-0.5 min, to 13%B at 2.5 min, to 100%B at 3.0 min held to 4.5 min, and followed by re-equilibration to initial condition at 2%B from 4.6-6.5 min. Analytes were detected by positive mode electrospray ionization using multi-reaction monitoring of precursor-product mass transitions for thiamine (265.0 > 122.1 m/z), thiamine-d3 (268.0 > 125.0 m/z), trimethoprim

(291.3 > 230.1 m/z), and trimethoprim-d9 (300.0 > 234 m/z) and quantified using internal standard methodology against 6-pt calibration curves.

Red blood cell (RBC) thiamine pyrophosphate was also measured by the Newman lab at the Western Human Nutrition Research Center by high performance liquid chromatography with fluorescence detection after thiochrome derivatization using minor modifications of previously published methods (*19*). Briefly, RBCs (~50 mg) were weighed into 1.5 mL amber Eppendorf tubes and enriched with 10 µL of 264 µM of the internal standard 4-deoxypyridine (DPN). Proteins were then precipitated by mixing with 13 µL 70% perchloric acid, agitating for 2 min, and centrifuging for 10 min at 15000g and 4°C. In a polypropylene 96-well plate, supernatant sub-aliquots (60 µL) were enriched with 5 µL universal pH indicator (Home Science Tools, Billings MT), and the thiochrome reactions were initiated by mixing with 35 µL of 12mM potassium ferricyanide in 3.35M sodium hydroxide. Samples were agitated for 1 min, incubated for 10 min, neutralized with 1M phosphoric acid, and then processed through 0.2 µm PVDF filter plates (Agilent Technologies) by spinning for 2 min at 2247g and 4°C. The analyte in the 25 µL injections was eluted on an Agilent 1200 HPLC equipped with a 4.6 x 150 mm, 5 µm Kinetex EVO C18 protected by 4 x 30 mm SecurityGuard C18 column (Phenomenex) using the following gradient of 0.15M dibasic potassium phosphate at pH7 (Solvent A) and methanol (Solvent B) at 45°C and 1.75 mL/min: 0 min 10%B to 20%B at 2 min, to 60% B at 4.5 min, and to initial conditions to 90%B at 4.8 min to re-equilibrate for 2.3 min to for a total run time of 7.1 min. Detection of the TPP derivative was accomplished by fluorescent detection with 367 nm/435 nm excitation/emission, while DPN was monitor by photo diode array detector absorption at 320 nm. Residues were quantified against 6-pt calibration curves after correction for matrix associated influence of derivatization efficiency assessed in each analytical batch using a common pooled RBC reference material. Intraday precision was 33.0+/-8%, while inter-day coefficient of variation was 33.0% over six different days.

3.3.3 Data cleaning and pharmacokinetic analyses

Data cleaning and imputation were performed using Jmp Pro 14.1 (SAS Institute, Carry, NC). Outliers identified by Huber M robust fit procedure were removed. Missing values were imputed using multivariate normal imputations. One of 180 plasma thiamine and 7 of 180 RBC TPP measures were imputed in the final data set.

Due to intra- and inter-subject variability in baseline thiamine concentrations, before any analyses were conducted, thiamine concentrations were adjusted by subtracting baseline thiamine concentrations (i.e. concentration at t = 0 hours) from thiamine concentrations at subsequent timepoints, respective to subject and cycle. Thiamine concentration at t = 0.25 hours was used for adjustment for one subject in one cycle since the concentration at t = 0 hours exceeded concentrations at all subsequent timepoints, and presumably represented a measurement error. Thiamine concentrations less than 0.005 nM post-adjustment were set to 0 nM.

Concentration-time profiles of thiamine were plotted using the ggplot2 package in R (version 3.4.0). PK parameters were determined by non-compartmental analysis using the PKNCA package (*20*) in R. Data are expressed as mean ± standard error unless otherwise noted. Differences in PK parameters were analyzed in R using paired t-tests.

3.3.4 Transporter inhibition studies

The OCT1 cell line stably transfected with SLC22A1 cDNA to HEK293 FlpIn cells (*21*) was cultured in DMEM supplemented with penicillin (100 U/mL), streptomycin (100 mg/mL) and 10% FBS. Cells were seeded at 80,000 cells per well onto poly-d-lysine coated 96-well plates for 16-24 hours to reach 95% confluence. To initiate the inhibition study, the cells were washed once in 100 µL warm HBSS and then incubated in 90 µL of the HBSS buffer containing trace amount of radiolabeled thiamine, [^{3}H]-thiamine (American Radiolabeled Chemicals) with 1 µM unlabeled thiamine together with various concentrations of trimethoprim at 37°C for 10 min. Each plate contained control wells with quinidine as canonical inhibitor of OCT1 which were used for normalization in data analysis. Following the incubation, the cells were washed twice with 200 µL ice-cold HBSS buffer. MicroScint-20 (Perkin Elmer) (100 µL) was added to the 96-well plate and sealed with an adhesive plastic cover. The plate was placed on a shaker for 1-2 hours. The plates were read in a MicroBeta2 (Perkin Elmer) using the dual counting mode.

3.3.5 Prediction of transporter-mediated inhibition

The DNI potential for trimethoprim at OCT1 was evaluated in accordance to the 2020 FDA Drug-Drug Interaction Guidance (https://www.fda.gov/media/134582/download). The estimated maximum plasma trimethoprim concentration at the inlet to the liver was calculated using the following equation: $I_{in,max} = I_{max} + (F_a \times F_g \times k_a \times Dose)/Q_h/R_B$. F_a and F_g were both estimated to be 1 since the bioavailability of trimethoprim is approximately 90-100% (*22*, *23*). Additionally, k_a, R_B, and Q_h were assumed to be 0.1 min^{-1}, 1, and 1.62 L/min, respectively. Lastly, the average maximum trimethoprim plasma concentration achieved (C_{max}) from our study was used for I_{max}.

Inhibition potency for OCT1 was determined using equation and cut-off: $R = 1 + ((f_{u,p} \times I_{in,max})/IC_{50}) \geq 1.1$, where $f_{u,p}$ was estimated to be 0.56 (*24*).

3.3.6 Thiamine Pyrophosphokinase 1 (TPK1) enzyme assay

To determine if trimethoprim is an inhibitor of human TPK1, adenosine monophosphate (AMP), a by-product of the enzymatic reaction between TPK1 and thiamine, levels were determined in a TPK1 enzyme reaction using AMP-Glo™ Assay (Promega). The 0.5 mL enzyme reaction mixture (pH 7.4), which contained 100 μM $MgCl_2$, 500 μM ATP, 15 μg human TPK1 (Novus Biologics, NBP19910210), and a substrate (with or without inhibitor), was incubated for 30 min at 37°C (*25*). Substrates that were tested in the enzyme reaction included 0.1 mM thiamine, 1 mM thiamine, and 1 mM pyrithiamine. Trimethoprim was tested as a substrate (1 mM) and inhibitor (1, 5, and 10 mM) in the enzyme reaction. A negative control (NC) reaction was prepared similarly to the enzyme reaction, however without TPK1.

After incubating the reaction in a 37°C water bath, samples were immediately transferred to ice and a 25 μL aliquot was transferred to a 96-well white plate. The reaction was terminated by adding an equal volume (25 μL) of AMPGlo™ Reagent I and incubated for 1 hour at room temperature. 50 μL of AMP Detection Solution was added to each sample and incubated for 1 hour at room temperature and luminescence was measured with a GloMax luminometer (Promega) (https://worldwide.promega.com/-/media/files/resources/protocols/technical-manuals/101/amp-glo-assay-protocol.pdf?la=en).

Data are expressed as mean ± standard deviation unless otherwise noted.

3.3.7 Real world data analyses

The UCSF Research Data Browser was utilized to search for patients diagnosed with HIV who had at least one laboratory test value reported for 1) triglyceride (“Triglycerides, serum”, “Triglycerides, Serum”; 5,079 patients), 2) LDL cholesterol (“LDL Cholesterol”, “Cholesterol, LDL”; 4,315 patients), or 3) total cholesterol (“Cholesterol, total”; 5,580 patients). ICD10 code B20 (which is associated with “human immunodeficiency virus [HIV] disease”) was used to identify and filter for HIV patients. Diagnoses with missing diagnosis start dates were excluded.

Laboratory values reported as an inequality were changed to a numerical value (i.e. < 0.5 mg/dL = 0.5 mg/dL). Laboratory values with missing values (i.e. DE-IDENTIFIED) and laboratory values without a laboratory collection date were excluded. Laboratory values taken before the initial HIV diagnosis start date were excluded (i.e. laboratories taken on or after diagnosis start date were included). Additionally, patients who did not have sex or date of birth recorded in the EHR were excluded from the analysis.

For each analysis, patients were divided into two groups depending on their medication prescriptions. Specifically, patients prescribed trimethoprim were grouped into the “on” drug group. Search terms for trimethoprim were as follows: “Bactrim”, “Cotrim”, “Polytrim” “Primsol”, “Proloprim”, “Septra”, “Sulfamethoprim”, “Sulfatrim”, “Sulmeprim”, “Trimeth”, “Trimethoprim”, “Trimpex”, “Uroplus”. There were 2,367 patients in the database with an HIV diagnosis and at least one medication order to trimethoprim (irrespective to timing or laboratories). Only medication orders with an oral route of administration and with a medication order start date were included in the analysis. Medication orders with a start date prior to initial HIV diagnosis start date were excluded. The remaining patients (i.e. individuals who were never prescribed trimethoprim) were grouped into the “off” drug group. Only patients with one laboratory value reported in their electronic health record were included in the “off” drug group.

Patients in the “on” drug group were further filtered based on their laboratory collection dates relative to their first and last medication order start dates. Laboratories collected after the patient’s last medication order start date were excluded. Additionally, laboratories collected before the patient's first medication order start date or within 7 days after their first medication order start date were excluded. A minimum of 7 days between first medication order start date and laboratory collection date was chosen to allow drug levels to reach steady-state and for an effect to be seen. For patients with more than one laboratory value, only the laboratory value closest to the first medication order start date was included. Lastly, patients were age- and sex-matched using the MatchIt package (*26*) in R to be comparable in both groups (**Supplemental Table 3.1**).

Two-sample Mann-Whitney U test were performed to evaluate if there was a significant difference in laboratory values when comparing “on” and “off” drug groups and ggplot2 was used to plot the data in R.

3.4 RESULTS

The results described here are largely obtained from six of the seven individuals who completed the clinical study. Original recruitment goals could not be met as a result of the impact of the COVID19 pandemic on shutting down clinical research operations at Tufts University.

3.4.1 Thiamine concentrations increase when co-administered with trimethoprim

A randomized, two-arm crossover DNI study was conducted in 7 healthy volunteers to determine the effect of trimethoprim on the absorption and disposition of thiamine. All subjects completed the study and no adverse events were reported. One subject was not included in the analysis due to incomplete sampling in the combination arm; thus, all analyses will be based on n = 6 subjects. The demographic and baseline characteristics of the healthy volunteers are shown in **Table 3.1**.

Results in these six volunteers showed that thiamine plasma concentrations increased following co-administration with trimethoprim (**Figure 3.1**). The maximum concentration achieved (C_{max}) and area under the curve from 0 to 4 hours (AUC_{0-4}) were significantly higher when thiamine was co-administered with trimethoprim (paired t-test p-value: 0.015 and 0.017, respectively). (**Table 3.2** and **Figure 3.1**).

Additionally, the ratio of unadjusted thiamine pyrophosphate to unadjusted thiamine (TPP/Thiamine) was increased in the thiamine only arm at every timepoint (**Supplemental**

Figure 3.1), suggesting increased parent (thiamine), decreased metabolite (TPP), or a combination of both.

3.4.2 Trimethoprim prevents metabolism of thiamine by inhibiting OCT1 and potentially TPK1

Organic cation transporter 1, OCT1 (SLC22A1), is a major hepatic uptake transporter for thiamine. *In vitro* data demonstrated that trimethoprim is a potent inhibitor of OCT1 (IC_{50}: 4.2 ± 0.6 μM) (**Figure 3.2**). Using the FDA guidance for evaluating transporter-mediated drug interactions, trimethoprim was predicted to cause a clinically relevant drug-nutrient interaction at OCT1 (R = 11.4) following a single 300 mg oral dose, which suggests that trimethoprim may inhibit OCT1-mediated thiamine uptake into the liver *in vivo,* thus reducing metabolism of thiamine to its metabolites, and elevating its plasma levels.

Preliminary data showed that thiamine (1 mM) and pyrithiamine significantly increased AMP luminescence in the TPK1 enzyme assay by 9.21 ± 0.158 and 11.4 ± 0.218-fold respectively, suggesting that both are substrates of TPK1, as noted in previous literature (*6, 27*). Trimethoprim (at 1 mM) did not increase AMP luminescence and is unlikely to be a substrate of TPK1. However, trimethoprim at high concentrations (1, 5, and 10 mM) reduced TPK1 activity by 30.7 ± 3.82, 46.0 ± 0.871, and 47.0 ± 0.931% respectively (**Figure 3.3**).

3.4.3 Electronic health record analyses complement in vitro OCT1 inhibition findings

To investigate the clinical relevance of trimethoprim, we mined the electronic health records (EHRs) database at UCSF. In particular, we compared specific laboratory values in HIV patients prescribed trimethoprim to the respective laboratory values in HIV patients not prescribed trimethoprim. Based on the inclusion and exclusion criteria described in the methods, we were able to classify patients as “on” drug (i.e. prescribed trimethoprim) or “off” drug. Triglyceride (p-value $< 2.2 \times 10^{-16}$, n = 464 “on” drug, n = 928 “off” drug), LDL cholesterol (p-value: 5.75×10^{-7}, n = 313 “on” drug, n = 1149 “off” drug), and total cholesterol (p-value: 5.82×10^{-7}, n = 483 “on” drug, n = 966 “off” drug) levels were significantly increased in HIV patients prescribed trimethoprim compared to age- and sex-matched HIV patients not prescribed trimethoprim, when comparing laboratories taken on or after initial HIV diagnosis start date, consistent with inhibition of OCT1 (**Figure 3.4** and **Table 3.3**).

Since statin use can influence lipid levels and be a confounding factor, we performed sub-analyses where we excluded patients who had at least one prescription to drugs (classified as antihyperlipidemic-HMG-CoA reductase inhibitors (statins)) in his/her electronic health record. In all three analyses, patients in the “on” drug group had significantly higher triglycerides, LDL cholesterol, and total cholesterol levels (respectively) compared to the “off” drug group (**Table 3.3**).

3.5 Discussion

Although membrane transporters are known targets for drug-drug interactions and are thoroughly investigated throughout the drug development process, DNIs with thiamine have been largely ignored until the fedratinib trial (*28*-*30*). Using multiple levels of evidence, this study suggests that in addition to OCT1 being an important target for drug-drug interactions, OCT1 may be a target for drug-nutrient interactions.

Though our study was interrupted by the COVID19 pandemic, and only seven volunteers completed the clinical study, the data from these individuals, which was complemented with real world data, are consistent with three major findings. First, systemic thiamine concentrations increase when the vitamin is co-administered with trimethoprim. Second, trimethoprim inhibits OCT1, and is predicted to inhibit the transporter at clinically relevant plasma concentrations. Finally, trimethoprim use is associated with increased lipid levels in data from EHRs, which is consistent with the drug inhibiting OCT1.

An unexpected finding was that thiamine concentrations increased when thiamine was co-administered with trimethoprim. Our initial hypothesis had been that trimethoprim would behave like fedratinib and inhibit intestinal ThTR-2, leading to reduced thiamine plasma levels. Although time to maximum thiamine concentration (T_{max}) was similar in both arms and to values reported in previous studies (*31-34*), C_{max} and AUC were significantly higher when thiamine was co-administered with trimethoprim. These data suggest that another mechanism was at play, which resulted in increased, rather than decreased, thiamine levels. Additionally, our preliminary data show that, contrary to our initial hypothesis, trimethoprim may be beneficial for patients who are diagnosed or at-risk for thiamine deficiency and should be considered when prescribing antibiotics to this patient population.

Thiamine is a known substrate of OCT1 (*35*); Oct1 knockout mice have increased plasma thiamine levels and reduced hepatic thiamine levels (*21, 35*). However, to our knowledge, before this study, the potential of trimethoprim to inhibit hepatic OCT1-mediated thiamine uptake has not been described. Based on the experimental IC_{50} determined in this study, trimethoprim is predicted to cause a clinically relevant drug-nutrient interaction at OCT1 in the liver. Although a recent study by Jensen et al did not find a significant difference in plasma thiamine concentrations relative to OCT1 genotype, this may have been because of the high dose of thiamine used in the study. A 200 mg dose of thiamine may have been too high to detect genotype-mediated differences in thiamine concentrations in their intensive PK study (i.e. thiamine concentrations in the portal vein exceeded the K_m). Further, differences in trough concentrations may have been missed in the second study due to intersubject variability (*33*).

Transporter interactions may be complex. For example, drugs such as fedratinib and trimethoprim inhibit multiple transporters and enzymes. Preclinical studies have shown that rats chronically dosed with clinically equivalent doses of fedratinib do not demonstrate neurological changes consistent with thiamine deficiency (*36, 37*). Further retrospective analyses of patients treated with fedratinib in the clinical trial suggest that pre-existing and underlying conditions (i.e. malnutrition) may have led to the symptoms observed since the mean thiamine levels from 161 patients were normal (*38*). Together, these data suggest that drug-induced thiamine deficiency may be complicated, affected by a patient's baseline health (e.g. patients suffering from malnutrition or alcoholism) and baseline thiamine levels as well as by the ability of drugs to interact with multiple transporters and enzymes.

Using electronic health records, we were able to use real world data to demonstrate that HIV patients prescribed trimethoprim had significantly higher triglycerides, LDL cholesterol, and total cholesterol levels, a known consequence to OCT1 inhibition (*21*), indicating that trimethoprim may be phenocopying the effect of a reduced function transporter. Mandal et al (*39*) previously showed that administration of trimethoprim to rats caused a significant increase in total serum lipid and cholesterol levels as well as modulated lipid and glycogen contents in the liver. The results reported in this study are consistent with the known phenotype of an OCT1 knockout mice, which exhibit higher triglycerides, LDL cholesterol, and total cholesterol levels (*21*). The EHR data suggest that HIV patients prescribed trimethoprim may be at an increased risk for comorbidities related to high lipid levels (*40-43*). Furthermore, drugs which may cause increased lipid levels as a result of off-target effects should be reconsidered in patients taking trimethoprim concomitantly.

There are a number of limitations to this study. First, trimethoprim was dosed orally, as we were interested in evaluating the effect of trimethoprim inhibition on intestinal SLC19A3-mediated thiamine absorption. Without an intravenous dose as well, we had no ability to detect the effects of trimethoprim on thiamine bioavailability. Additionally, our study design was modeled on the assumption that thiamine has a short half-life, which was not the case. Sampling time points past 24 hours post-dose are needed for accurate estimation of half-life and clearance. Finally, our EHR analysis was limited by the lack of data on SLC19A3 and OCT1 genotype of the patients, how long patients were on trimethoprim, and patient compliance. As more EHR data becomes available for research purposes, we will be able to account for these variables and covariates and increase the sample size and robustness of our analysis. Controlled, randomized clinical trials in both healthy volunteers and in patients diagnosed with HIV are needed to help address these limitations.

Overall, our study, though limited by the pandemic, demonstrates that trimethoprim increases thiamine concentrations. The mechanism probably involves inhibition of thiamine uptake via hepatic OCT1. Our study highlights that trimethoprim should be considered for patients who may be at-risk for thiamine deficiency; however, alternative anti-microbials should be considered for patients who may be predisposed to increased lipid levels and are chronically taking trimethoprim. This study suggests that although OCT1 is an established target for drug-drug interactions, OCT1 may be a target for drug-nutrient interactions as well. Additionally, this study, in combination with Chapter 2, highlights the importance of investigating transporter-mediated drug-nutrient interactions throughout drug development, both *in vitro* as well as in the clinic.

3.6 Acknowledgements

We would like to acknowledge and thank all subjects for their participation as well as the coordinators and site personnel involved in the clinical study including Dr. Andrew Greenberg, Kim Trinh, and Ryan Piccirillo. Additionally, we would like to thank Dr. John Newman, Dr. Theresa Pedersen, and Anita Wen for developing the plasma and red blood cell assays as well as for performing sample quantification and analysis. Additionally, we would like to thank Dr. Sook Wah Yee and Dr. Jessica Enogieru for generating the IC_{50} curves as well as performing the TPK1 assay. Lastly, we would like to thank Dr. Marina Sirota for helpful discussions regarding the EHR analyses.

3.7 Figures

A

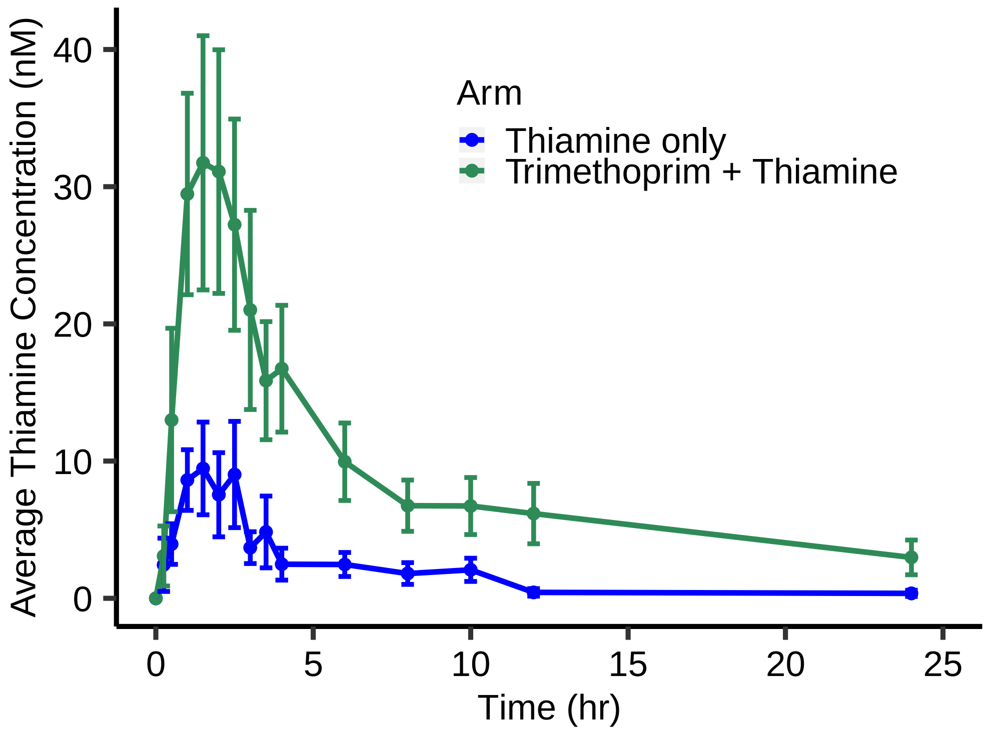

B

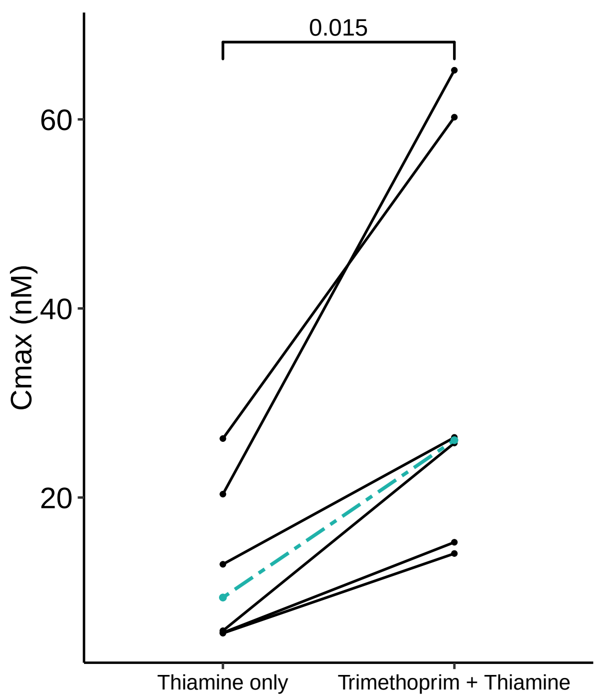

C

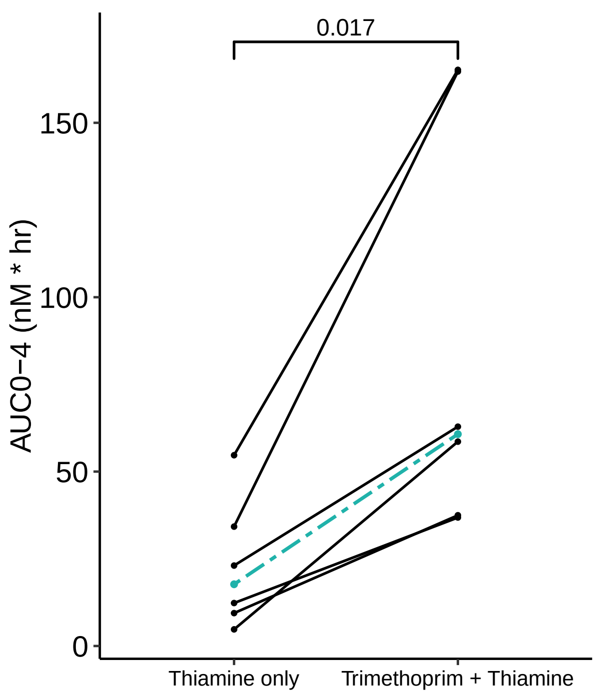

Figure 3.1 Average thiamine concentrations and pharmacokinetic parameters after administration of thiamine alone or in combination with trimethoprim in 6 healthy volunteers. (A) Thiamine concentrations were determined following a 5 mg oral dose of thiamine alone or with a 300 mg oral dose of trimethoprim. Data represent mean thiamine concentration ± standard error at each timepoint respective to arm. (B) Maximum concentration achieved (C_{max}) and (C) area under the concentration-time curve from t = 0 hours to t = 4 hours (AUC_{0-4}) were compared between both arms using a paired t-test. Median values are overlayed in green. One subject was not included in the analysis due to incomplete sampling in the combination arm; thus, the data shown here is from n = 6 subjects.

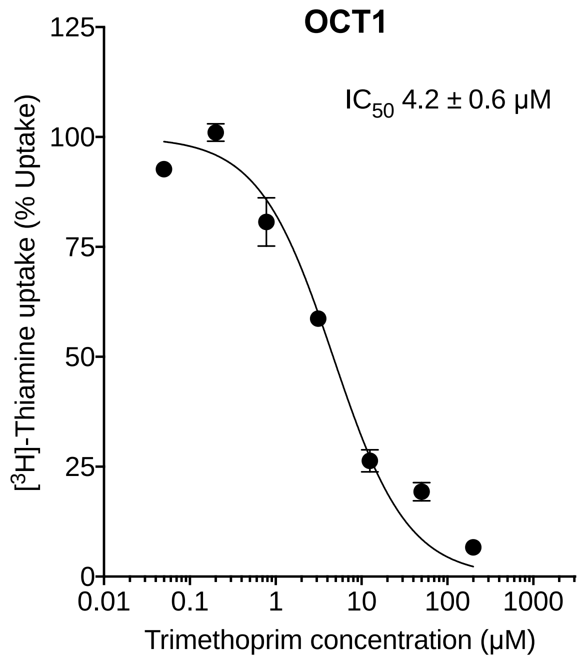

Figure 3.2 Inhibition of [^{3}H]-thiamine uptake by trimethoprim in HEK293-FlpIn cells overexpressing human OCT1 (SLC22A1). Circles represent mean ± SD from triplicate wells. IC_{50} value (mean ± SD) shown was from two independent studies in triplicate wells.

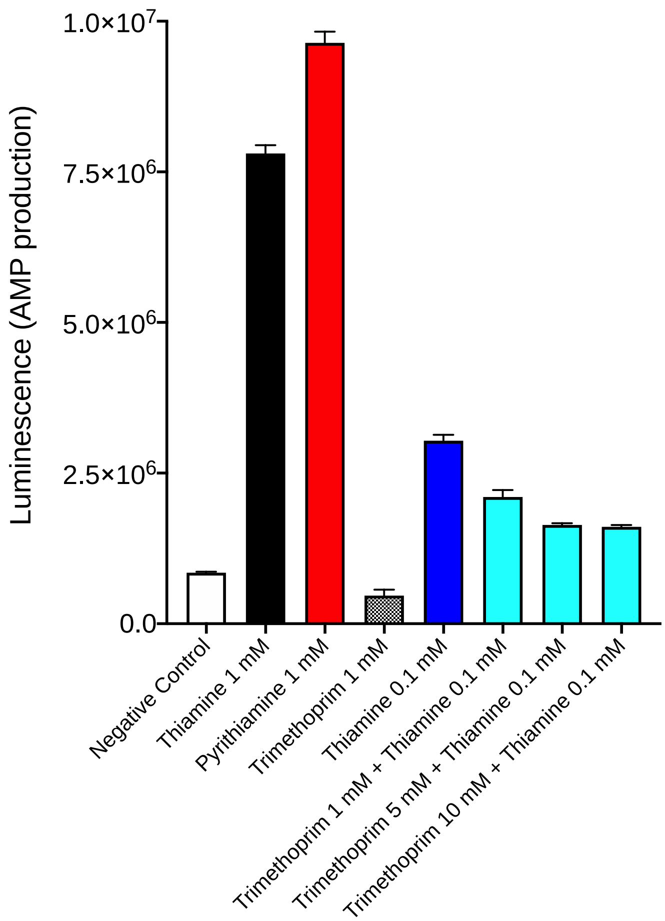

Figure 3.3 Results of the thiamine pyrophosphokinase 1 (TPK1) activity assay. Luminescence was measured as a marker for adenosine monophosphate (AMP) production in human TPK1 reactions following incubation with known substrates (thiamine and pyrithiamine). Trimethoprim was tested at various concentrations as a substrate and inhibitor. NC, negative control.

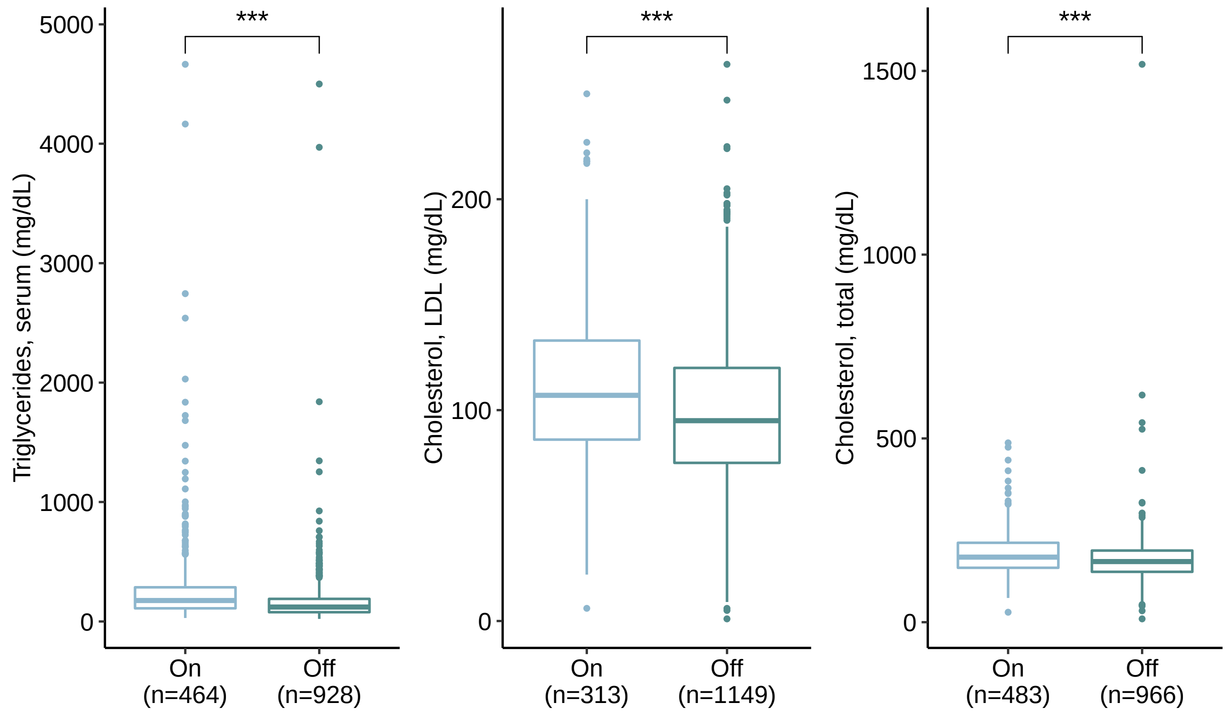

Figure 3.4 Endogenous biomarker levels in patients prescribed trimethoprim compared with levels in patients not prescribed trimethoprim using electronic health record data. Boxplots comparing triglycerides, LDL cholesterol, and total cholesterol laboratory values in HIV patients prescribed trimethoprim versus HIV patients not prescribed trimethoprim (p-value: $< 2.2 \times 10^{-16}$, 5.75×10^{-7}, 5.82×10^{-7}, respectively).

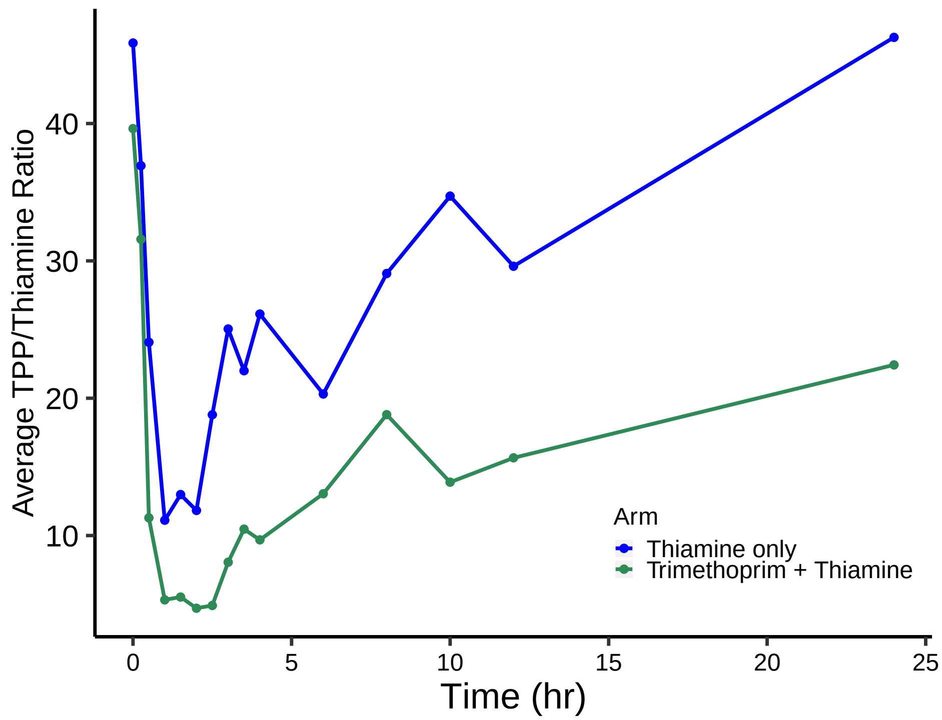

Supplemental Figure 3.1 Average thiamine pyrophosphate to thiamine ratio after administration of thiamine alone or in combination with trimethoprim in 6 healthy volunteers. Data represent mean ratio at each timepoint respective to arm. Ratio represents unadjusted thiamine pyrophosphate to unadjusted thiamine (TPP/Thiamine). One subject was not included in the analysis due to incomplete sampling in the combination arm; thus, the data shown here is from n = 6 subjects.

3.8 Tables

Table 3.1 Demographics of study cohort analyzed as part of the clinical trial.

Patient Demographics	
Number of patients (#)	6
Sex	
Female (#)	4
Male (#)	2
Age (years)	47.8 ± 6.36
Race	
Caucasian (#)	4
Other (#)	2
Hispanic	
Yes (#)	4
No (#)	2
Weight (kg)	74.7 ± 7.08
Height (cm)	169 ± 3.13
BMI (kg/m^2)	26.0 ± 2.00
Baseline Thiamine (nM)	9.91 ± 5.23

Age, weight, height, BMI, and baseline thiamine are reported as average ± standard error. Baseline thiamine was calculated using pre-dose thiamine concentrations from both treatment arms. Although seven individuals completed the clinical study, one subject was not included in the analysis due to incomplete sampling in the combination arm; thus, the data shown here is from n = 6 subjects.

Table 3.2 Summary of pharmacokinetic parameters of thiamine in six healthy volunteers with or without trimethoprim.

	Thiamine only	Thiamine + Trimethoprim	p-value
Thiamine			
T_{max} (hr)	1.5 (1 - 3)	1.5 (1 - 2.5)	0.530
C_{max} (nM)	12.8 ± 3.59	34.5 ± 9.19	0.0154
AUC_{0-4} (nM*hr)	23.1 ± 7.66	87.6 ± 24.8	0.017
AUC_{0-24} (nM*hr)	44.4 ± 10.9	206 ± 58.6	0.0234

All data are reported as mean ± standard error except for T_{max} which is reported as median (range). P-values were determined using paired t-tests. T_{max}, time to maximum plasma concentration; C_{max}, maximum plasma concentration achieved; $AUC_{0–4}$, area under the concentration-time curve from t = 0 hours to t = 4 hours; $AUC_{0–24}$, area under the concentration-time curve from t = 0 hours to t = 24 hours.

Table 3.3 Summary table of electronic health record analyses comparing laboratory values in patients prescribed trimethoprim versus patients not prescribed trimethoprim.

		Triglycerides	LDL cholesterol	Total cholesterol
Main analyses				
Total patients	On drug (N)	464	313	483
	Off drug (N)	1278	1149	1410
Matched patients	Ratio	1:2	all	1:2
	On drug (N)	464	313	483
	Off drug (N)	928	1149	966
	Average On drug (mg/dL)	275	112	185
	Average Off drug (mg/dL)	165	98.7	169
	Median On drug (mg/dL)	176	107	177
	Median Off drug (mg/dL)	121	95	165
	p-value	$< 2.2 \times 10^{-16}$	5.75×10^{-7}	5.82×10^{-7}
Sub-analyses: patients with prescription to statin(s) excluded				
Total patients	On drug (N)	391	248	402
	Off drug (N)	1089	959	1219
Matched patients	Ratio	1:2	all	All
	On drug (N)	391	248	402
	Off drug (N)	782	959	1219
	Average On drug (mg/dL)	264	109	178
	Average Off drug (mg/dL)	162	99.7	169
	Median On drug (mg/dL)	171	105	172
	Median Off drug (mg/dL)	120	97	165
	p-value	$< 2.2 \times 10^{-16}$	4.79×10^{-3}	1.69×10^{-3}

Supplemental Table 3.1 Demographics for on and off groups used in EHR analysis.

	On Drug	Off drug	p-value
Main analyses			
Triglycerides			
Number of patients (#)	464	928	NA
Average age (years)	42.7	42.9	0.606
% Male	89.0	90.4	0.469
LDL cholesterol			
Number of patients (#)	313	1149	NA
Average age (years)	44.2	45.6	0.079
% Male	85.6	87.3	0.495
Total cholesterol			
Number of patients (#)	483	966	NA
Average age (years)	42.9	42.9	0.963
% Male	87.2	88.6	0.473
Sub-analyses: patients with prescription to statin(s) excluded			
Triglycerides			
Number of patients (#)	391	782	NA
Average age (years)	42.0	42.2	0.679
% Male	88.2	89.4	0.621
LDL cholesterol			
Number of patients (#)	248	959	NA
Average age (years)	43.4	43.5	0.980
% Male	83.5	86.5	0.254
Total cholesterol			
Number of patients (#)	402	1219	NA
Average age (years)	42.3	42.9	0.362
% Male	85.8	87.4	0.476

Percent male and average age were computed for each group. NA, not applicable.

3.9 REFERENCES

1. A. Pardanani *et al.*, Safety and Efficacy of Fedratinib in Patients With Primary or Secondary Myelofibrosis: A Randomized Clinical Trial. *JAMA Oncol* **1**, 643-651 (2015).
2. A. Welsh, P. Rogers, F. Clift, Nonalcoholic Wernicke's encephalopathy. *CJEM* **18**, 309-312 (2016).
3. G. Sechi, A. Serra, Wernicke's encephalopathy: new clinical settings and recent advances in diagnosis and management. *Lancet Neurol* **6**, 442-455 (2007).
4. A. Mullally, J. Hood, C. Harrison, R. Mesa, Fedratinib in myelofibrosis. *Blood Adv* **4**, 1792-1800 (2020).
5. INREBIC [package insert]. Summit, NJ; Celgene Corporation.
6. L. Bettendorff, Thiamin. *Present Knowledge in Nutrition*, (2012).
7. H. M. Said, Water-soluble vitamins. *World Rev Nutr Diet* **111**, 30-37 (2015).
8. H. Said, in *Encyclopedia of Dietary Supplements*, P. Coates *et al.*, Eds. (Informa Healthcare, London and New York, 2010), pp. 748-753.
9. Q. Zhang *et al.*, The Janus kinase 2 inhibitor fedratinib inhibits thiamine uptake: a putative mechanism for the onset of Wernicke's encephalopathy. *Drug Metab Dispos* **42**, 1656-1662 (2014).
10. M. M. Giacomini *et al.*, Interaction of 2,4-Diaminopyrimidine-Containing Drugs Including Fedratinib and Trimethoprim with Thiamine Transporters. *Drug Metab Dispos* **45**, 76-85 (2017).
11. X. Liang *et al.*, Metformin Is a Substrate and Inhibitor of the Human Thiamine Transporter, THTR-2 (SLC19A3). *Mol Pharm* **12**, 4301-4310 (2015).

12. B. Vora *et al.*, Drug-nutrient interactions: discovering prescription drug inhibitors of the thiamine transporter ThTR-2 (SLC19A3). *Am J Clin Nutr* **111**, 110-121 (2020).
13. T. R. Kemnic, M. Coleman, in *StatPearls*. (StatPearls Publishing Copyright © 2020, StatPearls Publishing LLC., Treasure Island (FL), 2020).
14. R. Gleckman, N. Blagg, D. W. Joubert, Trimethoprim: mechanisms of action, antimicrobial activity, bacterial resistance, pharmacokinetics, adverse reactions, and therapeutic indications. *Pharmacotherapy* **1**, 14-20 (1981).
15. P. A. Masters, T. A. O'Bryan, J. Zurlo, D. Q. Miller, N. Joshi, Trimethoprim-sulfamethoxazole revisited. *Arch Intern Med* **163**, 402-410 (2003).
16. M. A. Fischl, G. M. Dickinson, L. La Voie, Safety and efficacy of sulfamethoxazole and trimethoprim chemoprophylaxis for Pneumocystis carinii pneumonia in AIDS. *JAMA* **259**, 1185-1189 (1988).
17. J. E. Kaplan *et al.*, Guidelines for prevention and treatment of opportunistic infections in HIV-infected adults and adolescents: recommendations from CDC, the National Institutes of Health, and the HIV Medicine Association of the Infectious Diseases Society of America. *MMWR Recomm Rep* **58**, 1-207; quiz CE201-204 (2009).
18. J. Ruskin, M. LaRiviere, Low-dose co-trimoxazole for prevention of Pneumocystis carinii pneumonia in human immunodeficiency virus disease. *Lancet* **337**, 468-471 (1991).
19. D. Hampel *et al.*, Thiamin and Riboflavin in Human Milk: Effects of Lipid-Based Nutrient Supplementation and Stage of Lactation on Vitamer Secretion and Contributions to Total Vitamin Content. *PLoS One* **11**, e0149479 (2016).

20. W. Denney, S. Duvvuri, C. Buckeridge, Simple, Automatic Noncompartmental Analysis: The PKNCA Package. *Journal of Pharmacokinetics and Pharmacodynamics* **42**, 11-107 (2015).

21. X. Liang *et al.*, Organic cation transporter 1 (OCT1) modulates multiple cardiometabolic traits through effects on hepatic thiamine content. *PLoS Biol* **16**, e2002907 (2018).

22. T. W. Chin, A. Vandenbroucke, I. W. Fong, Pharmacokinetics of trimethoprim-sulfamethoxazole in critically ill and non-critically ill AIDS patients. *Antimicrob Agents Chemother* **39**, 28-33 (1995).

23. M. E. Klepser *et al.*, Oral absorption of trimethoprim-sulfamethoxazole in patients with AIDS. *Pharmacotherapy* **16**, 656-662 (1996).

24. Trimethoprim [package insert]. Baltimore, MD; Lupin Pharmaceuticals, Inc.

25. W. Huang *et al.*, Reduced thiamine binding is a novel mechanism for TPK deficiency disorder. *Mol Genet Genomics* **294**, 409-416 (2019).

26. D. Ho, K. Imai, G. King, E. A. Stuart, MatchIt: Nonparametric Preprocessing for Parametric Causal Inference. *2011* **42**, 28 (2011).

27. J. Y. Liu, D. E. Timm, T. D. Hurley, Pyrithiamine as a substrate for thiamine pyrophosphokinase. *J Biol Chem* **281**, 6601-6607 (2006).

28. J. König, F. Müller, M. F. Fromm, Transporters and drug-drug interactions: important determinants of drug disposition and effects. *Pharmacol Rev* **65**, 944-966 (2013).

29. K. M. Giacomini *et al.*, Membrane transporters in drug development. *Nat Rev Drug Discov* **9**, 215-236 (2010).

30. F. Müller, M. F. Fromm, Transporter-mediated drug-drug interactions. *Pharmacogenomics* **12**, 1017-1037 (2011).

31. H. A. Smithline, M. Donnino, D. J. Greenblatt, Pharmacokinetics of high-dose oral thiamine hydrochloride in healthy subjects. *BMC Clin Pharmacol* **12**, 4 (2012).

32. C. M. Tallaksen, A. Sande, T. Bøhmer, H. Bell, J. Karlsen, Kinetics of thiamin and thiamin phosphate esters in human blood, plasma and urine after 50 mg intravenously or orally. *Eur J Clin Pharmacol* **44**, 73-78 (1993).

33. O. Jensen *et al.*, Variability and Heritability of Thiamine Pharmacokinetics With Focus on OCT1 Effects on Membrane Transport and Pharmacokinetics in Humans. *Clin Pharmacol Ther* **107**, 628-638 (2020).

34. D. Coats *et al.*, Thiamine pharmacokinetics in Cambodian mothers and their breastfed infants. *Am J Clin Nutr* **98**, 839-844 (2013).

35. L. Chen *et al.*, OCT1 is a high-capacity thiamine transporter that regulates hepatic steatosis and is a target of metformin. *Proc Natl Acad Sci U S A* **111**, 9983-9988 (2014).

36. A. S. Hazell, S. Afadlal, D. A. Cheresh, A. Azar, Treatment of rats with the JAK-2 inhibitor fedratinib does not lead to experimental Wernicke's encephalopathy. *Neurosci Lett* **642**, 163-167 (2017).

37. J. Hood, A. Hazell, Fedratinib Does Not Inhibit Thiamine Uptake or Induce Experimental Wernicke's Encephalopathy in Nonclinical Studies. *Blood* **130**, 4993-4993 (2017).

38. C. N. Harrison *et al.*, Case Series of Potential Wernicke's Encephalopathy in Patients Treated with Fedratinib. *Blood* **130**, 4197-4197 (2017).

39. B. Mandal, N. Hazra, A. Hui, C. R. Maity, Effect of trimethoprim administration on hepatic functions of albino rats. *Acta Physiol Pharmacol Bulg* **10**, 48-58 (1984).

40. B. A. Ference *et al.*, Low-density lipoproteins cause atherosclerotic cardiovascular disease. 1. Evidence from genetic, epidemiologic, and clinical studies. A consensus

statement from the European Atherosclerosis Society Consensus Panel. *Eur Heart J* **38**, 2459-2472 (2017).

41. N. Sarwar *et al.*, Triglycerides and the risk of coronary heart disease: 10,158 incident cases among 262,525 participants in 29 Western prospective studies. *Circulation* **115**, 450-458 (2007).

42. B. G. Talayero, F. M. Sacks, The role of triglycerides in atherosclerosis. *Curr Cardiol Rep* **13**, 544-552 (2011).

43. S. M. Grundy, Cholesterol and coronary heart disease. The 21st century. *Arch Intern Med* **157**, 1177-1184 (1997).

CHAPTER 4

Oxypurinol Pharmacokinetics and Pharmacodynamics in Healthy Volunteers: Influence of BCRP Q141K polymorphism and patient characteristics

4.1 ABSTRACT

Pharmacogenomics is the study of how genetic factors affect drug response. The missense variant, breast cancer resistance protein (BCRP) p.Q141K, which encodes a reduced function BCRP, has been linked to poor response to allopurinol. Using a multi-faceted approach, we aimed to characterize the relationship(s) between BCRP p.Q141K, the pharmacokinetics and pharmacodynamics (PKPD) of oxypurinol (the active metabolite of allopurinol), and serum uric acid (SUA) levels. A prospective clinical study (NCT02956278) was conducted in which healthy volunteers were given a single oral dose of 300 mg allopurinol followed by intensive blood sampling. Data were analyzed using non-compartmental analysis and population PKPD modeling. Additionally, electronic health records were analyzed to investigate whether clinical inhibitors of BCRP phenocopied the effects of the p.Q141K variant with respect to SUA.

---

*Modified from the publication: Vora B and Brackman DJ, Zou L, Garcia-Cremades M, Sirota M, Savic RM and Giacomini KM. (2021) "Oxypurinol Pharmacokinetics and Pharmacodynamics in Healthy Volunteers: Influence of BCRP Q141K polymorphism and patient characteristics." *Clinical and Translational Science*.

Subjects homozygous for p.Q141K had a longer half-life (34.2 ± 12.2 hours vs 19.1 ± 1.42 hours) of oxypurinol. The PKPD model showed that females had a 24.8% lower volume of distribution. Baseline SUA was affected by p.Q141K genotype and renal function; that is, it changed by 48.8% for every 1 mg/dL difference in serum creatinine. Real world data analyses showed that patients prescribed clinical inhibitors of BCRP have higher SUA levels than those that have not been prescribed inhibitors of BCRP, consistent with the idea that BCRP inhibitors phenocopy the effects of p.Q141K on uric acid levels. This study identified important covariates of oxypurinol PKPD that could affect its efficacy for the treatment of gout as well as a potential side effect of BCRP inhibitors on increasing uric acid levels, which has not been described previously.

4.2 Introduction

Gout, an inflammatory arthritis associated with high serum uric acid (SUA) levels, is a painful disease that is associated with comorbidities. Although there are several drugs on the market for the treatment of gout, such as febuxostat, allopurinol is recommended as first line treatment due to its tolerability, safety, and lower cost (*1*). As a xanthine oxidase inhibitor, allopurinol inhibits the formation of uric acid; however, response to the drug is highly variable, with studies showing as few as 21% of patients reaching an acceptable treatment endpoint (*2*). Thus, recognizing features and covariates that affect allopurinol response is vital in determining the right dose, schedule, and patient population.

Many studies have been performed to investigate the relationship between allopurinol and anti-hyperuricemic response. A spectrum of covariates, such as baseline SUA, diuretic use, creatinine clearance, and body weight, have been examined for use in predicting pharmacodynamic (PD) response, but results have been conflicting (*3-5*). Recently, breast cancer resistant protein (BCRP) p.Q141K (rs2231142) has been shown to associate with poor response to allopurinol (i.e. greater than the rheumatologist recommended SUA levels of < 6 mg/dL) (*6-8*).

Both allopurinol and oxypurinol, the active metabolite of allopurinol, are substrates of BCRP, which acts as an efflux pump on the apical membrane of the renal proximal tubule and intestinal epithelia and on the canalicular membrane of hepatocytes (*7*). Allopurinol is rapidly and extensively metabolized to oxypurinol, as reflected by its short half-life (1.2 hours). While the major route of elimination for allopurinol is metabolism to oxypurinol, oxypurinol is eliminated in the urine almost entirely as unchanged drug (*9*). Thus, BCRP can affect the pharmacokinetics of allopurinol and/or oxypurinol by reducing absorption of allopurinol following an oral dose, limiting distribution of allopurinol and oxypurinol, and aiding in the elimination of both. BCRP p.Q141K has been shown to alter the PK and PD of many substrates, such as rosuvastatin, and is typically associated with increased systemic levels and improved pharmacologic response. Thus, it is difficult to understand the mechanisms by which the variant associates with poor response to allopurinol (*10*).

Using a multi-faceted approach, we aimed to characterize the relationship(s) between BCRP p.Q141K, oxypurinol PKPD, and SUA levels. Specifically, we: (1) characterized the PKPD relationship of oxypurinol and SUA; (2) quantified the effects of covariates affecting the PKPD of oxypurinol, including the effects of BCRP p.Q141K; and (3) determined whether clinical inhibitors of BCRP phenocopy the effects of the p.Q141K variant on SUA levels.

4.3 METHODS

4.3.1 Study participants

Healthy human volunteers between 18 and 50 years of age were recruited for this study and 19 subjects were enrolled. All subjects were evaluated to be healthy on the basis of medical history provided by a study questionnaire. Volunteers were excluded if they were taking any medications that are known to interact with uric acid levels, BCRP function, or allopurinol PK. Individuals with elevated liver enzymes (>1.5x normal range), elevated creatinine concentrations (>1.5x normal range), and abnormal platelet and/or white blood cell count levels were also excluded. Individuals carrying the HLA-B*58:01 allele were excluded from this study because of the increased risk for allopurinol-induced Stevens-Johnson syndrome. All participants gave written, informed consent and the study was registered on clinicaltrials.gov (NCT02956278).

4.3.2 Genotyping

BCRP p.Q141K (rs2231142) was genotyped by TaqMan assay (Applied Biosystems, assay ID C__15854163_70, Foster City, CA) in DNA extracted from a cheek swab. The reaction mixture consisted of 5-10 ng DNA, 12.5µL of TaqMan Genotyping Master Mix (Applied Biosystems, Foster City, CA), 1.25µL of TaqMan genotyping assay mix, and 11.25µL of distilled water. The cycling conditions were as follows: 95°C for 10 minutes and 40 cycles of 95°C for 15 seconds then 60°C for 1 minute. The reaction was run on a BioRad MyCycler (Bio-Rad, Hercules, CA) and allele discrimination determined by ABI 7900 Fast HT Sequence Detection Systems (Applied Biosystems, Foster City, CA).

4.3.3 Clinical study design

This study protocol was reviewed and approved by Western Institutional Review Board. Healthy individuals of European or Asian heritage were recruited into this study and informed consent was obtained from each subject. Prior to their enrollment in the study, subjects were screened. The screening included two stages: (1) a questionnaire on health, medications, and self-reported ethnicity as well as a cheek swab to determine BCRP p.Q141K genotype and (2) a blood sample to measure complete blood count (CBC), hepatic function, renal function, uric acid, and HLA-B*58:01 genotype.

Subjects were enrolled under two protocols. The first protocol incorporated a multi-dose design, in which subjects were asked to arrive at the site following an overnight fast. An initial blood sample was taken to establish baseline SUA and serum creatinine before drug was administered. An oral dose of 300 mg of allopurinol was administered to all subjects, followed by blood sampling at: 0.5, 1, 1.5, 2, 3, 4, 5, 6, 8, 10, and 24 hours post-dose. The subjects were then asked to take allopurinol 300 mg once daily and return to the site on Day 6 for their final dose of allopurinol. Blood samples were drawn at 0, 0.5, 1, 1.5, 2, 3, 4, 5, 6, 8, 10, 24, 48, and 72 hours after the final dose.

For the second protocol, subjects were asked to arrive at the site following an overnight fast. An initial blood draw was taken to establish baseline SUA and serum creatinine before drug was administered. A single dose of 300 mg of allopurinol was administered to all subjects, followed by blood sampling at: 0.5, 1, 1.5, 2, 3, 4, 5, 6, 8, 10, 24, 48, and 72 hours post-dose.

Samples collected following a single dose of allopurinol (from both protocols) were used for subsequent analyses.

Serum was isolated from blood samples using clotting and centrifugation and stored at -80°C for analysis of uric acid, creatinine, allopurinol, and oxypurinol concentrations.

4.3.4 Bioanalytical methods

Allopurinol and oxypurinol were analyzed by Quintara Discovery (Hayward, CA) using a validated liquid chromatography tandem mass spectrometry (LC/MS-MS) method. Samples were diluted as needed. An aliquot of 20 μL of serum samples was treated with 200 μL of 25% Methanol 75% acetonitrile containing internal standard (Fulvestrant). The mixture was vortexed on a shaker for 15 minutes and subsequently centrifuged at 4000rpm for 15 minutes. The supernatant was transferred to a microtiter plate for the injection to the LC-MS/MS. Calibration standards and quality control samples were prepared by spiking the test compound into corresponding blank matrix and processed with the unknown samples. The quantification limit was 2 ng/mL for serum.

Uric acid and creatinine levels were analyzed by Open Medicine Institute according to standard spectrophotometry protocol.

4.3.5 Non-compartmental PK analysis

The concentration-time profiles of allopurinol and oxypurinol were plotted using GraphPad Prism 8.4 (GraphPad Software, San Diego, CA). PK parameters of allopurinol and oxypurinol were determined by non-compartmental analysis using the PKNCA package (*11*) in R (version 3.4.0). Values below the limit of quantification were excluded from the analysis.

Data are expressed as mean ± standard error unless otherwise noted. Differences in demographics, clinical characteristics, and PK parameters relative to genotype were analyzed in R using a one-way ANOVA followed by Tukey's post-hoc test for multiple test correction (TukeyHSD). P-values less than 0.05 were considered statistically significant.

4.3.6 Collection of mouse luminal contents

All animal experiments were approved by the University of California, San Francisco (UCSF) IACUC. Experiments were performed using 12-week-old male C57BL/6 mice (Charles River). The method of collection was described previously (*12*) with modifications. In brief, mouse intestine was evenly divided into four segments and opened longitudinally. The contents were gently removed using forceps without scraping the surface and resuspended in 1 mL of solution (50 mM Tris-HCl (pH 7.0), 50 mM Mannitol, 2 mM EGTA, 8 μg/ml Aprotinin, 10 μg/ml Leupeptin, 2mM DTT). Protein concentration was quantified by the BCA assay (Thermo Scientific).

4.3.7 Xanthine oxidase assay

Xanthine oxidase activities in the mouse luminal contents were determined according to the manufacture's protocol (Abcam, ab102522). In brief, in a black wall 96-well plate, 10 μL of sample solution was added in 50 μL of Reaction Mix containing assay buffer, hypoxanthine, and OxiRed probe, with or without oxypurinol (1 mM), an inhibitor of xanthine oxidase. ddH_2O was added to adjust the total volume to 100 μL. 10 mU of xanthine oxidase enzyme was used as the positive control. The plate was incubated at 37°C for 1 hour, protected from light. The fluorescent signal was measured at Ex/Em= 535/590nm.

4.3.8 Population PKPD model

Longitudinal oxypurinol PK and SUA data were linked using the population approach using non-linear mixed effects modeling software NONMEM version 7.3.0 (ICON Development Solutions, Ellicott City, Maryland). The analysis was performed sequentially. First, the PK analysis was performed. In this analysis, F_m was used to represent the fraction of the allopurinol dose systemically available as oxypurinol and K_{fm} denotes the formation rate constant, similar to a previous model for oxypurinol (*13*). Values below the limit of quantification were excluded from the analysis. Nine out of 250 samples were either missing/not collected or below the limit of quantification.

Secondly, an E_{max} model was used to link the predicted individual oxypurinol PK concentration data with the SUA data (PD). Genotype (discrete), gender (discrete), race (discrete), serum creatine (continuous), and weight (continuous) were all assessed as potential covariates for every PKPD parameter in both the PK and PKPD model. Covariate selection was guided by using the stepwise covariate modelling (SCM) approach with the PsN software (version 4.8.1). This method consists of stepwise testing different covariate-parameter relationships with forward inclusion and backward exclusion approaches with significance levels of 0.05 and 0.01, respectively. The inclusion of covariates in the final model was done by considering scientific plausibility, significance, and clinical relevance following stepwise covariate selection.

Model parameters were estimated using first order conditional estimation (FOCE) method with the option for interaction. Between subject variability (BSV) was modeled exponentially and residual variability was modeled using a combination of additive and proportional error. Model selection was based on goodness-of-fit (GOF) plots and the difference in the objective function value (OFV) between nested models. Final models were internally validated through simulation-based diagnostics using visual predictive check plots (VPC) (1000 simulations). The precision of the final parameter estimates was evaluated using 1000 simulated bootstrap datasets using PsN software (*14*).

Model development, diagnostics, and graphing were done using R (version 3.4.0) including packages such as ggplot2 and Xpose (*15*). Percent CV was calculated as follows: sqrt(OMEGA) * 100. The final PKPD model was used to simulate (n = 500) SUA profiles after 30 days of once daily dosing of 300 mg of allopurinol as a post-hoc analysis of covariate effects.

4.3.9 Electronic health record analyses to evaluate uric acid levels in patients prescribed clinical inhibitors of BCRP

To investigate whether drugs that are clinical inhibitors of BCRP can phenocopy the effect of p.Q141K on baseline SUA, we mined the electronic health records (EHRs) at UCSF and identified subjects both on and off BCRP inhibitors with SUA levels in the database. The UCSF Research Data Browser was utilized to search for patients who had a numeric serum/plasma uric acid laboratory test value reported, giving a total of 26,328 patients and 120,570 laboratory values. Values reported as an inequality were changed to a numerical value (i.e. < 0.5 mg/dL = 0.5 mg/dL). Lab values with missing values (i.e. DE-IDENTIFIED) and lab values without a lab collection date were excluded.

Patients were divided into two groups depending on their medication prescriptions. Specifically, patients prescribed cyclosporine and/or eltrombopag, both of which are identified as clinical inhibitors of BCRP by the Food and Drug Administration (https://www.fda.gov/drugs/drug-interactions-labeling/drug-development-and-drug-interactions-table-substrates-inhibitors-and-inducers), were grouped into the "on" drug group. Search terms included: "Cyclosporine", "Sandimmune", "Neoral", "Gengraf", "Eltrombopag", and "Promacta". Only medication orders with an oral route of administration and with a medication order start date were included in the analysis, which resulted in 1,785 patients. The remaining patients (i.e. individuals who were never prescribed cyclosporine or eltrombopag) were grouped into the "off" drug group. Only patients with one uric acid level reported in their electronic health record were included in the "off" drug group, which reduced the sample size to 15,042 individuals. Additionally, for both groups, patients with a prescription to any uric acid lowering medication were excluded from the analysis.

Patients in the “on” drug group were further filtered based on their laboratory collection date relative to their first medication order start date. Serum/plasma uric acid laboratory tests collected before the patient's first medication order start date or within 7 days after their first medication order start date were excluded. A minimum of 7 days between medication order start date and laboratory value collection date was chosen to allow drug levels to reach steady-state and for an effect to be seen. For patients with more than one lab value, only the lab value closest to the first medication order start date was included. In total, 273 patients met these criteria and were in the “on” drug group. Lastly, patients were age- and sex- matched using the MatchIt package (*16*) in R to be comparable in both groups which resulted in a final sample sizes of 273 patients “on” drug and 2,730 patients “off” drug (**Figure 4.4** and **Supplemental Table 4.1**).

In order to address the possibility that underlying disease or drug class contributed to the differences seen in uric acid levels, for the therapeutic class-specific analysis looking at immunosuppressants, patients were further assigned to subgroups. More specifically, patients in the “on cyclosporine” drug group were filtered to only include patients with a prescription to cyclosporine and exclude patients with prescriptions for any other immunosuppressants. Conversely, the “on other immunosuppressants” drug group was filtered to only include patients with at least one prescription for an immunosuppressant, but exclude patients with a prescription to cyclosporine. In addition to the inclusion/exclusion criteria above, patients with prescriptions to eltrombopag were also excluded from both groups. This resulted in 174 patients in the “on cyclosporine" drug group and 3,503 patients in the "on other immunosuppressants" drug group who met the medication order inclusion/exclusion criteria and had at least one serum/plasma uric acid level reported. Patients in both groups were further filtered based on their laboratory collection date relative to their first medication order start date for cyclosporine for the "on cyclosporine" drug group and any other immunosuppressant (except cyclosporine) for the "on other immunosuppressants" drug group, respectively. The rest of the analysis was performed as described for the "on" drug group above; after age- and sex- matching the groups, we had 119 patients in the "on cyclosporine" drug group and 833 patients in the "on other immunosuppressants" drug group (**Figure 4.4** and **Supplemental Table 4.1**).

Wilcoxon rank sum test with continuity correction was performed to evaluate if there was a significant difference in laboratory values when comparing both groups and ggplot2 was used to plot the data in R (version 3.4.0).

4.4 RESULTS

4.4.1 Study cohort

Healthy volunteers of European or Asian ancestry were screened for participation in this study. These ethnicities were chosen due to the high minor allele frequencies of BCRP p.Q141K in individuals of Asian (29%) and European (9%) ancestries (*17*). Of the 178 subjects screened, 19 completed the study and allopurinol was well tolerated. Most subjects were excluded based on *ABCG2* genotype, some were excluded based on HLA-B*58:01 genotype and concomitant medications. Demographics of the study subjects by genotype can be found in **Table 4.1**. There was a significant difference in serum creatinine (SCr) concentrations between the homozygous reference (CC) and heterozygous (CA) groups (adjusted p-value: 2.99×10^{-7}) and homozygous reference (CC) and homozygous variant (AA) groups (adjusted p-value: 1.19×10^{-6}). Additionally, baseline SUA was significantly different between the homozygous reference (CC) and heterozygous (CA) groups (adjusted p-value: 5×10^{-4}). If we exclude females from this comparison given the higher ratio of females to males in the CC group compared with the other groups (CA and AA), we continue to see a significant difference in serum creatinine (SCr) concentrations between the CC and CA groups (adjusted p-value: 0.00338) and CC and AA groups (adjusted p-value: 1.73×10^{-5}) as well as a slight difference between the CA and AA groups (adjusted p-value: 0.0474). In addition, excluding females from the analysis results in a greater significant difference in baseline SUA among the various genotype groups: CC and CA (adjusted p-value: 5.29×10^{-13}), CC and AA (adjusted p-value: 0.00176), and CA and AA (adjusted p-value: 0.0163).

4.4.2 BCRP p.Q141K associates with a longer half-life of oxypurinol and the concentration-time profile of oxypurinol demonstrates enterohepatic recycling

Plasma concentration-time profiles and the non-compartmental PK parameters were similar for allopurinol regardless of genotype (**Table 4.2** and **Figure 4.1**). Oxypurinol half-life was significantly longer in patients homozygous for the p.Q141K variant compared to patients homozygous for the reference allele when using a one-way ANOVA followed by Tukey's post-hoc test for multiple test correction (34.2 ± 12.2 hours vs 19.1 ± 1.42 hours, adjusted p-value: 0.047) (**Table 4.2** and **Figure 4.1**). However, BCRP p.Q141K genotype had no statistically significant effect on any other PK parameter such as maximum concentration achieved (C_{max}), area under the curve (AUC), and time to maximum concentration (T_{max}) (**Table 4.2**).

Additionally, multiple peaks were observed in the individual concentration-time profiles of oxypurinol, suggesting that enterohepatic recycling may be occurring (**Supplemental Figure 4.1**). Experimental studies showed that xanthine oxidase activity is present in mouse intestinal lumen (**Supplemental Figure 4.2**), suggesting that the intestinal lumen is a potential site of action for oxypurinol.

4.4.3 PKPD covariate model shows a significant effect of gender on oxypurinol volume of distribution and genotype and SCr on baseline SUA

A one compartment PK model with first order absorption was found to best fit the oxypurinol concentration-time data. Parameter and BSV estimates (noted in parentheses) for clearance (CL/F_m), volume of distribution (V/F_m), and the formation rate constant (K_{fm}) were 1.74 L/hr (23.6%), 57.0 L (18.7%), and 0.771 hr^{-1}(55.2%) respectively (**Table 4.3**). In the PKPD model, BSV was estimated for baseline SUA (13.3%). The rest of parameter estimates can be found in **Table 4.3**.

Gender, genotype, race, serum creatinine, and weight were tested for their effects on the PK parameters of oxypurinol as well as the effects of oxypurinol on SUA. The final PKPD model included gender as a significant covariate on apparent volume of distribution. BCRP p.Q141K genotype and SCr were also included as significant covariates for baseline SUA (**Table 4.3**). Females had a 24.8% lower V/F_m compared to males. Baseline SUA changed by 48.8% for every

1 mg/dL difference in SCr. Additionally, baseline SUA increased by 35.4% and 24.4% for the genotypes of CA or AA, respectively, as compared to reference BCRP p.Q141K (CC). Based on the results from our non-compartmental analysis where half-life was significantly longer in patients homozygous for the BCRP p.Q141K variant, we were interested in exploring the effect of genotype on clearance and volume of distribution. In our model, apparent clearance also appeared to correlate with genotype; however, it was not significant and thus BCRP p.Q141K genotype was not included as a covariate for clearance nor volume of distribution in the final model. Visual predictive checks and goodness of fit plots confirmed that the final PKPD model adequately described the observed data (**Figure 4.2**, **Supplemental Figure 4.3**, and **Supplemental Figure 4.4**).

Simulations were performed to visualize the role of genotype and SCr on the pharmacodynamic effects of oxypurinol after 30 days of once daily dosing of 300 mg of allopurinol. Simulations confirmed that individuals who have at least one variant allele or SCr levels > 0.78 mg/dL (the average SCr value in our dataset) have 1) higher baseline SUA levels on average and 2) are less likely to achieve and maintain the target concentration of < 6 mg/dL given a flat dose of allopurinol (**Figure 4.3**).

4.4.4 Electronic health record analyses show clinical inhibitors of BCRP can phenocopy the p.Q141K variant

To investigate whether drugs that are clinical inhibitors of BCRP can phenocopy the effect of p.Q141K on baseline SUA, we mined the electronic health records (EHRs) at UCSF and identified subjects both on and off BCRP inhibitors with SUA levels in the database.

Specifically, we compared uric acid levels in patients prescribed cyclosporine and/or eltrombopag, both of which are identified as clinical inhibitors of BCRP by the Food and Drug Administration (https://www.fda.gov/drugs/drug-interactions-labeling/drug-development-and-drug-interactions-table-substrates-inhibitors-and-inducers), to uric acid levels in patients not prescribed either of those drugs. Based on the inclusion and exclusion criteria described in the methods, we were able to classify patients as "on" drug (i.e., prescribed cyclosporine and/or eltrombopag) or "off" drug (**Figure 4.4**).

A significant difference in uric acid levels was observed between the two groups (p-value: 1.74×10^{-6}; n = 273 "on" drug, n = 2730 "off" drug), with patients prescribed at least one clinical inhibitor of BCRP having higher levels compared to age- and sex-matched patients not prescribed either (5.95 mg/dL vs 5.36 mg/dL) (**Figure 4.4**). To test the sensitivity of this analysis and selection of controls, 10 iterations were performed of randomly selected 273 age- and sex-matched patients from the "off" drug group to allow for a 1:1 ratio between the "on" drug and "off" drug groups; the "on" drug group had significantly higher uric acid levels compared to the "off" drug group in every iteration tested (**Supplemental Figure 4.5**). Additional analyses with a maximum separation date of one year between the first medication order start date and lab collection date still showed a significant difference (p-value = 0.00074) in uric acid levels between the "on" drug (n = 199) and "off" drug (n = 1990) groups, further demonstrating the robustness of our analysis.

In order to address the possibility that underlying disease or drug class contributed to the differences seen in uric acid levels, additional analyses were performed within the class of immunosuppressants. Uric acid levels in patients prescribed cyclosporine were compared to those prescribed other immunosuppressants (**Figure 4.4**). Individuals prescribed cyclosporine (and no other immunosuppressants) had significantly higher uric acid levels (p-value: 0.00462; n = 119 “on cyclosporine”, n = 833 “on other immunosuppressants”) compared to age- and sex-matched individuals prescribed other immunosuppressants (5.98 mg/dL vs 5.58 mg/dL) (**Figure 4.4**).

4.5 Discussion

BCRP p.Q141K has the potential to affect the pharmacokinetics and pharmacodynamics of many drugs by reducing efflux and increasing systemic levels. However, interestingly, p.Q141K has been associated with poor response to allopurinol in two GWAS (*6*, *7*) and in candidate gene studies (*8, 18*). The current study provides the first investigation into the relationship between 1) BCRP p.Q141K and allopurinol/oxypurinol PKPD in a prospective clinical trial and 2) BCRP inhibition and uric acid levels using real world data.

This study resulted in three major findings. First, we found that p.Q141K associated with a longer half-life of oxypurinol. Second, we showed that gender was a significant covariate for oxypurinol volume of distribution and higher baseline SUA levels caused by factors such as BCRP genotype and kidney function may lead to inadequate response to allopurinol. Finally, we found that clinical inhibitors of BCRP (cyclosporine and eltrombopag) associated with increased SUA levels, suggesting the potential of these drugs to cause hyperuricemia and increased risk for gout in susceptible patient populations.

One of our major findings was that the half-life of oxypurinol was significantly longer in subjects who were homozygous for the reduced function variant compared to those who were homozygous for the reference allele of BCRP. Since half-life is dependent on CL and V, this effect may have been driven by slight (albeit not significant) decreases in CL/F and increases in V/F in individuals homozygous for the variant allele compared to those homozygous for the reference allele (**Table 4.2**). CL of oxypurinol is determined to a large extent by kidney function. Data from BioBank Japan suggest that the reduced function allele, p.Q141K, associates with reduced kidney function (lower eGFR and thus increased serum creatinine levels) in Asian subjects (*19*), consistent with a trend towards reduced CL in the individuals homozygous for p.Q141K, which was observed in both our non-compartmental analysis and PK model. The slight increases in V/F in individuals homozygous for the variant allele may reflect increased distribution of oxypurinol into tissues in which BCRP is expressed (e.g., intestine, colon, liver, kidney, brain, and thyroid (*20*)), consistent with a reduced ability of the variant transporter to protect these tissues. Despite this finding, the overall exposure and C_{max} of oxypurinol remained similar between genotype groups (**Table 4.2**). Further, the finding that oxypurinol half-life is increased with BCRP genotype may be confounded by the limited sampling time in some subjects (24 hours) compared to the oxypurinol half-life; however, the trend remains when excluding these subjects.

To our knowledge, no other study has demonstrated enterohepatic recycling of oxypurinol and these findings need to be confirmed in additional PK studies. Preliminary studies identified xanthine oxidase activity in the contents obtained from the mouse intestinal lumen

(**Supplemental Figure 4.2**). This result is consistent with a previous electron microscopic study showing the presence of the enzyme in the mucous of the duodenum (*21*) and reports suggesting that the enzyme may be secreted into the intestinal lumen (*22*, *23*) or be expressed and secreted by gut microbiota (*24*). Though speculative, intestinal lumen xanthine oxidase may be a target of oxypurinol, and enterohepatic recycling of oxypurinol may contribute to its overall pharmacological effects on reducing SUA. An intestinal lumen target for oxypurinol is consistent with GWAS results suggesting that individuals who harbor the reduced function variant of BCRP (who would have less enterohepatic recycling) have a poorer response to the drug (*6*-*8*).

Employing EHRs as real world evidence, clinical inhibitors of BCRP associated with increased SUA levels, demonstrating that prescription drug inhibitors of BCRP may phenocopy the BCRP p.Q141K variant. Our therapeutic-class analysis suggested that these observations were a result of inhibition of BCRP and not due to a drug class or underlying disease effect. The list of drugs used in the "on other immunosuppressants" drug group were: azathioprine, mycophenolic acid, mycophenolate mofetil, tacrolimus, and sirolimus, and the literature suggests that none of these drugs appear to interact with BCRP at clinically relevant concentrations; however, limited to no information was found about clinical inhibition of BCRP by mycophenolate mofetil, mycophenolic acid, and azathioprine or its metabolite, 6-mercaptopurine (*25*-*27*).

Simulations after 300 mg once daily dosing of allopurinol showed that subjects with higher baseline SUA due to BCRP p.Q141K genotype or SCr levels were less likely to maintain healthy (< 6 mg/dL) uric acid levels. Baseline SUA is an important determinant of allopurinol response, as shown in previous studies (*28*-*31*). The results of this current study suggest that concomitant

BCRP inhibitors may also contribute to increases in SUA levels and may contribute to hyperuricemia, and therefore allopurinol response. Subjects with higher baseline SUA for any reason may require higher doses of allopurinol to achieve and maintain healthy uric acid levels. However, effect sizes observed in these simulations are based on a small sample size and need to be further investigated and validated.

There are a number of limitations to this study. First, allopurinol was dosed orally, as allopurinol for IV injection is only indicated for prevention of tumor lysis syndrome (*32*). Oral dosing limited our ability to precisely detect effects of BCRP p.Q141K on bioavailability, and therefore on clearance and volume of distribution of the drug. Additionally, sample size of this trial was small, which was powered to detect large differences in oxypurinol clearance. Thus, there may be differences in oxypurinol PK parameters among genotype groups that went undetected in our study. Similarly, our model was limited due to the small sample size and study design; a larger study with a multiple dose regimen in patients diagnosed with gout is needed to better compare genotype groups, identify significant covariates, capture the multiple peaks in the concentration-time profile, and improve our simulations. Although we attempted to include enterohepatic circulation in the model by evaluating different previously published modeling approaches (*33*), this addition was not significant in terms of objective function and did not adequately capture the multiple peaks, most likely due to the limited data and large variation observed. Finally, our EHR analysis was limited by lack of data on the BCRP genotype of the patients, the indication for which the patients were prescribed the respective medications, and how long they were on each medication. As more EHR data becomes available for research purposes, we will be able to account for these variables and covariates, increase the sample size and robustness of our analysis, and potentially perform a joint GWAS and EHR analysis in the future.

The renewed interest in the treatment of gout stems from its growing prevalence and associated morbidities. Allopurinol remains the first-line treatment, but recent GWAS have indicated that subjects harboring the BCRP p.Q141K variant may not respond as well to allopurinol (*6*-*8*). Overall, our comprehensive study was able to identify covariates important in the PK and PD of oxypurinol and use real world data to phenocopy the p.Q141K variant using clinical inhibitors of BCRP. Additionally, this study provides evidence that individuals who harbor the reduced function variant of BCRP may have lower levels of oxypurinol in their intestine. If further studies show the intestine to be an important site of action for oxypurinol, this could help explain the poor response seen in these individuals, despite the similar systemic exposure of oxypurinol. This study highlights how genetic variants can influence the pharmacodynamics of a drug through transporter-mediated drug-variant interactions.

4.6 FIGURES

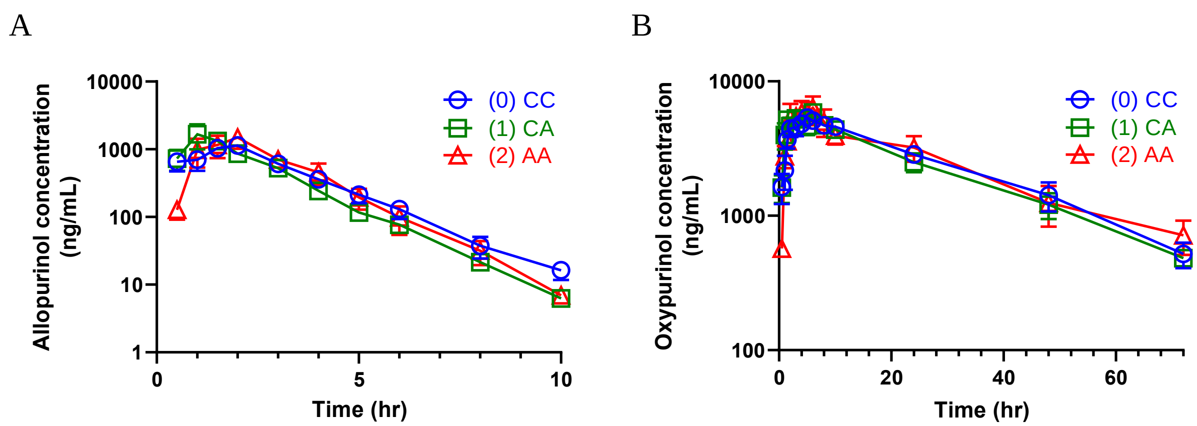

Figure 4.1 Concentration time profiles for (A) allopurinol and (B) oxypurinol after a single dose of allopurinol to healthy volunteers. Allopurinol and oxypurinol concentrations were determined following a 300 mg single oral dose of allopurinol. (0) CC, homozygous reference; (1) CA, heterozygous; (2) AA, homozygous variant. Data represent the mean ± standard error from 19 individuals of various genotypes (see **Table 4.1**); note that data were missing or below the limit of quantification at several timepoints so not all mean ± standard error are representative of all (n = 19) subjects. No error bars are present if the standard error is encompassed within the point.

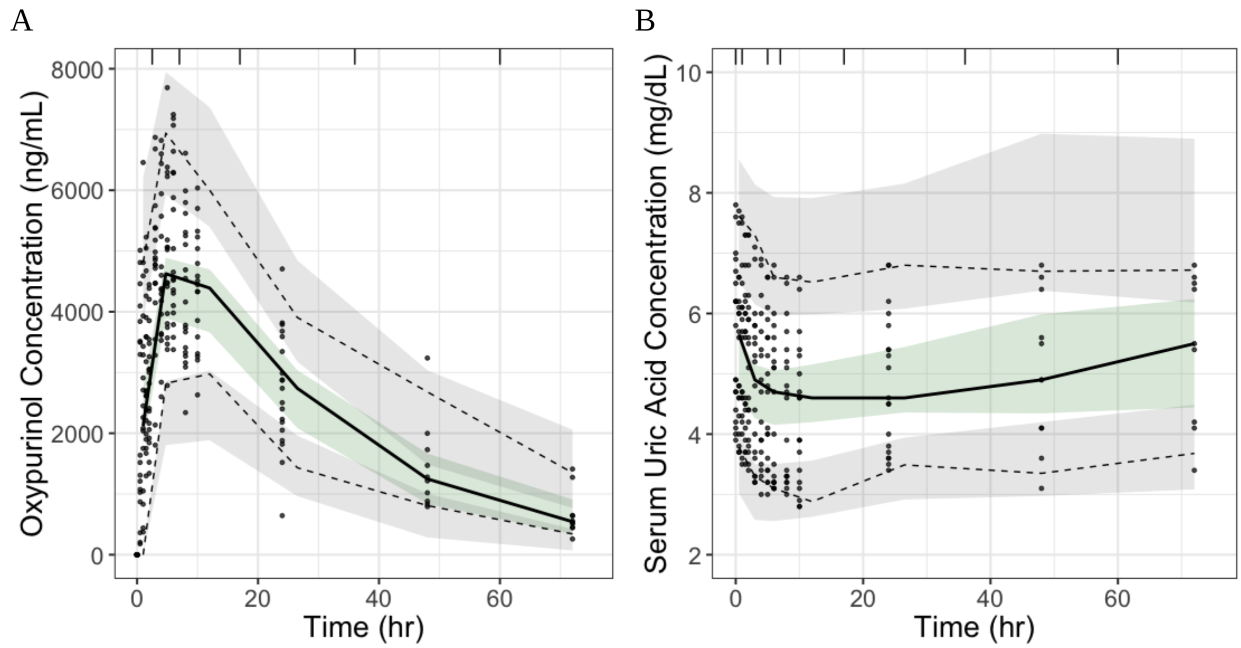

Figure 4.2 Evaluation of oxypurinol PK and PKPD models through visual predictive checks. PK and PKPD model evaluation of oxypurinol concentrations and serum uric acid concentrations after single dose administration of allopurinol. Visual predictive checks show the observed data (grey dots), the median (solid line) and 5th and 95th percentiles (dashed lines) of the observed data, and the 95% confidence intervals of the model simulated data (shaded areas) for (A) plasma oxypurinol concentrations and (B) serum uric acid concentrations.

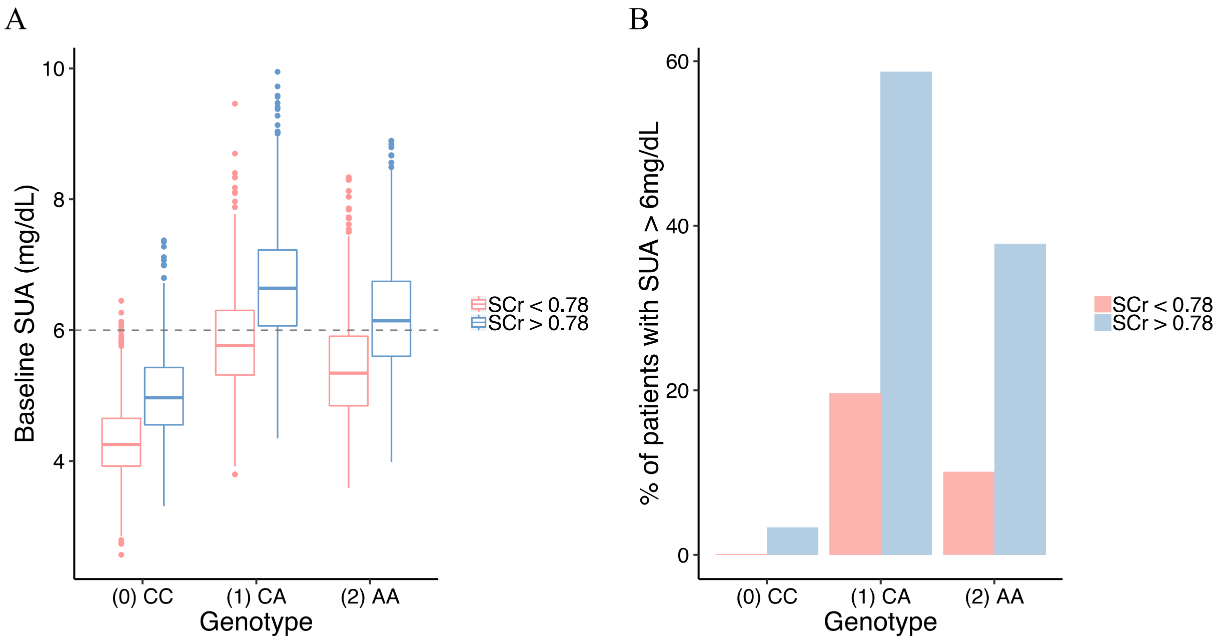

Figure 4.3 Simulated plasma concentrations of serum uric acid (SUA) at (A) baseline and (B) following allopurinol administration. Model predicted (A) baseline serum uric acid concentrations and (B) percentage of patients with SUA levels greater than 6 mg/dL on Day 31 after 30 days of once daily dosing of 300 mg of allopurinol stratified by serum creatinine and genotype. Simulations were run using 1000 patients per genotype + SCr group (total n = 6000). Percentages reported were calculated for each of the six genotype + SCr groups.

A

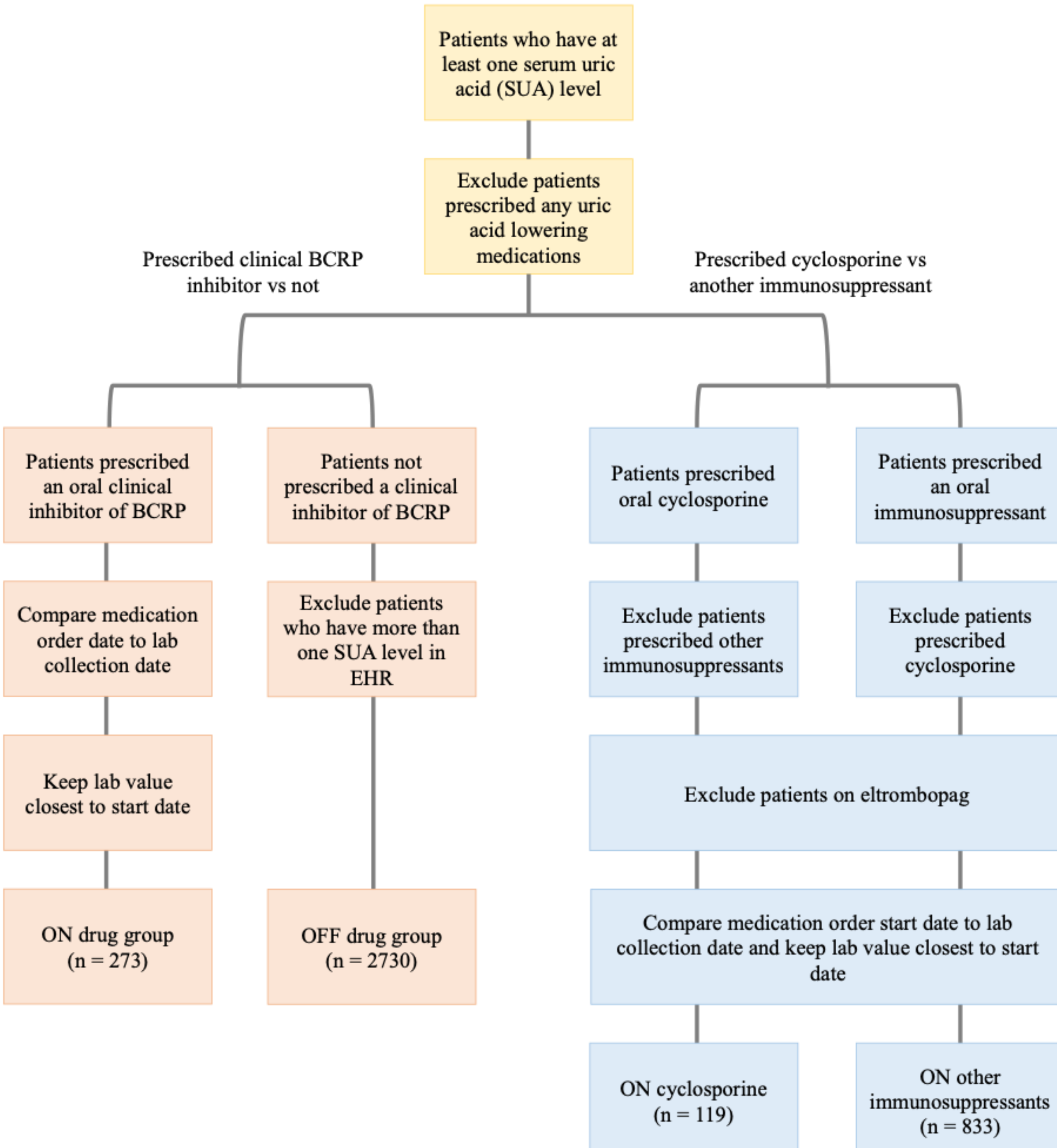
Patients who have at least one serum uric acid (SUA) level
Exclude patients prescribed any uric acid lowering medications
Prescribed clinical BCRP inhibitor vs not
Prescribed cyclosporine vs another immunosuppressant
Patients prescribed an oral clinical inhibitor of BCRP
Patients not prescribed a clinical inhibitor of BCRP
Patients prescribed oral cyclosporine
Patients prescribed an oral immunosuppressant
Compare medication order date to lab collection date
Exclude patients who have more than one SUA level in EHR
Exclude patients prescribed other immunosuppressants
Exclude patients prescribed cyclosporine
Keep lab value closest to start date
Exclude patients on eltrombopag
ON drug group (n = 273)
OFF drug group (n = 2730)
Compare medication order start date to lab collection date and keep lab value closest to start date
ON cyclosporine (n = 119)
ON other immunosuppressants (n = 833)

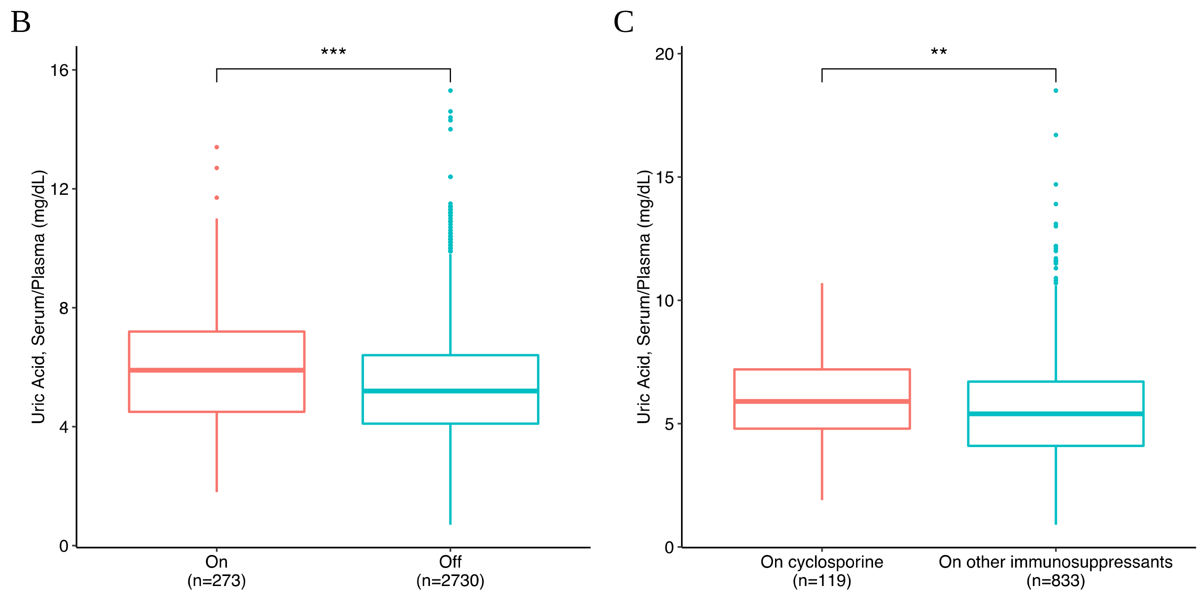

Figure 4.4 Uric acid levels in patients prescribed at least one clinical inhibitor of BCRP compared with levels in patients not prescribed a clinical inhibitor of BCRP from electronic health record data. (A) Flow chart describing the inclusion/exclusion criteria for the analyses and (B) boxplots comparing uric acid laboratory values in patients prescribed cyclosporine and/or eltrombopag versus patients not prescribed cyclosporine and/or eltrombopag (p-value: 1.74×10^{-6}) and (C) patients prescribed cyclosporine (and no other immunosuppressant) versus patients prescribed other immunosuppressants (except cyclosporine) (p-value: 0.00462).

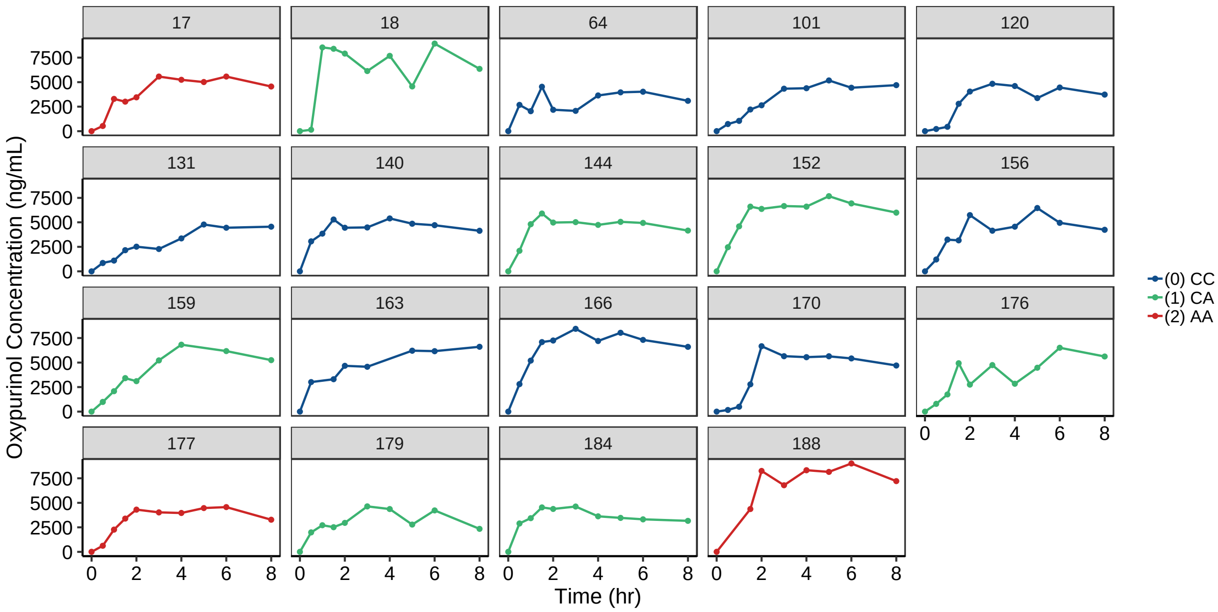

Supplemental Figure 4.1 Individual concentration-time profiles for oxypurinol up to 8 hours post-dose after a 300mg single dose of allopurinol in 19 healthy volunteers. The numbers at the top of each plot are the subject identification number.

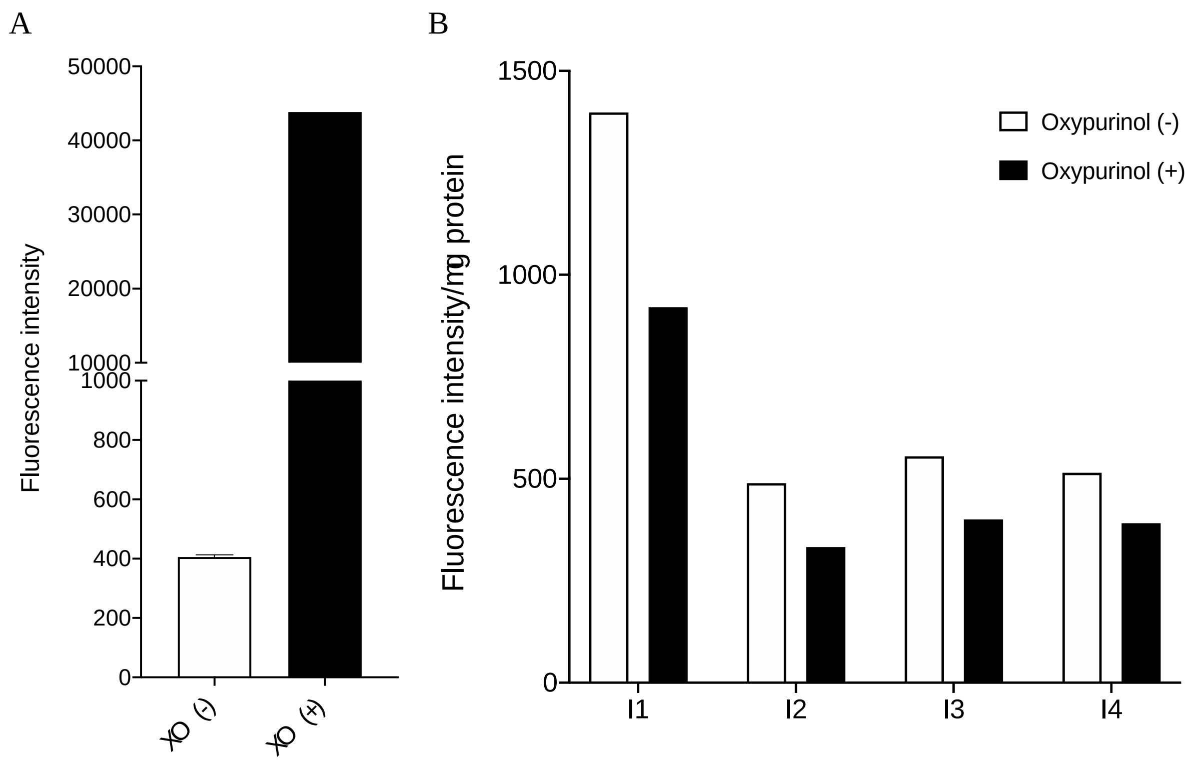

Supplemental Figure 4.2 Xanthine oxidase activity in mouse intestinal contents. (A) Xanthine oxidase activity in reaction buffer (white bar) and a reaction mix with 10 mU of xanthine oxidase (black bar). (B) Fluorescence signal generated by intestinal contents obtained from different segments of the intestine without (white bar) or with (black bar) 1 mM oxypurinol. The fluorescence intensity is normalized by the amount of protein added in reaction mixture. The difference between the white bar and the black bar represents the xanthine oxidase activity.

A

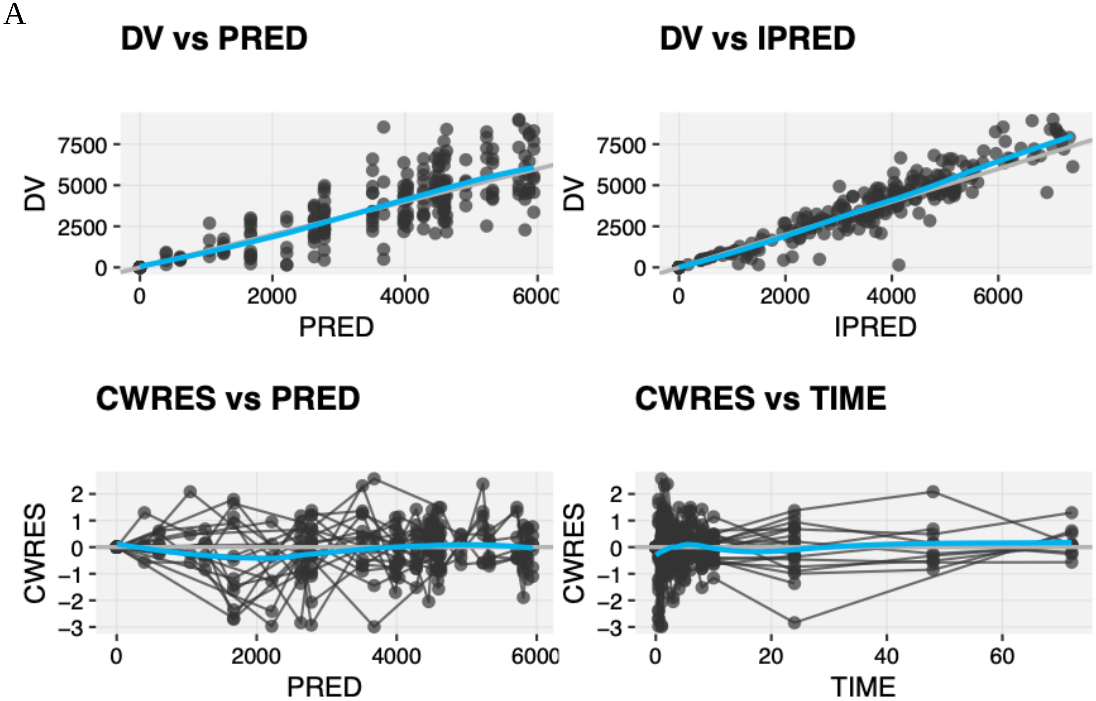

B

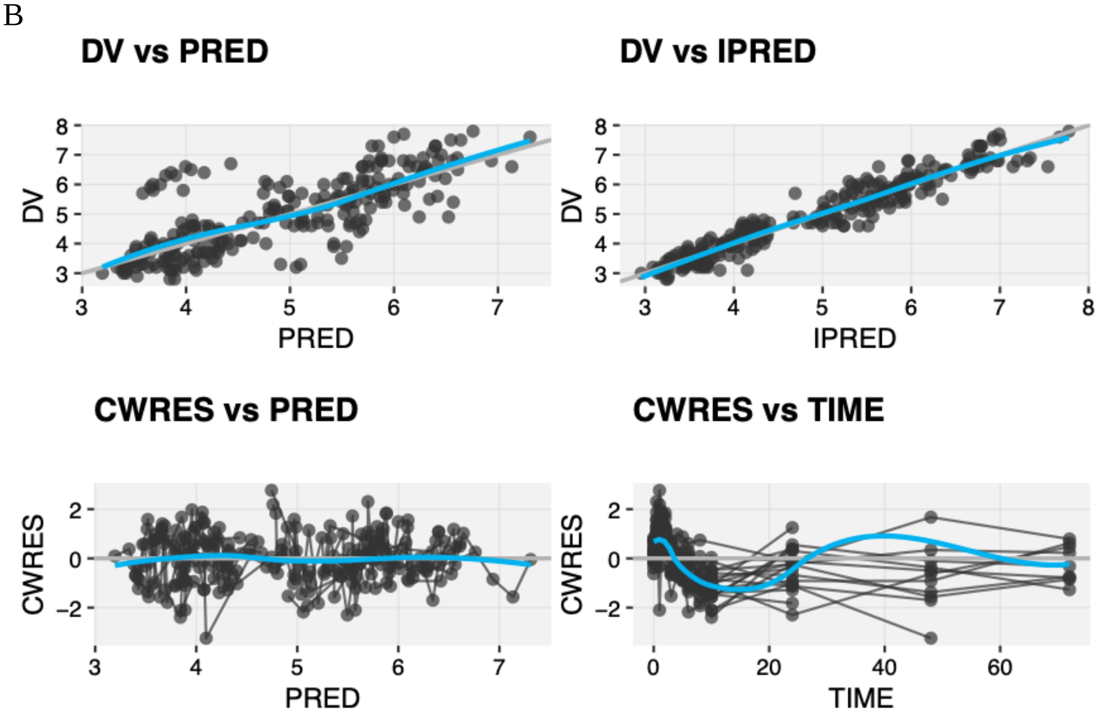

Supplemental Figure 4.3 Goodness of Fit (GoF) plots for (A) oxypurinol PK and (B) serum uric acid levels. DV, observed concentration; PRED, predicted concentration; IPRED, individual predicted concentration; CWRES, conditional weighted residuals.

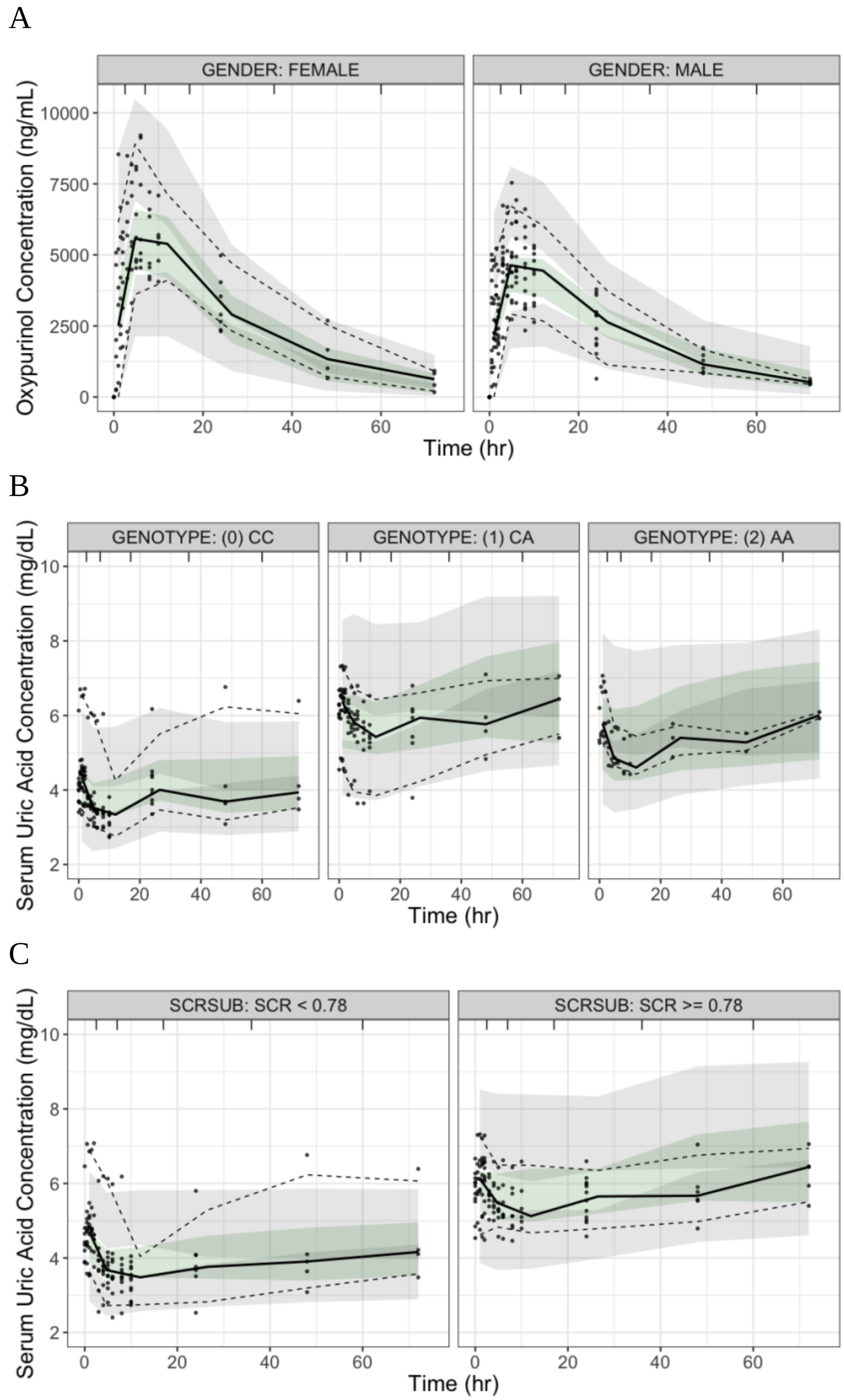

Supplemental Figure 4.4 Visual predictive checks (VPCs). VPCs show the observed data (grey dots), the median (solid line) and 5th and 95th percentiles (dashed lines) of the observed data and the 95% confidence intervals of the model simulated data (shaded areas) for plasma oxypurinol concentrations stratified by (A) gender and serum uric acid concentration stratified by (B) genotype and (C) serum creatinine.

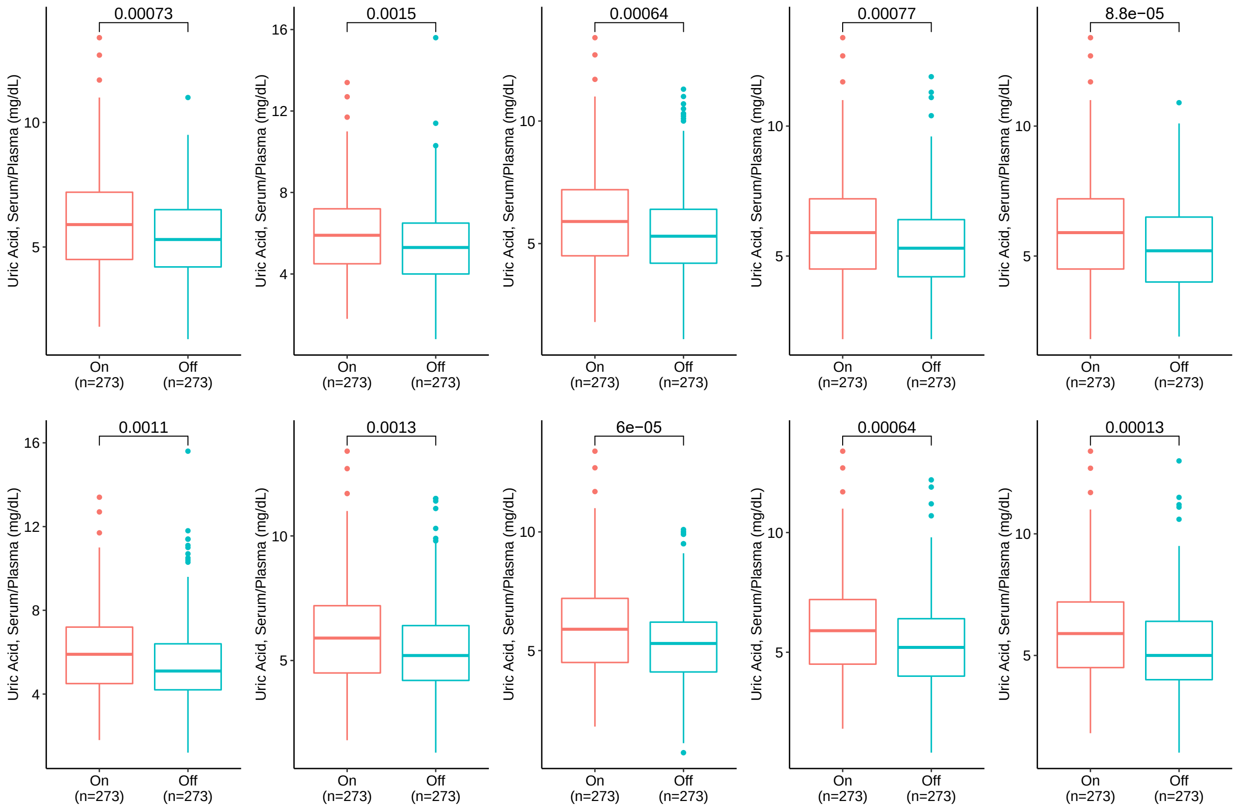

Supplemental Figure 4.5 Sensitivity analysis comparing patients prescribed at least one clinical inhibitor of BCRP vs patients not prescribed a clinical inhibitor of BCRP at a 1:1 ratio. Ten iterations of sampling the "off" drug group at a 1:1 ratio showed that the "on" drug group had significantly higher serum/plasma uric acid levels in each of the ten iterations.

4.7 TABLES

Table 4.1 Demographics and clinical characteristics of study cohort.

	Genotype		
Demographics & Clinical Characteristics	(0) CC	(1) CA	(2) AA
Number of patients (#)	9	7	3
Male/Female (#)	4/5	6/1	2/1
Weight (kg)	71.5 ± 6.25	69.9 ± 7.31	73.4 ± 4.54
Male (kg)	72.3 ± 8.89	71.7 ± 8.37	73.8 ± 7.82
Female (kg)	70.9 ± 9.63	59.0	72.6
Race			
East Asian (#)	4	5	1
South Asian (#)	2	1	0
Filipino (#)	0	1	1
European (#)	1	0	0
Mixed (#)	2	0	1
Serum creatinine (mg/dL)	0.716 ± 0.010	0.819 ± 0.016*	0.844 ± 0.023*
Baseline serum uric acid (mg/dL)	4.62 ± 0.284	6.70 ± 0.368**	6.07 ± 0.133

Weight, serum creatinine, and baseline serum uric acid are reported as average ± standard error. All statistical tests were done using one-way ANOVA followed by Tukey's post-hoc test for multiple test correction. *Serum creatinine was significantly different between (0) CC and (1) CA (adjusted p-value: 2.99×10^{-7}) and between (0) CC and (2) AA (adjusted p-value: 1.19×10^{-6}). **Baseline serum uric acid was significantly different between (0) CC and (1) CA (adjusted p-value: 5×10^{-4}). (0) CC, homozygous reference; (1) CA, heterozygous; (2) AA, homozygous variant.

Table 4.2 Summary of the effect of the BCRP p.Q141K variant allele on the pharmacokinetic parameters of allopurinol and oxypurinol computed by non-compartmental analysis.

Parameter	(0) CC	(1) CA	(2) AA
Number of patients (#)	9	7	3
Allopurinol			
C_{max} (ng/mL)	1370 ± 130	1930 ± 617	1550 ± 453
T_{max} (hr)	1.5 (0.5 - 2)	1 (0.5 - 2)	2 (1 - 2)
AUC_{0-10} (μg*hr/mL)[a]	3.78 ± 0.346	3.47 ± 0.549	2.76 ± 0.637
CL/F (L/hr)	94.5 ± 9.73	97.8 ± 12.5	92.8 ± 26.6
V/F (L)	149 ± 17.0	160 ± 22.3	148 ± 40.9
$t_{1/2}$ (hr)	1.10 ± 0.060	1.14 ± 0.078	1.11 ± 0.025
Oxypurinol			
C_{max} (ng/mL)	5930 ± 409	6440 ± 592	6380 ± 1350
T_{max} (hr)	4 (1.5 - 10)	4 (1.5 - 6)	6 (3 - 6)
AUC_{0-24} (μg*hr/mL)	93.9 ± 8.07	93.4 ± 9.99	105 ± 20.6
CL/F (L/hr)[b]	1.89 ± 0.227	1.81 ± 0.276	1.38 ± 0.466
V/F (L)[b]	49.9 ± 4.53	61.9 ± 9.58	56.6 ± 11.6
$t_{1/2}$ (hr)[b]	19.1 ± 1.42	23.9 ± 1.35	34.2 ± 12.2*

All data are reported as mean ± standard error except for T_{max} which is reported as median (range). *Half-life was significantly longer in the homozygous variant group compared to the homozygous reference group when using an ANOVA comparison followed by Tukey's post-hoc test for multiple test correction (adjusted p-value: 0.047). [a] n = 16 for AUC_{0-10} since three subjects had concentrations below the limit of quantification at t = 10 hours. [b] n = 18 since terminal half-life could not be accurately estimated for one subject. (0) CC, homozygous reference; (1) CA, heterozygous; (2) AA, homozygous variant; C_{max}, maximum plasma concentration; T_{max}, time to maximum concentration; AUC_{0-10}, area under the concentration-time curve from t = 0 hours to t = 10 hours; CL/F, apparent clearance; V/F, apparent volume of distribution; $t_{1/2}$, half-life; AUC_{0-24}, area under the concentration-time curve from t = 0 hours to t = 24 hours.

Table 4.3 Parameter estimates in the final oxypurinol PKPD covariate model.

Parameter	Estimate (%RSE) [95% CI]	BSV (%RSE) [95% CI]
PK model		
K_{fm} (1/hr)	0.771 (17.8) [0.535, 1.06]	55.2% (38.1) [29.0, 69.6]
CL/F_m (L/hr)	1.74 (7.18) [1.51, 2.00]	23.6% (41.5) [9.61, 29.5]
V/F_m (L) = θ_{V/F_m} x (1 + θ_{gender})	θ_{V/F_m} = 57.0 (8.05) [48.1, 65.6]	18.7% (41.7) [7.53, 22.9]
	$\theta_{gender\ (male)}$ = 0	-
	$\theta_{gender\ (female)}$ = -0.248 (35.7) [-0.395, -0.067]	-
PKPD model		
E_{max}	1	-
C_{50} (ng/mL)	2590 (11.6) [2170, 3330]	-
Baseline SUA (mg/dL) = $\theta_{Baseline\ SUA}$ x (1 + $\theta_{genotype}$) x (1 + θ_{SCR} x (SCr – 0.78))	$\theta_{Baseline\ SUA}$ = 4.61 (5.64) [4.19, 5.23]	13.3% (61.4) [4.07, 18.6]
	$\theta_{genotype\ (CC)}$ = 0	-
	$\theta_{genotype\ (CA)}$ = 0.354 (29.3) [0.139, 0.543]	-
	$\theta_{genotype\ (AA)}$ = 0.244 (40.4) [0.047, 0.452]	-
	θ_{SCR} = 0.488 (24.6) [0.246, 0.717]	-
Residual variability		
Proportional error for PK (%CV)	25.4 (11.1) [19.6, 30.7]	-
Proportional error for PD (%CV)	7.67 (5.54) [6.81, 8.45]	-

BSV is reported as percent coefficient of variation (%CV). CL/F_m, apparent clearance of oxypurinol; V/F_m, apparent volume of distribution; K_{fm}, formation rate constant; BSV, between subject variability; E_{max}, maximum effect; C_{50}, concentration needed to achieve 50% effect; SUA, serum uric acid; SCr, serum creatinine; F_m refers to the fraction of the allopurinol dose which can be converted into oxypurinol. The additive part of the combined residual error model was fixed to 0 mg/dL (PD model) and to 0.01 ng/mL (PK model). Residual standard errors (%RSE) and 95% confidence intervals (95% CI) and were obtained from the bootstrap analyses.

Supplemental Table 4.1 Demographics for on and off groups used in EHR analysis.

	On drug	Off drug	p-value
Prescribed a clinical inhibitor of BCRP vs not			
% Male	58.6	58.6	1.0
Average age	42.4	42.4	0.999
Prescribed a clinical inhibitor of BCRP vs not (cut-off of 365 days)			
% Male	57.3	57.3	1.0
Average age	41.3	41.3	1.0
	On cyclosporine	**On other immunosuppressants**	**p-value**
Prescribed cyclosporine vs other immunosuppressants			
% Male	55.5	51.9	0.524
Average age	39.4	41.7	0.222

Percent male and average age were computed for each group.

4.8 References

1. J. D. FitzGerald *et al.*, 2020 American College of Rheumatology Guideline for the Management of Gout. *Arthritis Rheumatol* **72**, 879-895 (2020).
2. M. A. Becker *et al.*, Febuxostat Compared with Allopurinol in Patients with Hyperuricemia and Gout. *New England Journal of Medicine* **353**, 2450-2461 (2005).
3. D. F. Wright *et al.*, Predicting allopurinol response in patients with gout. *Br J Clin Pharmacol* **81**, 277-289 (2016).
4. N. Dalbeth, S. Kumar, L. Stamp, P. Gow, Dose adjustment of allopurinol according to creatinine clearance does not provide adequate control of hyperuricemia in patients with gout. *J Rheumatol* **33**, 1646-1650 (2006).
5. D. R. W. Kannangara *et al.*, Individualising the dose of allopurinol in patients with gout. *Br J Clin Pharmacol* **83**, 2015-2026 (2017).
6. D. J. Brackman *et al.*, Genome-Wide Association and Functional Studies Reveal Novel Pharmacological Mechanisms for Allopurinol. *Clin Pharmacol Ther* **106**, 623-631 (2019).
7. C. C. Wen *et al.*, Genome-wide association study identifies ABCG2 (BCRP) as an allopurinol transporter and a determinant of drug response. *Clin Pharmacol Ther* **97**, 518-525 (2015).
8. M. C. Wallace *et al.*, Association between ABCG2 rs2231142 and poor response to allopurinol: replication and meta-analysis. *Rheumatology (Oxford)* **57**, 656-660 (2018).
9. R. O. Day *et al.*, Clinical pharmacokinetics and pharmacodynamics of allopurinol and oxypurinol. *Clin Pharmacokinet* **46**, 623-644 (2007).

10. D. J. Brackman, K. M. Giacomini, Reverse Translational Research of ABCG2 (BCRP) in Human Disease and Drug Response. *Clin Pharmacol Ther* **103**, 233-242 (2018).

11. W. Denney, S. Duvvuri, C. Buckeridge, Simple, Automatic Noncompartmental Analysis: The PKNCA Package. *Journal of Pharmacokinetics and Pharmacodynamics* **42**, 11-107 (2015).

12. H. Li *et al.*, The outer mucus layer hosts a distinct intestinal microbial niche. *Nat Commun* **6**, 8292 (2015).

13. S. L. Stocker *et al.*, The pharmacokinetics of oxypurinol in people with gout. *Br J Clin Pharmacol* **74**, 477-489 (2012).

14. L. Lindbom, P. Pihlgren, E. N. Jonsson, N. Jonsson, PsN-Toolkit--a collection of computer intensive statistical methods for non-linear mixed effect modeling using NONMEM. *Comput Methods Programs Biomed* **79**, 241-257 (2005).

15. R. J. Keizer, M. O. Karlsson, A. Hooker, Modeling and Simulation Workbench for NONMEM: Tutorial on Pirana, PsN, and Xpose. *CPT Pharmacometrics Syst Pharmacol* **2**, e50 (2013).

16. D. Ho, K. Imai, G. King, E. A. Stuart, MatchIt: Nonparametric Preprocessing for Parametric Causal Inference. *2011* **42**, 28 (2011).

17. G. R. Abecasis *et al.*, An integrated map of genetic variation from 1,092 human genomes. *Nature* **491**, 56-65 (2012).

18. R. L. Roberts *et al.*, ABCG2 loss-of-function polymorphism predicts poor response to allopurinol in patients with gout. *Pharmacogenomics J* **17**, 201-203 (2017).

19. A. Nagai *et al.*, Overview of the BioBank Japan Project: Study design and profile. *J Epidemiol* **27**, S2-S8 (2017).

20. A. E. Fohner, D. J. Brackman, K. M. Giacomini, R. B. Altman, T. E. Klein, PharmGKB summary: very important pharmacogene information for ABCG2. *Pharmacogenet Genomics* **27**, 420-427 (2017).

21. R. J. Van Den Munckhof, H. Vreeling-Sindelarova, J. P. Schellens, C. J. Van Noorden, W. M. Frederiks, Ultrastructural localization of xanthine oxidase activity in the digestive tract of the rat. *Histochem J* **27**, 897-905 (1995).

22. K. Vettenranta, K. O. Raivio, Xanthine oxidase during human fetal development. *Pediatr Res* **27**, 286-288 (1990).

23. R. Harrison, Milk xanthine oxidase: Properties and physiological roles. *International Dairy Journal* **16**, 546-554 (2006).

24. Z. Guo *et al.*, Intestinal Microbiota Distinguish Gout Patients from Healthy Humans. *Sci Rep* **6**, 20602 (2016).

25. A. Pawarode *et al.*, Differential effects of the immunosuppressive agents cyclosporin A, tacrolimus and sirolimus on drug transport by multidrug resistance proteins. *Cancer Chemother Pharmacol* **60**, 179-188 (2007).

26. K. Köck, K. L. R. Brouwer, A perspective on efflux transport proteins in the liver. *Clinical pharmacology and therapeutics* **92**, 599-612 (2012).

27. C. de Wolf *et al.*, Contribution of the drug transporter ABCG2 (breast cancer resistance protein) to resistance against anticancer nucleosides. *Mol Cancer Ther* **7**, 3092-3102 (2008).

28. A. Köttgen *et al.*, Genome-wide association analyses identify 18 new loci associated with serum urate concentrations. *Nat Genet* **45**, 145-154 (2013).

29. H. Matsuo *et al.*, ABCG2/BCRP dysfunction as a major cause of gout. *Nucleosides Nucleotides Nucleic Acids* **30**, 1117-1128 (2011).

30. H. Matsuo *et al.*, Genome-wide association study of clinically defined gout identifies multiple risk loci and its association with clinical subtypes. *Ann Rheum Dis* **75**, 652-659 (2016).

31. A. Nakayama *et al.*, ABCG2 is a high-capacity urate transporter and its genetic impairment increases serum uric acid levels in humans. *Nucleosides Nucleotides Nucleic Acids* **30**, 1091-1097 (2011).

32. M. S. Cairo, B. Coiffier, A. Reiter, A. Younes, T. E. Panel, Recommendations for the evaluation of risk and prophylaxis of tumour lysis syndrome (TLS) in adults and children with malignant diseases: an expert TLS panel consensus. *Br J Haematol* **149**, 578-586 (2010).

33. M. Okour, R. C. Brundage, Modeling Enterohepatic Circulation. *Current Pharmacology Reports* **3**, 301-313 (2017).

Chapter 5

Drugs in COVID19 Clinical Trials: Predicting transporter-mediated drug-drug interactions using in vitro assays and real world data

5.1 Abstract

Numerous drugs are currently under accelerated clinical investigation for the treatment of COVID19; however, well-established safety and efficacy data for these drugs are limited. The goal of this study was to predict the potential of 25 small molecule drugs in clinical trials for COVID19 to cause clinically relevant drug-drug interactions (DDIs), which could lead to potential adverse drug reactions (ADRs) with the use of concomitant medications. We focused on 11 transporters, which are targets for DDIs. *In vitro* potency studies in membrane vesicles or HEK293 cells expressing the transporters coupled with DDI risk assessment methods revealed that 21 of the 25 drugs met the criteria from regulatory authorities to trigger consideration of a DDI clinical trial. Analyses of real world data from electronic health records, including a database representing nearly 120,000 COVID19 patients, were consistent with several of the

*Modified from material under review: Yee SW and Vora B, Oskotsky TT, Zou L, Jakobsen S, Enogieru OJ, Koleske ML, Kosti I, Rödin M, Sirota M, Giacomini KM. "Drugs in COVID19 clinical trials: Predicting transporter-mediated drug-drug interactions using in vitro assays and real-world data."

drugs causing transporter-mediated DDIs (e.g., sildenafil, chloroquine, and hydroxychloroquine). This study suggests that COVID19 patients, who are often older and on various concomitant medications, should be carefully monitored for ADRs.

5.2 INTRODUCTION

Adverse drug reactions (ADRs) are often a result of drug-drug interactions (DDIs), especially in patients for whom polypharmacy is common. It is estimated that the prevalence of clinically relevant drug-drug interactions is about 50% in those taking five, and almost 100% in those taking ten, medications (*1*, *2*). DDIs can influence drug efficacy and toxicity by affecting pharmacokinetics through the inhibition or induction of drug metabolizing enzymes and transporters in the intestine, liver, and kidney (*3*, *4*).

As the COVID19 pandemic, caused by the severe acute respiratory syndrome coronavirus 2 (SARS-CoV2), continues to plague the world, approved drugs and new molecular entities are being evaluated at an unprecedented pace. Patients diagnosed with COVID19 may be increasingly vulnerable to incur a significant DDI, especially older patients who are more susceptible to comorbidities associated with COVID19 and in whom pre-existing multimorbidity and polypharmacy (*5*) are most common.

Membrane transporters are important targets for DDIs as they play critical roles in the absorption, distribution, and elimination of drugs and nutrients (*6*). Recently, the U.S. Food and Drug Administration (FDA) released two guidances for drug developers, which include recommendations for conducting *in vitro* and clinical studies of transporter-mediated DDIs. Further, they provided a list of substrates and/or inhibitors for characterizing interactions mediated by nine membrane transporters: two efflux (P-gp and BCRP) and seven influx (OATP1B1, OATP1B3, OAT1, OAT3, OCT2, MATE1 and MATE2) (https://www.fda.gov/drugs/drug-interactions-labeling/drug-development-and-drug-interactions-table-substrates-inhibitors-and-inducers#major). These transporters not only play an important role in the disposition of drugs but also endogenous metabolites, such as creatinine (OCT2, MATE1, and MATE2) and uric acid (OAT1, OAT3, and BCRP).

In this study, we conducted extensive *in vitro* experiments aimed at predicting the potential for 25 small molecule drugs in clinical trials for COVID19 to cause transporter-mediated DDIs (**Figure 5.1**). More specifically, we 1) performed *in vitro* studies to determine the inhibition potential of the 25 drugs against 11 membrane transporters, and 2) predicted the likelihood for these drugs to cause a clinical transporter-mediated DDI using literature reported plasma concentrations and criteria suggested by the FDA. Finally, using electronic health records (EHRs), we demonstrated that the levels of endogenous compounds that are known substrates of specific transporters are significantly elevated in individuals on the drugs that are predicted inhibitors of the transporters. Overall, these findings suggest that individuals with COVID19 who may be prescribed these medications are at risk for transporter-mediated DDIs.

5.3 METHODS

5.3.1 Selection of COVID19 drugs used in clinical trials

The following three website and databases were searched between March 17th and April 1st, 2020 to select drugs being evaluated in clinical trials for COVID19: clinicaltrials.gov (https://clinicaltrials.gov/ct2/results/details?cond=COVID19), DRUGBANK (https://www.drugbank.ca/covid-19), IUPHAR/BPS Guide to Pharmacology (https://www.guidetopharmacology.org/GRAC/CoronavirusForward). Twenty-five small molecule drugs, which were in clinical trials as of April 1st, 2020, were selected for studying transporter-mediated drug-drug interactions.

5.3.2 Cell lines used for inhibition studies

Transient cells were used for determining the transporter inhibition at one concentration, 100 µM, unless mentioned otherwise. HEK293 Flp-In cells stably overexpressing human OATP2B1 (*7*), OCT1 (*8*), OCT2 (*9*), OAT1 (*10*), OAT3 (*11*), MATE1 (*12*), and MATE2 (*13*) were used for determining the inhibition potencies, IC_{50} values, of selected drugs (see next section). See Supplementary Information for more information, including methods to establish transient cells expressing OATP1B1, OATP1B3, OATP2B1, OCT1, OCT2, OAT1, OAT3, MATE1, and MATE2 in HEK293 Flp-In cells.

5.3.3 Transporter inhibition studies

Twenty-five COVID19 drugs were screened against 11 transporters at a concentration of 100 µM, except for azithromycin (50 µM), baricitinib (50 µM) and tetrandrine (10 µM) due to solubility. The substrate used for each transporter is listed in **Supplemental Table 5.1**. For OATP1B1, OATP1B3, OATP2B1, OCT1, OCT2, OAT1, OAT3, MATE1, and MATE2, drugs were screened in cells transiently overexpressing each of the transporters. For P-gp and BCRP, membrane vesicles were used and the vesicular transport assays were performed as reported previously (*14*) with modifications. See Supplementary Information for detailed methods.

5.3.4 Prediction of transporter-mediated inhibition

The DDI potential for each drug was evaluated in accordance to the 2020 FDA Drug-Drug Interaction Guidance (*4*) by calculating the ratio of predicted clinically relevant drug concentration (I) to IC_{50} (I/IC_{50}). See Supplementary Information for description on the formulas and cutoff values used to predict *in vivo* DDI potential. Clinical pharmacokinetic characteristics (such as C_{max}, plasma protein binding percentage, and R_b) were collected from PubMed and FDA-approved labeling (Drugs@FDA) (**Supplemental Table 5.2**). If no information was available, $f_{u,p}$ and R_b were both estimated to be 1. The highest possible single dose, and respective C_{max} value, was used for all calculations. If a C_{max} value following the highest possible single dose was not available, the C_{max} was scaled linearly to fit the dose.

5.3.5 Electronic health record analyses

Two electronic health record databases were used to extract information about patient medication use as well as perform real world data analyses, UCSF Research Data Browser and Cerner's Real World COVID19 Database.

The UCSF Research Data Browser with UCSF patient data from 1982 to September 2020 was utilized to search for patients (both inpatients and outpatients) who had at least one laboratory test value reported for 1) serum/plasma uric acid, 2) triglyceride, 3) LDL cholesterol, 4) total cholesterol or 5) bilirubin. For each analysis, patients were divided into the "on" or "off" drug group depending on their medication prescriptions for sildenafil, ritonavir, darunavir, and/or lopinavir. See Supplementary Information for detailed methods.

The Cerner COVID19 database includes EMR data from 62 healthcare facilities across the United States from January 2015 to July 2020 of patients who were in an Emergency Room (ER) or admitted to a hospital for COVID19. We searched for patients who had (a) at least one positive lab test result for SARS-CoV2 and (b) at least two laboratory test values reported for serum creatinine (**Supplemental Figure 5.1**). Patients were divided into the "on" or "off" drug group depending on their medication prescription(s) for chloroquine (CQ) or hydroxychloroquine (HCQ). See Supplementary Information for detailed methods

In all analyses comparing patient groups, patients were matched by covariates, including age and sex, using the MatchIt package (*15*) in R to be comparable in both groups.

The Cerner COVID19 database was also utilized to search for the number of patients who have prescriptions for drugs that are known substrates or inhibitors of the transporters, P-gp, BCRP, OATP1B1, OATP1B3, OCT1, OCT2, MATE1, MATE2, OAT1 and OAT3 (https://www.fda.gov/drugs/drug-interactions-labeling/drug-development-and-drug-interactions-table-substrates-inhibitors-and-inducers#major). See Supplementary Information for detailed methods.

5.3.6 Statistical analyses

Two-sample two-sided Mann–Whitney U tests with continuity correction were performed to compare "on" and "off" drug groups. Among patients without elevated "pre" creatinine levels, enrichment of elevated "post" creatinine level for those on HCQ or CQ in comparison to the matched control group was calculated by Chi-squared test with Yates correction. ggplot2 was used to plot the data in R (version 3.4.0).

5.4 RESULTS

5.4.1 In vitro studies determine inhibition potencies of 25 drugs used in clinical trials for COVID19

Among the 25 drugs screened, 14 (56%) were anti-microbial agents and 10 (40%) were anti-inflammatory drugs. Eleven or more compounds reduced transport activity of P-gp, OATP2B1, OATP1B1, OATP1B3, OCT1, MATE1, MATE2, and OAT3 by > 50% (**Supplemental Table 5.1**). In contrast, five or fewer compounds inhibited BCRP, OCT2, and OAT1 by > 50%. Twenty drugs, which showed greater than 50% inhibition of transporter activity in our initial screen, were characterized further to estimate their IC_{50} (inhibitor concentration at which transporter activity is reduced to 50%) (**Table 5.1**). For drugs with transporter inhibition of < 50%, IC_{50} was predicted based on a single point determination; however, for those that showed no transporter inhibition when screened at 100 µM, IC_{50} was not estimated. When inhibition potency data were available in the literature, those values were recorded and used in predicting the potential to cause clinical transporter-mediated DDI (**Supplemental Table 5.1** and **Supplemental Table 5.4**). In general, experimentally estimated IC_{50} values (**Table 5.1**) were in agreement with published data (**Supplemental Table 5.4**).

Substrate-dependent inhibition of OATP1B1 and OATP1B3

We compared differences in potency of inhibition of various drugs using EG and ES or cholecystokinin (CCK) as probe substrates for OATP1B1 and OATP1B3, respectively. In general, inhibition potencies of the drugs tested were lower when [^{3}H]-EG was used as the probe substrate in comparison to [^{3}H]-ES as the probe substrate (**Table 5.1**), as also reported by Izumi *et al.* (*16*). Darunavir, losartan, remdesivir, and ritonavir all were estimated to inhibit [^{3}H]-EG at concentrations one-tenth (or lower) than those that inhibited [^{3}H]-ES; that is, potency differences of the inhibitors for the two probes were greater than 10-fold. Differences in inhibition potency of compounds were not as stark when [^{3}H]-EG and [^{3}H]-CCK were used as probe substrates for OATP1B3 (**Table 5.1**). Seven drugs had potency differences within 2-fold; however, remdesivir showed a 14-fold lower IC_{50} with [^{3}H]-EG as a substrate compared with [^{3}H]-CCK whereas darunavir was 5-fold more potent in inhibiting the uptake of [^{3}H]-CCK in comparison to that of [^{3}H]-EG (**Table 5.1**).

Similarity and differences in potencies between transporters of close homology

In general, experimental IC_{50} values for OATP2B1, OATP1B1, and OATP1B3 were significantly correlated for the 10 drugs where IC_{50} values were experimentally determined (Spearman correlation coefficient, r, ranges from 0.74 to 0.82, $p < 0.02$). Triazavirin is the only drug that was selective for OATP2B1 (IC_{50} = 17 ± 4 μM), showing no inhibition of OATP1B1 and OATP1B3 at 100 μM. For MATE1 and MATE2, nine drugs (out of 15) had IC_{50} values within 5-fold of each other; however, three drugs (ritonavir, remdesivir, and tofacitinib) had IC_{50} values that were greater than 25-fold different. In contrast, larger differences in IC_{50} values were observed when comparing the two organic cation transporters, OCT1 and OCT2, or the two organic anion transporters, OAT1 and OAT3 (**Table 5.1**). Camostat, chloroquine, colchicine, darunavir, hydroxychloroquine, prazosin, remdesivir, ritonavir, and umifenovir inhibited OCT1 ≥ 10-fold more potently relative to OCT2, when comparing predicted or actual IC_{50} values. Similarly, baricitinib (*17*), leflunomide, piclidenoson, remdesivir, ruxolitinib, and sildenafil inhibited OAT3 ≥ 10-fold more potently relative to OAT1 when comparing predicted or actual IC_{50} values.

5.4.2 Clinically relevant transporter-mediated drug-drug interactions are predicted for 21 drugs

Using the FDA guidance for evaluating transporter-mediated drug interactions, a total of 86 potentially clinically relevant drug-transporter interactions were identified (**Table 5.2**, **Supplemental Table 5.5**, and **Figure 5.2**). Twenty-one out of the 25 drugs screened were predicted to inhibit at least one of the studied transporters at clinical concentrations. Favipiravir, ritonavir, darunavir, and umifenovir were the most promiscuous clinical inhibitors, with each compound predicted to inhibit at least six transporters at clinically achievable drug levels. In contrast, baricitinib, colchicine, fingolimod, and prazosin were not predicted to cause any transporter mediated DDIs. Intestinal and hepatic transporters appeared to be more easily inhibited compared to renal transporters, reflecting higher drug concentrations and exposure in the intestine and liver compared with the kidney. Additionally, intestinal P-gp appeared to be highly inhibitable with 16 of the 25 drugs predicted to inhibit the transporter at estimated intestinal concentrations.

Since the first whitepaper by the International Transporter Consortium (ITC) was published (*6*), many drug labels include information on whether a drug is a substrate or inhibitor of certain transporters. For the drugs in this study that were approved prior to 2010 (n = 14), many clinically relevant transporter interactions were predicted. In particular, 54 interactions were predicted for these drugs. Five drugs approved during or after 2010 were predicted to have limited potential to inhibit these transporters *in vivo* with the exception remdesivir (approved in October 2020). Remdesivir inhibited five transporters at clinically relevant concentrations (**Table 5.2**). Interestingly, for the six drugs that have not been approved by the FDA (**Table 5.2**), 25 potentially relevant drug-transporter interactions were identified. For example, favipiravir, umifenovir, and triazavirin each were predicted to cause five or more clinically relevant drug-transporter interactions. Camostat and leflunomide are rapidly converted to their active metabolites, precluding I/IC_{50} calculations for hepatic and renal transporters.

5.4.3 Electronic health record analyses complement in vitro findings on clinically relevant transporter-mediated DDIs

To investigate the clinical relevance of the inhibitors identified *in vitro*, we mined the electronic health record (EHR) database from the UCSF Research Data Browser (n = 2,888,884 total patients from the general population). Specifically, we compared specific lab values in patients prescribed commonly used drugs (i.e. sildenafil, darunavir, ritonavir, lopinavir) to lab values in patients not prescribed the respective drug. Endogenous biomarkers chosen and compared for each of these analyses were driven by literature-based evidence (**Supplemental Table 5.6**).

To assess whether sildenafil, which was predicted to inhibit BCRP at clinical concentrations, actually inhibited the transporter in patients, we used uric acid levels from the UCSF database as a biomarker of BCRP activity; higher uric acid levels have been previously associated with reduced BCRP activity. Patients prescribed sildenafil had significantly higher uric acid levels (average: 6.84 mg/dL vs 5.94 mg/dL) compared to age- and sex- matched controls not prescribed sildenafil (p-value $< 2.2 \times 10^{-16}$, n = 636 “on” drug, n = 3,180 “off” drug), consistent with inhibition of BCRP (**Figure 5.3** and **Table 5.3**). Additional sensitivity analyses including (1) a maximum separation date of one year between the first medication order start date and lab collection date, (2) limiting our analysis to patients diagnosed with pulmonary hypertension and (3) further filtering to only include lab values taken on or after initial diagnosis start date, (4) only including Sildenafil (i.e. excluding Viagra and Revatio) medication orders with a dose greater than 25mg in the medication name, and (5) excluding male patients, showed a significant difference between the two groups, where patients “on” drug had higher uric acid levels compared to patients “off” drug (**Table 5.3**). Furthermore, to test the sensitivity of these analyses and selection of controls, multiple iterations were performed for each analysis where the ratio used to sex- and age- match the two groups was varied; in every iteration, the “on” drug group had significantly higher uric acid levels compared to the “off” drug group (**Supplemental Table 5.7**).

To assess the potential of ritonavir and darunavir to inhibit OCT1 at clinical concentrations, we used pharmacodynamic endpoints using data from the UCSF database. That is, reduction in the function of OCT1 has been associated with higher lipid levels (*18*). Triglyceride, LDL cholesterol, and total cholesterol levels were significantly increased in HIV patients prescribed ritonavir compared to age- and sex- matched HIV patients not prescribed ritonavir, when comparing labs taken on or after initial HIV diagnosis start date, consistent with inhibition of OCT1 (**Figure 5.3** and **Table 5.3**). A similar, significant increase was seen in HIV patients prescribed darunavir (**Table 5.3**). Percentage of patients with at least one statin prescription was higher in the "on" drug group or comparable between both groups for all ritonavir & darunavir analyses when comparing prescriptions to drugs (classified as antihyperlipidemic-HMG-CoA reductase inhibitors (statins)) with a medication order start date within one year before the lab collection date (**Supplemental Table 5.3**).

HIV patients prescribed ritonavir and/or lopinavir had significantly higher total bilirubin levels compared to HIV patients not prescribed ritonavir and/or lopinavir, when comparing labs taken on or after initial HIV diagnosis start date, consistent with inhibition of OATP1B1 and OATP1B3 (**Table 5.3**).

Serum creatinine levels are determined by renal function, but also by secretion via renal transporters including MATE1 (*19*). Thus, we used the change in creatinine level over time in patients prescribed hydroxychloroquine (HCQ) and chloroquine (CQ), which are predicted to inhibit MATE1, to determine whether these drugs may actually inhibit this transporter clinically (**Table 5.4**). We used the Cerner COVID19 database (n = 117,496 total COVID19 patients) to identify patients prescribed HCQ and CQ (**Table 5.4** and **Supplemental Figure 5.1**). The Cerner database contains data about medication order status (e.g. 'complete', 'incomplete') that informs about medication administration as well as timestamps for labs and medications that provide a temporal relationship between events of interest, and thus used for this analysis instead of the UCSF Research Data Browser.

In the analysis of COVID19 patients in the Cerner database who have "pre" creatinine levels within the upper limit of normal range, the "on drug" cohort had a significantly higher prevalence of "post" creatinine levels that were elevated above the normal range than the "off drug" control cohort matched using a propensity score that included age, sex, race, ethnicity, and outcome (death), with a 1:2 ratio (15.41% vs 11.47%. Chi-square test, p-value = 0.024) (**Table 5.4**). As serum creatinine levels can be confounded by underlying kidney disease and by chronic conditions such as systemic lupus erythematosus (SLE) for which long-term therapy with HCQ or CQ can be prescribed, we conducted a sensitivity analysis which excluded those with chronic renal disease and matched patients in the "on drug" and "off drug" cohorts by medication indication for HCQ and CQ. For the COVID19 patients with "pre" creatinine levels within the upper limit of normal range and without chronic renal disease, the "on drug" cohort had a significantly higher prevalence of "post" creatinine levels elevated above the normal range than the "off drug" control cohort matched using a propensity score which included age, sex, race, ethnicity, outcome (death), and medication indication (SLE, discoid lupus, and rheumatoid arthritis, and malaria), with a 1:2 ratio (14.23% vs 8.37%. Chi-square test, p-value = 4.6×10^{-4}, **Table 5.4** and **Supplemental Table 5.3**). Creatinine elevations are consistent with inhibition of MATEs.

5.5 DISCUSSION

In the present study, we determined the inhibition potency of 25 drugs (18 approved drugs, six investigational drugs, and one recently approved) in COVID19 clinical trials against 11 transporters and evaluated their potential to cause transporter-mediated DDIs. COVID19 patients are often older and taking multiple medications, many of which are substrates of transporters and thus, subject to transporter-mediated DDI. For example, furosemide (OAT1 and OAT3 substrate), atorvastatin (OATP1B1 and OATP1B3 substrate), and morphine (OCT1 substrate) are known substrates of transporters and are commonly used in COVID19 patients to treat co-existing conditions (**Supplemental Table 5.8**).

This study resulted in three major findings. First, many of the drugs tested, which are in clinical trials for COVID19, inhibited transporters in cellular assays with certain transporters being sensitive to inhibition by multiple drugs. Second, most of the drugs (21 out of 25) were predicted to cause at least one clinical DDI; that is, the concentrations of these drugs that inhibited the transporters in cellular assays were equal to or greater than drug levels known to result in clinical DDIs. Finally, real world data from EHRs were consistent with our predictions of transporter-mediated DDIs. In particular, recorded levels of certain solutes (such as creatinine and uric acid), which are endogenous substrates of particular transporters, were significantly elevated in individuals taking drugs predicted to inhibit the transporters clinically, in comparison to matched subjects not taking the drugs (**Table 5.3** and **Table 5.4**). Below, we discuss each of these findings.

5.5.1 Drugs in clinical trials for COVID19 inhibited membrane transporters that are targets for clinical DDIs

Seventeen of the 25 drugs tested in this study have been reported to be substrates or inhibitors of one or more of the eleven membrane transporters that are targets for DDIs (**Supplemental Table 5.1**); however, none of them have been assessed against all eleven transporters in a single study. Although the FDA recommends transporter studies for nine of these transporters, we included OCT1 based on the recommendation by the European Medicine Agency (EMA) and OATP2B1 because of increasing evidence for its role in mediating intestinal drug absorption (*20*). There were eight drugs where no information was available about their interactions with any of the eleven transporters, including: 1) three drugs (HCQ, ribavirin and thalidomide) which were approved before 2000 and have no information about transporter inhibition reported in their FDA approved labels, their product inserts, or the literature, 2) two drugs (fingolimod and ruxolitinib) which were approved after 2010 but have limited information about their IC_{50} values in their labels and product inserts, and 3) three drugs (piclidenoson, triazavirin and umifenovir) which have not been approved. Examination of the data suggest that hepatic uptake transporters including OATP1B1, OATP1B3, and OCT1 are subject to inhibition by multiple drugs in clinical trials for COVID19. These hepatic transporters are known to interact with structurally diverse molecules from a range of pharmacologic classes and play critical roles in xenobiotic detoxification (*21*, *22*). OATP2B1, also in the liver and intestine, similarly interacts with multiple drugs. In the kidney, MATE1 and MATE2 were inhibited by several drugs (**Figure 5.2** and **Table 5.2**). These transporters are known to interact with many drugs (*23*), and clinically relevant DDIs have been reported between inhibitors of MATE1 such as cimetidine and the commonly prescribed anti-diabetic drug, metformin (*24*). In contrast, the renal transporters OCT2 and OAT1, and the intestinal efflux transporter, BCRP, were not subject to inhibition by multiple drugs (**Table 5.1** and **Figure 5.2**). The majority of the drugs on the market that inhibit OCT2 are more potent inhibitors of MATE1 and MATE2 at clinically relevant concentrations, such as pyrimethamine and trimethoprim (*25*). OAT1, which is responsible for the renal secretion of many acidic drugs such as tenofovir, is inhibited by a few prescription drugs such as probenecid, but is considered a less promiscuous paralog than OAT3, which interacts with a more diverse array of drugs and their metabolites (*11*). The fact that BCRP was not inhibited by most of the drugs tested (**Table 5.1**) is interesting. BCRP has an endogenous role in the elimination of uric acid (**Supplemental Table 5.6**), and drugs that inhibit this transporter may increase risk for hyperuricemia and gout.

5.5.2 Most of the drugs (21 out of 25) tested were predicted to cause at least one transporter-mediated clinical DDI

A surprising finding of our study was that many of the drugs in clinical trials for COVID19 had the potential to cause at least one transporter-mediated DDI. In particular, 21 out of the 25 drugs screened were predicted to inhibit at least one of the eleven transporters at clinically achievable concentrations (**Table 5.2**). Ten of the 21 drugs have supporting information in the literature suggesting that they cause DDIs in humans or mice or have reported adverse events that are consistent with transporter inhibition (**Supplemental Table 5.6**). The finding that the drugs may cause DDIs mediated by one or more transporters is consistent with the notion that these transporters work together with drug metabolizing enzymes to detoxify a plethora of xenobiotics including environmental toxins, exogenous chemicals, and prescription drugs. Thus, transporters and enzymes interact with structurally diverse molecules and are subject to inhibition interactions. For example, azithromycin, a known *in vivo* P-gp inhibitor, increases plasma levels of the non-sedating antihistamine, fexofenadine, and the anticoagulant, ximelagatran, both of which are substrates of P-gp (*26, 27*). The anti-viral combination drugs, lopinavir/ritonavir or lopinavir/darunavir, are known *in vivo* inhibitors of OATP1B1, OATP1B3, and P-gp. As such, they are associated with increase plasma levels of rosuvastatin, which is a substrate of OATP1B1/B3 and BCRP (*28, 29*), and fexofenadine, which is a P-gp substrate (*30*). The effectiveness and cardiac safety of hydroxychloroquine, chloroquine, and azithromycin in COVID19 patients have been the subject of considerable discussion in the literature (*31-34*). One of the major adverse events of these drugs is prolongation of the QT interval. This study and others have shown that azithromycin, hydroxychloroquine, and chloroquine are substrates and inhibitors of P-gp (*26, 27, 35, 36*). Therefore, the use of azithromycin in combination with chloroquine or hydroxychloroquine needs to be carefully assessed and monitored.

5.5.3 Real world data from electronic health records were consistent with our predictions of transporter-mediated DDIs

Human genetic association studies and knockout mouse studies have shown that reduced function genetic variants of BCRP, OAT1, and OAT3 are associated with higher uric acid levels (*10, 37, 38*). Similarly, genetic variants in OCT2 and MATE1 are associated with higher serum creatine levels and hence, reduced estimated glomerular filtration rate (eGFR) (*39-41*). Finally, genetic variants of OATP1B1 and OATP1B3 are associated with increased bilirubin levels (*42*). All of these metabolites are also substrates of the respective transporters. Additionally, reduced function polymorphisms in OCT1 and Oct1 knockout mice have been shown to have increased plasma levels of LDL cholesterol, total cholesterol, and triglycerides (*18*). Since levels of uric acid, creatinine, bilirubin, and various lipids are routinely measured and recorded in the EHR, these levels may be exploited to validate predictions from *in vitro* transporter assays of clinically relevant DDIs. Sildenafil has been shown to increase risk of gout (**Supplemental Table 5.6**), and we found that patients who were prescribed sildenafil, a potent inhibitor of BCRP, had significantly elevated serum uric acid levels relative to patients not prescribed sildenafil (**Table 5.3** and **Figure 5.3**). In our study, average serum uric acid levels in the "on" drug group ranged from 6.8 - 7.4 mg/dL whereas the average levels for the "off" drug group ranged from 5.0 - 6.3 mg/dL, across all analyses. Previous studies have reported incidents of sildenafil-induced gouty arthritis (*43, 44*). In contrast, other inhibitors of phosphodiesterase 5 (PDE-5), such as vardenafil and tadalafil, are weak inhibitors of BCRP (*45*) and serum uric acid levels have been shown to significantly decrease following a one year treatment with vardenafil (*46*).

In addition to exploiting uric acid as an endogenous substrate of BCRP, we used lipid levels as biomarkers of OCT1 activity. That is, patients prescribed ritonavir and/or darunavir, both of which are OCT1 inhibitors (**Table 5.1** and **Table 5.2**), had significantly higher triglyceride, LDL cholesterol, and total cholesterol levels, compared with patients not prescribed either of these drugs (**Table 5.3** and **Figure 5.3**). Increases in cholesterol and triglyceride levels are listed as possible side effects in the FDA product label for ritonavir, as well as the Warnings and Precautions section to ensure these levels are monitored before and during therapy (*47*). Though multiple mechanisms may account for the observed increases in lipid levels associated with these drugs, reduced OCT1 activity is consistent with the elevated lipid levels (*18*).

The *in vitro* studies and *in vivo* DDI risk predictions were focused on 25 drugs, selected during the beginning of the COVID19 shelter-in-place; therefore, the numbers of drugs were limited. The EHR analyses were limited by lack of data on how long patients were on each respective medication, patient compliance (i.e. picking up medication from pharmacy, abiding by dosing schedule), and robust controls (i.e. other PDE-5 and protease inhibitors) as well as difficulty in getting measurable outcomes and noisy data. As more EHR data become available for research purposes, we will be able to account for these variables and covariates as well as increase the sample size and robustness of our analysis. Importantly, the endogenous solutes and lipids measured may be elevated for other reasons beyond transporter inhibition (e.g. creatinine elevation can result from dehydration and elevation of lipids, in particular triglycerides, can be detected for hours after high fat meals); thus, the EHR results need to be interpreted cautiously and only as supporting information. Additional studies such as controlled randomized clinical trials of DDIs or use of validated biomarkers for transporter-mediated DDIs need to be conducted (*48*, *49*).

This study highlights that many of the currently used drugs for COVID19 have the potential to cause transporter-mediated DDIs. Our study suggests that COVID19 patients, who are often older and on various concomitant medications, should be carefully monitored for known ADRs.

5.6 FIGURES

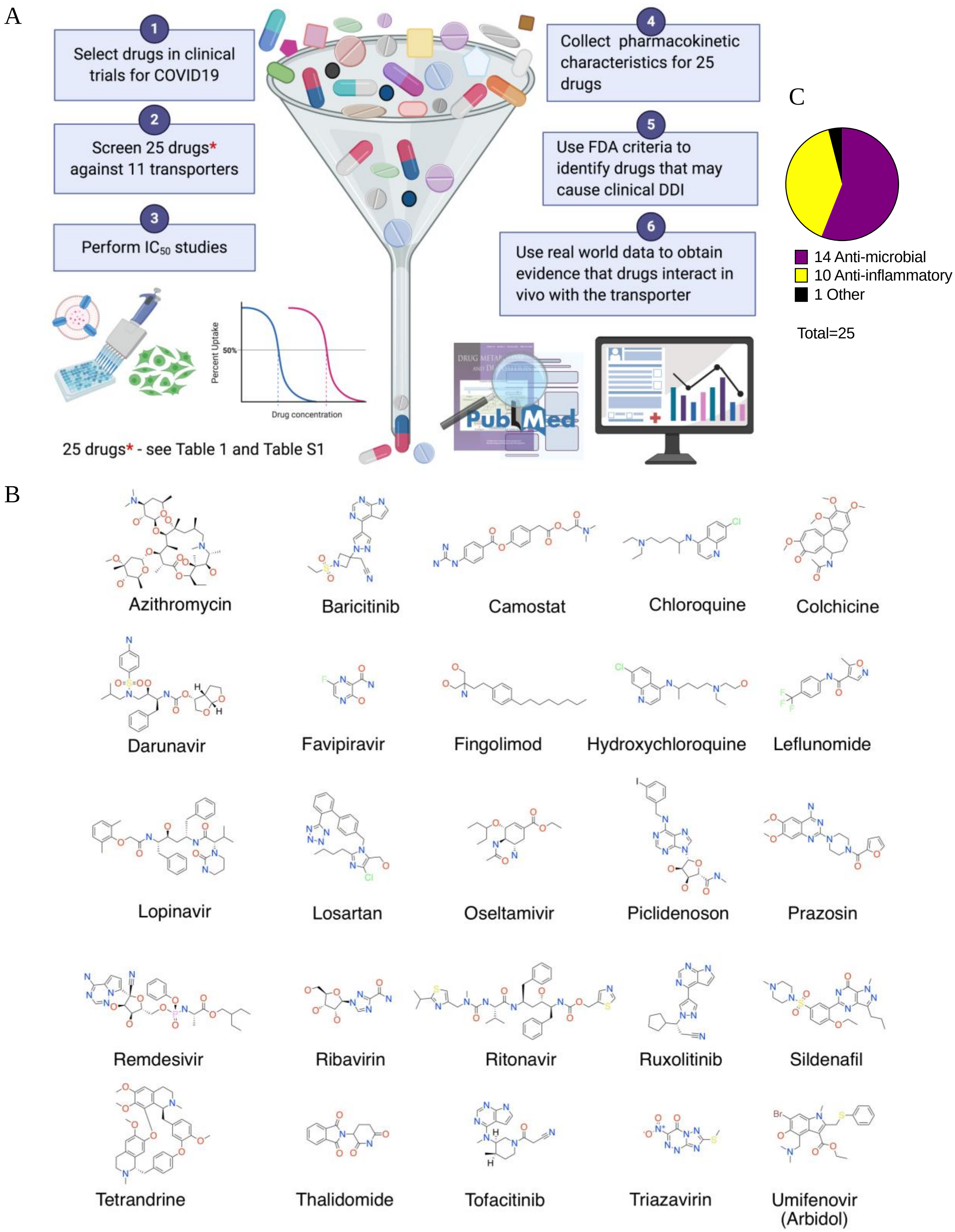
A
1
Select drugs in clinical trials for COVID19
2
Screen 25 drugs* against 11 transporters
3
Perform IC50 studies
Percent Uptake
50%
Drug concentration
25 drugs* - see Table 1 and Table S1
4
Collect pharmacokinetic characteristics for 25 drugs
5
Use FDA criteria to identify drugs that may cause clinical DDI
6
Use real world data to obtain evidence that drugs interact in vivo with the transporter
PubMed
C
14 Anti-microbial
10 Anti-inflammatory
1 Other
Total=25
B
Azithromycin
Baricitinib
Camostat
Chloroquine
Colchicine
Darunavir
Favipiravir
Fingolimod
Hydroxychloroquine
Leflunomide
Lopinavir
Losartan
Oseltamivir
Piclidenoson
Prazosin
Remdesivir
Ribavirin
Ritonavir
Ruxolitinib
Sildenafil
Tetrandrine
Thalidomide
Tofacitinib
Triazavirin
Umifenovir (Arbidol)

Figure 5.1 Overall study approach to assess the risks for transporter-mediated drug-drug interactions (DDI) of 25 drugs in clinical trials to treat COVID19 patients. (A) Multiple approaches were used in this study, starting with *in vitro* assays to determine transporter inhibition (1-3), followed by applying predictive methods to evaluate the potential for DDIs (4-5), and leveraging real world data from electronic health records (6) to validate drug-transporter interactions clinically. (B, C) Chemical structures of 25 drugs, which include 14 anti-microbial and 10 anti-inflammatory drugs.

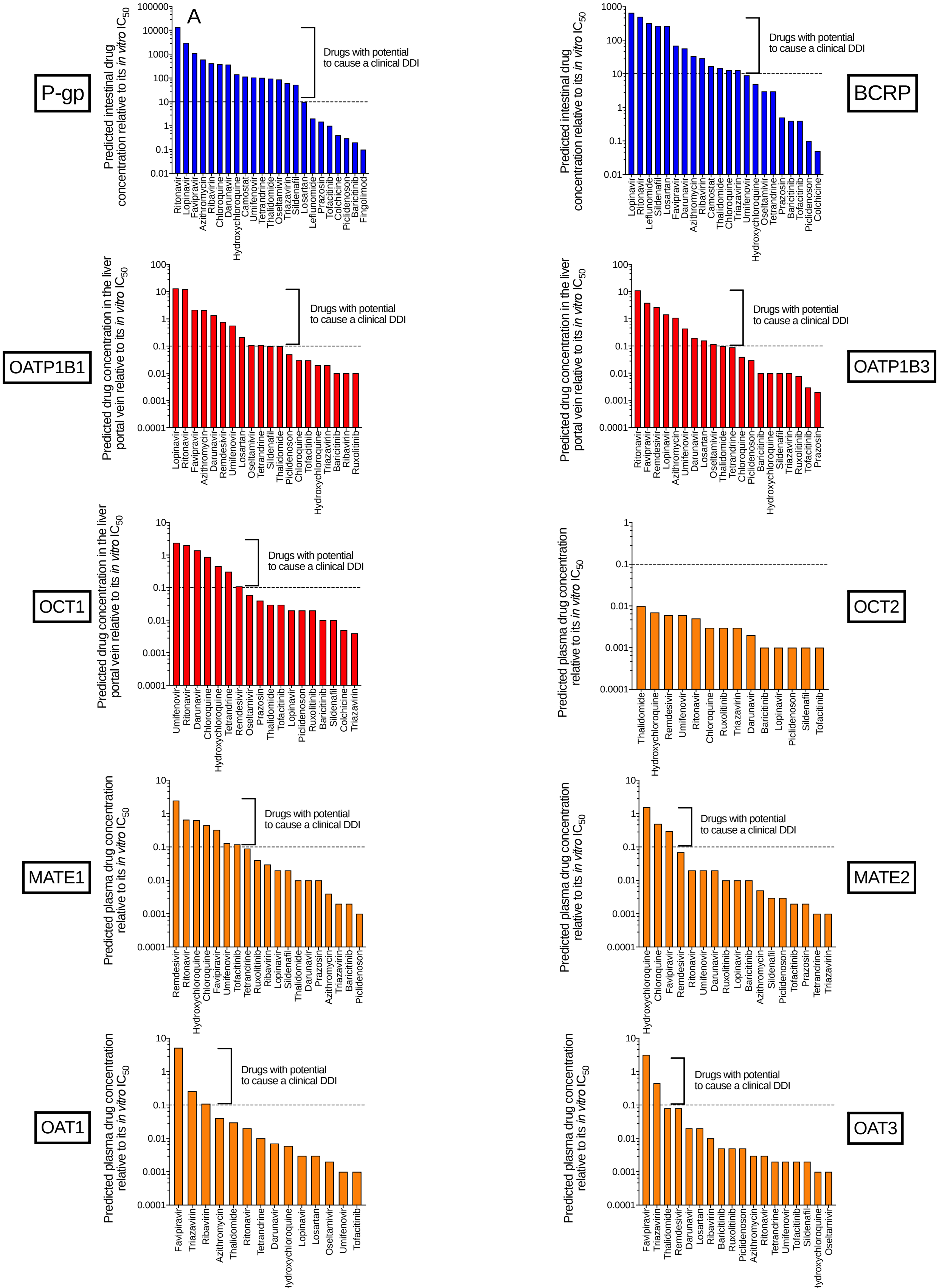
A
P-gp
Predicted intestinal drug concentration relative to its in vitro IC50
Drugs with potential to cause a clinical DDI
Ritonavir Lopinavir Favipiravir Azithromycin Ribavirin Chloroquine Darunavir Hydroxychloroquine Camostat Umifenovir Tetrandrine Thalidomide Oseltamivir Triazavirin Sildenafil Losartan Leflunomide Prazosin Tofacitinib Colchicine Piclidenoson Baricitinib Fingolimod
BCRP
Predicted intestinal drug concentration relative to its in vitro IC50
Drugs with potential to cause a clinical DDI
Lopinavir Ritonavir Leflunomide Sildenafil Losartan Favipiravir Darunavir Azithromycin Ribavirin Camostat Thalidomide Chloroquine Triazavirin Umifenovir Hydroxychloroquine Oseltamivir Tetrandrine Prazosin Baricitinib Tofacitinib Piclidenoson Colchicine
OATP1B1
Predicted drug concentration in the liver portal vein relative to its in vitro IC50
Drugs with potential to cause a clinical DDI
Lopinavir Ritonavir Favipiravir Azithromycin Darunavir Remdesivir Umifenovir Losartan Oseltamivir Tetrandrine Sildenafil Thalidomide Piclidenoson Chloroquine Tofacitinib Hydroxychloroquine Triazavirin Baricitinib Ribavirin Ruxolitinib
OATP1B3
Predicted drug concentration in the liver portal vein relative to its in vitro IC50
Drugs with potential to cause a clinical DDI
Ritonavir Favipiravir Remdesivir Lopinavir Azithromycin Umifenovir Darunavir Losartan Oseltamivir Thalidomide Tetrandrine Chloroquine Piclidenoson Baricitinib Hydroxychloroquine Sildenafil Triazavirin Ruxolitinib Tofacitinib Prazosin
OCT1
Predicted drug concentration in the liver portal vein relative to its in vitro IC50
Drugs with potential to cause a clinical DDI
Umifenovir Ritonavir Darunavir Chloroquine Hydroxychloroquine Tetrandrine Remdesivir Oseltamivir Prazosin Thalidomide Tofacitinib Lopinavir Piclidenoson Ruxolitinib Baricitinib Sildenafil Colchicine Triazavirin
OCT2
Predicted plasma drug concentration relative to its in vitro IC50
Thalidomide Hydroxychloroquine Remdesivir Umifenovir Ritonavir Chloroquine Ruxolitinib Triazavirin Darunavir Baricitinib Lopinavir Piclidenoson Sildenafil Tofacitinib
MATE1
Predicted plasma drug concentration relative to its in vitro IC50
Drugs with potential to cause a clinical DDI
Remdesivir Ritonavir Hydroxychloroquine Chloroquine Favipiravir Umifenovir Tofacitinib Tetrandrine Ruxolitinib Ribavirin Lopinavir Sildenafil Thalidomide Darunavir Prazosin Azithromycin Triazavirin Baricitinib Piclidenoson
MATE2
Predicted plasma drug concentration relative to its in vitro IC50
Drugs with potential to cause a clinical DDI
Hydroxychloroquine Chloroquine Favipiravir Remdesivir Ritonavir Umifenovir Darunavir Ruxolitinib Lopinavir Baricitinib Azithromycin Sildenafil Piclidenoson Tofacitinib Prazosin Tetrandrine Triazavirin
OAT1
Predicted plasma drug concentration relative to its in vitro IC50
Drugs with potential to cause a clinical DDI
Favipiravir Triazavirin Ribavirin Azithromycin Thalidomide Ritonavir Tetrandrine Darunavir Hydroxychloroquine Lopinavir Losartan Oseltamivir Umifenovir Tofacitinib
OAT3
Predicted plasma drug concentration relative to its in vitro IC50
Drugs with potential to cause a clinical DDI
Favipiravir Triazavirin Thalidomide Remdesivir Darunavir Losartan Ribavirin Baricitinib Ruxolitinib Piclidenoson Azithromycin Ritonavir Tetrandrine Umifenovir Tofacitinib Sildenafil Hydroxychloroquine Oseltamivir

Figure 5.2 Results of predictions of 25 drugs in COVID19 clinical trials to cause *in vivo* transporter-mediated drug-drug interactions (DDIs). Predictions are based on *in vitro* inhibition potency data and are expressed as the clinical drug concentration (e.g., intestinal, portal vein, or systemic unbound concentration) relative to the *in vitro* IC_{50} value for each transporter. The stippled lines indicate the FDA recommended values above which sponsors are asked to consider conducting a clinical DDI trial. Drugs that have negligible inhibition and have $[I]/IC_{50}$ ratio < 0.001 are not shown. To illustrate the interpretation of these figures, consider ritonavir (marked A in the upper left panel). Its estimated concentration in the intestine after a therapeutic dose is 10,000 times greater than the ritonavir concentration required to inhibit 50% of P-gp activity in an *in vitro* experiment.

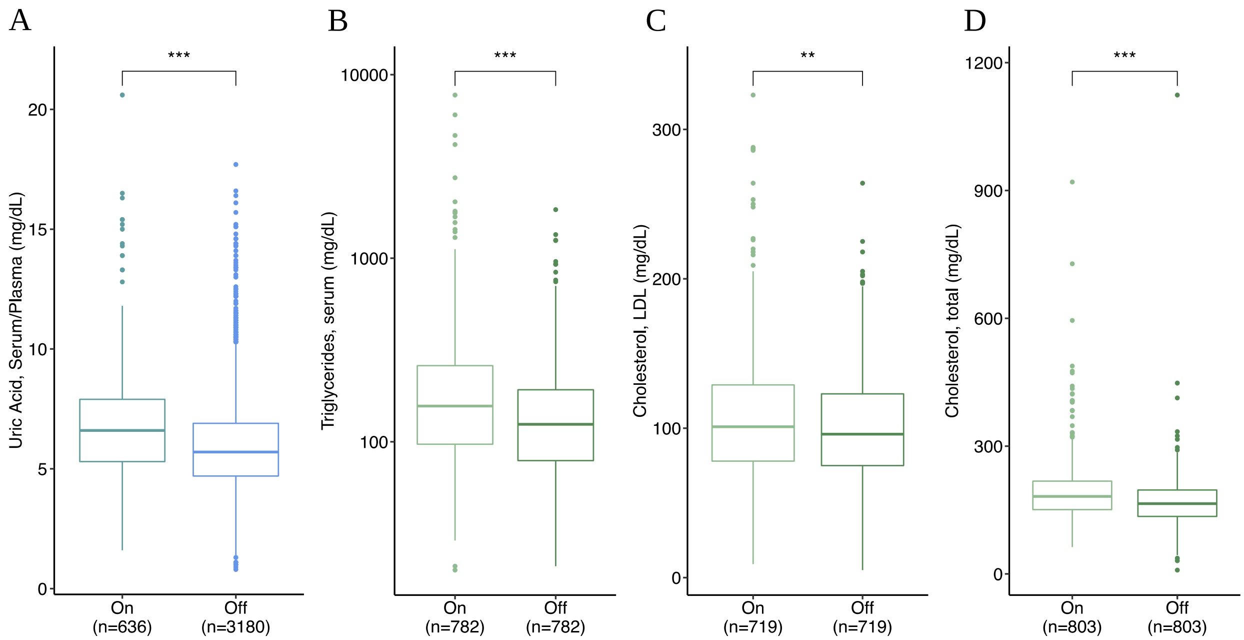

Figure 5.3 Endogenous levels of transporter biomarkers in patients prescribed drugs that are predicted to cause a transporter-mediated DDI. Levels of each biomarker were obtained from patient electronic health records. Boxplots compare (A) levels of uric acid, a biomarker of BCRP activity, in patients prescribed sildenafil versus patients not prescribed sildenafil (p-value $< 2.2 \times 10^{-16}$) and (B-D) levels of triglycerides, LDL cholesterol, and total cholesterol, biomarkers of OCT1 activity, in HIV patients prescribed ritonavir versus HIV patients not prescribed ritonavir (p-value: 7.8×10^{-12}, 0.0033, 3.1×10^{-13}, respectively). **Figure 5.3B** is plotted on a log scale.

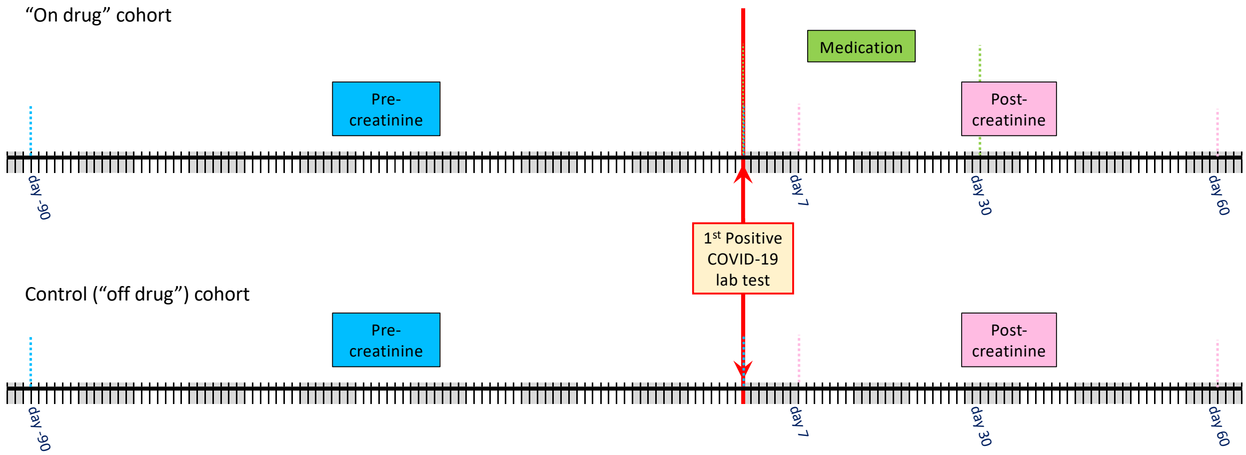

Supplemental Figure 5.1 Schematic for Cerner Real World COVID19 data mining and real world data analysis. The Cerner Real World COVID19 dataset was queried for patients who had at least two serum creatinine lab test values ("pre" and "post") within specific timeframes relative to the time of the first positive COVID19 lab test (red line). For the "on drug" cohort, the serum creatinine value that was reported 7 to 30 days after the earliest HCQ or CQ medication start date was used for the "post" creatinine. When multiple lab values were found within a defined time frame, the result closest to the time of the first positive COVID19 lab test (red line) was included.

5.7 TABLES

Table 5.1 Summary table showing the inhibition potencies of drugs in COVID19 clinical trials against transporters that are mediators of drug-drug interactions (DDIs).

A) Major intestinal transporters: P-gp, BCRP, and OATP2B1

COVID19 Drug	P-gp	BCRP	OATP2B1
Azithromycin	18	314	414
Baricitinib	175	107	217
Camostat	35	238	NI
Chloroquine	20.0	596	1332
Colchicine	42	320	NI
Darunavir	16	103	30.6 ± 7.7
Favipiravir	55	890	NI
Fingolimod	89	NI	298
Hydroxychloroquine	51.8 ± 20.6	1484	1084
Leflunomide	629	4.53[a]	81.9 ± 36.1
Lopinavir	1.7[a]	7.66[a]	0.72[a]
Losartan	128	4.8 ± 1.1	2.5 ± 0.7
Oseltamivir	44	1286	6593
Piclidenoson	50	105	12.3 ± 4.7
Prazosin	70.7[a]	221	137
Remdesivir	14	25 ± 6.0	3.5 ± 0.4
Ribavirin	47	675	1628
Ritonavir	36, 0.24[a]	19.5, 6.6[a]	3.7 ± 1.1
Ruxolitinib	NI	NI	17.4 ± 8.6
Sildenafil	16	3.1 ± 2.5	39.0 ± 12.8
Tetrandrine	3.8 ± 1.1	113	NI
Thalidomide	65	427	NI
Tofacitinib	178	295	NI
Triazavirin	72	325	17.4 ± 4.0
Umifenovir (Arbidol)	16.0 ± 2.0	186	3.5 ± 1.2

B) Major liver transporters: OATP1B1, OATP1B3, and OCT1

COVID19 Drug	**OATP1B1 (ES)**	**OATP1B1 (EG)**	**OATP1B3 (CCK)**	**OATP1B3 (EG)**	**OCT1**
Azithromycin	211	69	98	137	NI
Baricitinib	124	30	55	47	22.9 ± 18.0
Camostat	251	152	90	135	20.3 ± 21.3
Chloroquine	326	289	192	251	10.7 ± 10.4
Colchicine	345	42	147	365	29.7 ± 38.6
Darunavir	82.5 ± 21.0	6.2 ± 1.4	7.6 ± 1.3	42.9 ± 12.9	6.0 ± 6.6
Favipiravir	635	323	187	182	NI
Fingolimod	228	204	180	254	543
Hydroxychloroquine	475	580	159	820	20.0 ± 15.9
Leflunomide	247	33.3 ± 4.9	21.2 ± 2.0	128	490
Lopinavir	0.6 ± 0.1	0.3 ± 0	4.2 ± 0.6	2.7 ± 1.7	209
Losartan	26.3 ± 14.8	1.4 ± 0.5	4.0 ± 1.0	1.8 ± 2.1	NI
Oseltamivir	933	217	134	203	390
Piclidenoson	17.0 ± 0.1	6.3 ± 0.5	12.9 ± 5.0	9.0 ± 3.9	16.5 ± 10.9
Prazosin	78.9 ± 22.8	47.1 ± 6.2	36.7 ± 2.8	40.6 ± 4.8	1.8 ± 2.0
Remdesivir	36.1 ± 24.4	1.4 ± 0.02	5.5 ± 1.2	0.4 ± 0.04	10.1 ± 0.01
Ribavirin	929	1190	219	NI	NI
Ritonavir	18.7 ± 1.7	0.6 ± 0.15	1.6 ± 0.6	0.7 ± 0.2	3.8 ± 0.1
Ruxolitinib	47.9 ± 3.6	12.7 ± 1.4	19.1 ± 2.9	23.9 ± 11.8	9.7 ± 4.3
Sildenafil	13.3 ± 2.2	3.0 ± 0.8	12.8 ± 0.04	20.7 ± 1.4	19.8 ± 6.4
Tetrandrine	25	24	79	31	8.6
Thalidomide	717	464	NI	448	1776
Tofacitinib	126	39	NI	423	41.4 ± 13.0
Triazavirin	1140	190	102	318	1071
Umifenovir (Arbidol)	17.5 ± 11.9	5.1 ± 0.6	NI	6.5 ± 1.7	1.2 ± 0.1

C) Major kidney transporters: OCT2, MATE1, MATE2, OAT1, and OAT3

COVID19 Drug	OCT2	MATE1	MATE2	OAT1	OAT3
Azithromycin	NI	700	511	58	923
Baricitinib	48	36.0 ± 24.0	6.7 ± 5.6	233	12.7 ± 5.0
Camostat	161	3.4 ± 2.9	2.0 ± 1.3	102	550
Chloroquine	103 ± 45.7	0.8 ± 0.8	0.7 ± 0.2	NI	5923
Colchicine	1015	394	NI	69	942
Darunavir	279	43.8 ± 14.4	30.7 ± 20.2	95	37.9 ± 9.5
Favipiravir	NI	822	914	52	84.2 ± 19.5
Fingolimod	2287	1862	6164	64	1000
Hydroxychloroquine	187	1.9 ± 0.3	0.8 ± 0.1	202	841
Leflunomide	730	9.5 ± 5.5	12.6 ± 4.0	325	4.1a
Lopinavir	385	22.5 ± 4.0	25.1 ± 9.6	141	NI
Losartan	NI	484	752	12a	1.6a
Oseltamivir	445	347	934	90	211
Piclidenoson	40.7 ± 9.4	29.2 ± 19.6	15.2 ± 6.7	NI	8.7 ± 0.9
Prazosin	140	0.5 ± 0.2	2.4 ± 0.9	NI	29.8a
Remdesivir	183	0.4 ± 0.1	15.2 ± 9.7	NI	14.0 ± 1.7
Ribavirin	NI	338	NI	99	1248
Ritonavir	101	0.5 ± 0.3	12.6 ± 8.2	89	99
Ruxolitinib	10.7 ± 3.7	0.7 ± 0.01	3.7 ± 2.3	NI	6.1 ± 0.6
Sildenafil	68.0 ± 20.1	2.4 ± 0.1	14.4 ± 1.3	1002	20.5 ± 3.1
Tetrandrine	1045	1.2 ± 0.2	81	11	45
Thalidomide	335	318	NI	145 ± 26.8	54.6 ± 2.4
Tofacitinib	209	1.0 ± 0.5	68.5 ± 6.2	89	51.6 ± 7.0
Triazavirin	321	543	1042	4.1 ± 0.7	2.3 ± 0.4
Umifenovir (Arbidol)	14.9 ± 4.9	0.7 ± 0.2	4.1 ± 1.6	187	58.6 ± 21.9

IC_{50} (µM)	<= 5	>5-20	>20-40	>40-60	>60-100	>60 or NI

[a]IC_{50} from the literature. NI = No inhibition at the one concentration tested (and thus IC_{50} could not be predicted). Inhibition potencies are expressed as mean ± SD (µM). IC_{50} values for each transporter are based on experimental data (see Methods). Values shown are from two or more independent experiments. When only a single value is shown without a SD, the value represents a predicted IC_{50}. Predicted IC_{50} ($prIC_{50}$) was calculated using the equation: $\mathbf{V} = \mathbf{V_0}/\{1 + [(\mathbf{I})/prIC_{50}]\}$, where **V** and $\mathbf{V_0}$ are the activity with and without inhibitor, respectively, and **I** is the inhibitor concentration.

Table 5.2 Summary of drugs in clinical trials for COVID19 predicted to cause a transporter-mediated DDI.

<u>Intestinal transporters</u> (I_{gut}/IC_{50})

COVID19 drug	FDA approval date	Dose, mg	Transporters inhibited at clinical concentrations	P-gp	BCRP	OATP2B1
Azithromycin	1991	2000	5/11	**593**	**34**	**26**
Baricitinib	2018	4	0/11	0.2	0.4	0.2
Camostat	Not approved	400	2/11	**115**	**17**	NI
Chloroquine	1949	1000	5/11	**375**	**13**	6
Colchicine	1961	1.5	0/11	0.4	0.05	NI
Darunavir	2006	800	6/11	**365**	**57**	**191**
Favipiravir	Not approved	2400	8/11	**1111**	**69**	NI
Fingolimod	2010	0.5	0/11	0.1	NI	0.02
Hydroxychloroquine	1955	800	4/11	**143**	5	7
Leflunomide	1998	100	2/11	2	**327**[a]	**18**
Lopinavir	2000	800	5/11	**2994**[a]	**664**[a]	**7068**[a]
Losartan	1995	150	5/11	**10**	**268**	**518**
Oseltamivir	1999	300	3/11	**87**	3	1
Piclidenoson	Not approved	2	1/11	0.3	0.1	1.3
Prazosin	1976	10	0/11	1.5[a]	0.5	1
Remdesivir	2020	200	5/11	NA	NA	NA
Ribavirin	1998	1200	4/11	**418**	**29**	**12**
Ritonavir	2000	600	7/11	**13871**[a]	**504**[a]	**907**
Ruxolitinib	2011	25	1/11	NI	NI	**19**
Sildenafil	1998	100	4/11	**53**	**270**	**22**
Tetrandrine	Not approved	60	3/11	**102**	3	NI
Thalidomide	1998	400	4/11	**95**	**15**	NI

COVID19 drug	**FDA approval date**	**Dose, mg**	**Transporters inhibited at clinical concentrations**	**P-gp**	**BCRP**	**OATP2B1**
Tofacitinib	2012	10	1/11	1	0.4	NI
Triazavirin	Not approved	250	5/11	**61**	**13**	**252**
Umifenovir	Not approved	200	6/11	**105**	9	**481**

Liver transporters ($I_{u,in,max}/IC_{50}$)

COVID19 drugs	OATP1B1	OATP1B3	OCT1	P-gp	BCRP	OATP2B1
Azithromycin	**2.1**	**1.1**	NI	**8.2**	**0.47**	**0.36**
Baricitinib	0.01	0.01	0.01	0.002	0.003	0.001
Camostat	NC	NC	NC	NC	NC	NC
Chloroquine	0.03	0.04	**0.88**	**0.47**	0.02	0.01
Colchicine	0.004	<0.001	0.005	0.004	<0.001	NI
Darunavir	**1.36**	**0.2**	**1.4**	**0.53**	0.08	**0.28**
Favipiravir	**2.18**	**3.9**	NI	**12.8**	**0.79**	NI
Fingolimod	<0.001	<0.001	<0.001	<0.001	NI	<0.001
Hydroxychloroquine	0.02	0.01	**0.46**	**0.18**	0.01	0.01
Leflunomide	NC	NC	NC	NC	NC	NC
Lopinavir	**13.2**	**1.46**	0.02	**2.32**[a]	**0.52**[a]	**5.48**[a]
Losartan	**0.21**	**0.16**	NI	0.002	0.06	**0.12**
Oseltamivir	**0.11**	**0.12**	0.06	**0.55**	0.02	0.004
Piclidenoson	0.05*	0.03*	0.02*	0.006	0.003	**0.11***
Prazosin	0.002	0.002	0.04	0.001[a]	<0.001	0.001
Remdesivir	**0.78**	**2.72**	**0.11**	0.08	0.04	**0.31**
Ribavirin	0.01	NI	NI	**0.34**	0.02	0.01
Ritonavir	**12.7**	**11.2**	**2.03**	**31.9**[a]	**1.16**[a]	**2.08**
Ruxolitinib	0.01	0.008	0.02	NI	NI	0.01
Sildenafil	**0.1**	0.01	0.01	0.02	0.09	0.01
Tetrandrine	**0.11***	0.09*	**0.31***	**0.7***	0.02*	NI
Thalidomide	**0.1**	**0.1**	0.03	**0.71**	**0.11**	NI
Tofacitinib	0.03	0.003	0.03	0.01	0.004	NI
Triazavirin	0.02	0.01	0.004	0.06	0.01	**0.26**
Umifenovir	**0.57**	**0.44**	**2.39**	**0.18**	0.02	**0.83**

<u>Kidney transporters</u> ($C_{u,max}/IC_{50}$)

COVID19 drug	OCT2	MATE1	MATE2-K	OAT1	OAT3	P-gp	BCRP
Azithromycin	NI	0.004	0.005	0.04	0.003	**0.14**	0.01
Baricitinib	0.001	0.002	0.01	<0.001	0.005	<0.001	0.001
Camostat	NC	NC	NC	NC	NC	NC	NC
Chloroquine	0.003	**0.46**	**0.5**	NI	<0.001	0.02[a]	0.001
Colchicine	<0.001	<0.001	NI	<0.001	<0.001	<0.001	<0.001
Darunavir	0.002	0.01	0.02	0.007	0.02	0.04	0.006
Favipiravir	NI	**0.33**	**0.3**	**5.2**	**3.21**	**4.9**	**0.3**
Fingolimod	<0.001	<0.001	<0.001	<0.001	<0.001	<0.001	NI
Hydroxychloroquine	0.007	**0.64**	**1.57**	0.006	0.001	0.02	0.001
Leflunomide	NC	NC	NC	NC	NC	NC	NC
Lopinavir	0.001	0.02	0.01	0.003	NI	**0.22[a]**	0.05[a]
Losartan	NI	<0.001	<0.001	0.003[a]	0.02[a]	<0.001	0.007
Oseltamivir	<0.001	<0.001	<0.001	0.002	0.001	0.004	<0.001
Piclidenoson	0.001*	0.001*	0.003*	NI	0.005*	0.001*	<0.001*
Prazosin	<0.001	0.01	0.002	NI	<0.001[a]	<0.001[a]	<0.001
Remdesivir	0.006	**2.48**	0.05	NI	0.08	0.08	0.04
Ribavirin	NI	0.03	NI	**0.11**	0.01	**0.23**	0.02
Ritonavir	0.005	**0.66**	0.02	0.02[a]	0.003	**1.27[a]**	0.05[a]
Ruxolitinib	0.003	0.04	0.01	NI	0.005	NI	NI
Sildenafil	0.001	0.02	0.003	<0.001	0.002	0.003	0.02
Tetrandrine	<0.001*	0.09*	0.001*	0.01*	0.002*	0.03*	0.001*
Thalidomide	0.01	0.01	NI	0.03	0.08	0.07	0.01
Tofacitinib	0.001	**0.12**	0.002	0.001	0.002	0.001	<0.001
Triazavirin	0.003	0.002	0.001	**0.26**	**0.45**	0.01	0.003
Umifenovir	0.006	**0.13**	0.02	0.001	0.002	0.006	0.001

[a]IC_{50} is from literature.
*Protein binding not reported so $f_{u,p}$ assumed to be 1.

I/IC_{50} for each organ (intestine, liver, and kidney) and their respective transporters. Values shown in **bold** meet FDA criteria to consider a clinical DDI study. Predictions are expressed as estimated clinical concentration relative to *in vitro* inhibition potency. NI, no inhibition; NA, not applicable; NC, not calculated due to missing C_{max} values.

Table 5.3 Summary table of electronic health record analyses comparing endogenous biomarkers in patients prescribed predicted clinical inhibitors of transporters versus patients not prescribed predicted clinical inhibitors.

Analysis	Total patients		Matched patients					
Sildenafil	**On drug (N)**	**Off drug (N)**	**Ratio**	**On drug (N)**	**Off drug (N)**	**Average SUA On/Off drug (mg/dL)**	**Median SUA On/Off drug (mg/dL)**	**p-value**
Main analysis	636	53808	1:5	636	3180	6.84 / 5.94	6.6 / 5.7	< 2.2E-16
1) Criteria: exclude lab values taken more than one year after first medication order start date	319	53808	1:5	319	1595	6.97 / 5.91	6.7 / 5.7	2.2E-13
2) Criteria: exclude patients without a diagnosis of pulmonary hypertension	175	1483	1:5	175	875	7.35 / 6.19	6.9 / 5.6	6.1E-07
3) Criteria: exclude lab values taken before diagnosis of pulmonary hypertension	152	1017	1:5	152	760	7.41 / 6.31	7.2 / 5.7	6.1E-06
4) Criteria: only include Sildenafil medication orders with dose > 25mg in medication name	183	53808	1:5	183	915	6.86 / 6.1	6.8 / 5.9	1.2E-08
5) Criteria: exclude male patients	76	27659	1:5	76	380	7.29 / 5.04	7 / 4.6	2.9E-11

Analysis	Total patients		Matched patients					
Ritonavir	**On drug (N)**	**Off drug (N)**	**Ratio**	**On drug (N)**	**Off drug (N)**	**Average On/Off drug (mg/dL)**	**Median On/Off drug (mg/dL)**	**p-value**
Triglyceride	782	1249	1:1	782	782	252 / 162	156 / 124	7.8E-12
LDL cholesterol	719	1058	1:1	719	719	106 / 99.5	101 / 96	0.0033
Total cholesterol	803	1410	1:1	803	803	190 / 168	182 / 165	3.1E-13
Darunavir	**On drug (N)**	**Off drug (N)**	**Ratio**	**On drug (N)**	**Off drug (N)**	**Average On/Off drug (mg/dL)**	**Median On/Off drug (mg/dL)**	**p-value**
Triglyceride	386	1407	1:2	386	772	180 / 160	137 / 118	0.00022
LDL cholesterol	357	1234	1:2	357	714	105 / 98.7	100 / 95	0.0077
Total cholesterol	364	1572	1:2	364	728	183 / 170	180 / 166	5.18E-06
Ritonavir and/or Lopinavir	**On drug (N)**	**Off drug (N)**	**Ratio**	**On drug (N)**	**Off drug (N)**	**Average On/Off drug (mg/dL)**	**Median On/Off drug (mg/dL)**	**p-value**
Total bilirubin	1089	1697	1:1	1089	1089	1.39 / 0.91	0.9 / 0.7	< 2.2E-16

SUA, serum uric acid; LDL, low-density lipoproteins. Sildenafil is predicted to be a clinical inhibitor of BCRP; ritonavir and darunavir are predicted to be clinical inhibitors of OCT1; ritonavir and lopinavir are predicted to be clinical inhibitors of OATP1B1 and OATP1B3.

Table 5.4 Table of electronic health record analyses comparing serum creatinine levels in patients prescribed hydroxychloroquine (HCQ) and chloroquine (CQ) versus patients not prescribed hydroxychloroquine and chloroquine (control).

Analysis		Creatinine above normal level	total	% Creatinine above normal level	X-squared	P-value
Main	on HCQ/CQ	90	584	15.41%	5.07	0.024
Main	control	134	1168	11.47%		
1	on HCQ/CQ	74	520	14.23%	12.26	4.6E-04
1	control	87	1040	8.37%		

In the main analysis, patients were matched by age, sex, race, ethnicity, and outcome (mortality). In analysis 1, patients with chronic kidney disease were excluded and patients were matched by age, sex, race, ethnicity, outcome (mortality), and medication indication. Chi-squared tests were performed to compare the percent of patients who have creatinine levels within the upper limit of normal range in the on drug group and the control (off) drug group.

Supplemental Table 5.1 Results of screening 25 drugs used in COVID19 clinical trials at one concentration across eleven transporters.

Drugs used in COVID19 Clinical trials	Tetrandrine	Thalidomide	Tofacitinib	Triazavirin	Umifenovir
Purpose	Anti-inflammatory	Anti-inflammatory	Anti-inflammatory	Anti-microbial	Anti-microbial
Screening concentration	10 µM	100 µM	100 µM	100 µM	100 µM
P-gp (NMN)	90.2	60.5	36.0	58.1	92.3
BCRP (CCK)	8.1	19.0	25.3	23.6	35.0
OATP2B1 (ES)	-22.9	-28.4	-32.3	83.5	80.4
OATP1B1 (ES)	36.9	12.8	46.3	9.2	80.9
OATP1B1 (EG)	31.8	19.2	77.9	37.3	99.9
OATP1B3 (CCK)	24.6	-63.5	1.0	22.0	9.1
OATP1B3 (EG)	41.9	31.7	33.2	41.5	98.9
OCT1 (Metformin)	69.4	6.9	55.5	-3.1	110.4
OCT2 (Metformin)	-5.9	17.6	27.6	21.1	86.2
MATE1 (Metformin)	72.8	38.9	86.2	7.7	116.2
MATE2 (Thiamine)	27.0	4.0	63.9	30.3	115.3
OAT1 (PAH)	24.8	60.0	35.7	95.2	3.9
OAT3 (ES)	20.0	61.8	69.2	99.3	70.7

Drugs used in COVID19 Clinical trials	Remdesivir	Ribavirin	Ritonavir	Ruxolitinib	Sildenafil
Purpose	Anti-microbial	Anti-microbial	Anti-microbial	Anti-inflammatory	Anti-inflammatory
Screening concentration	100 µM	100 µM	100 µM	100 µM	100 µM
P-gp (NMN)	88.0	67.9	91.4	-7.8	86.6
BCRP (CCK)	53.8	12.9	82.7	-3.3	58.7
OATP2B1 (ES)	99.1	6.7	90.2	83.5	81.6
OATP1B1 (ES)	63.0	10.2	78.2	55.9	86.2
OATP1B1 (EG)	99.7	8.4	98.9	98.8	100.8
OATP1B3 (CCK)	106.7	53.2	103.0	99.8	97.2
OATP1B3 (EG)	89.1	-1.5	108.3	87.9	93.6
OCT1 (Metformin)	78.9	-7.7	87.8	84.5	74.9
OCT2 (Metformin)	30.8	-8.2	46.2	95.7	62.5
MATE1 (Metformin)	85.8	-4.5	84.6	84.6	101.2
MATE2 (Thiamine)	68.6	0.0	85.4	97.7	103.3
OAT1 (PAH)	-87.9	31.1	33.6	-3.8	-38.9
OAT3 (ES)	89.1	8.1	55.0	99.6	88.3

Drugs used in COVID19 Clinical trials	Leflunomide	Lopinavir	Losartan	Oseltamivir	Piclidenoson	Prazosin
Purpose	Anti-inflammatory	Anti-microbial	Other	Anti-microbial	Anti-microbial	Anti-inflammatory
Screening concentration	100 µM	100 µM	100 µM	100 µM	100 µM	100 µM
P-gp (NMN)	13.7	90.8	43.9	69.5	66.5	79.1
BCRP (CCK)	33.5	79.6	88.9	7.2	48.8	31.1
OATP2B1 (ES)	76.7	95.3	88.6	1.7	85.5	48.7
OATP1B1 (ES)	30.2	93.4	82.6	10.1	84.6	44.1
OATP1B1 (EG)	93.3	100.4	101.8	34.1	101.1	93.2
OATP1B3 (CCK)	94.5	104.4	99.7	69.2	91.7	82.8
OATP1B3 (EG)	76.2	106.8	105.7	57.4	111.3	103.4
OCT1 (Metformin)	21.8	41.6	0.1	26.3	81.3	89.5
OCT2 (Metformin)	5.9	15.1	-12.9	12.7	68.3	37.7
MATE1 (Metformin)	78.3	74.8	28.6	36.5	85.0	87.8
MATE2 (Thiamine)	40.1	43.8	28.5	24.5	85.0	114.6
OAT1 (PAH)	-14.0	14.6	88.9	31.2	-65.9	-55.5
OAT3 (ES)	98.9	-19.0	99.9	35.2	99.0	81.7

Drugs used in COVID19 Clinical trials	Colchicine	Darunavir	Favipiravir	Fingolimod	Hydroxychloroquine
Purpose	Anti-inflammatory	Anti-microbial	Anti-microbial	Anti-inflammatory	Anti-microbial
Screening concentration	100 µM	100 µM	100 µM	100 µM	100 µM
P-gp (NMN)	70.5	86.3	64.4	53.0	81.6
BCRP (CCK)	23.8	49.3	10.1	-21.5	6.3
OATP2B1 (ES)	-7.1	87.3	-17.2	29.0	9.8
OATP1B1 (ES)	23.5	57.6	14.2	31.9	18.2
OATP1B1 (EG)	76.2	99.9	25.5	35.5	15.9
OATP1B3 (CCK)	66.2	110.8	58.1	59.3	63.4
OATP1B3 (EG)	37.4	97.0	61.5	49.1	18.9
OCT1 (Metformin)	61.1	84.2	-2.0	20.0	80.2
OCT2 (Metformin)	2.7	21.3	-10.1	-2.5	30.3
MATE1 (Metformin)	33.3	74.4	19.1	10.5	108.3
MATE2 (Thiamine)	0.0	22.6	24.8	8.8	132.5
OAT1 (PAH)	43.1	31.8	54.7	44.7	0.4
OAT3 (ES)	10.5	55.8	38.6	10.0	11.6

Drugs used in COVID19 Clinical trials	Azithromycin	Baricitinib	Camostat	Chloroquine
Purpose	Anti-microbial	Anti-inflammatory	Anti-microbial	Anti-microbial
Screening concentration	50 µM	50 µM	100 µM	100 µM
P-gp (NMN)	74.0	22.3	73.9	83.4
BCRP (CCK)	13.7	31.8	29.6	14.4
OATP2B1 (ES)	12.4	21.6	-64.9	8.1
OATP1B1 (ES)	20.0	30.0	29.8	24.6
OATP1B1 (EG)	45.4	67.5	42.9	27.8
OATP1B3 (CCK)	56.5	76.4	83.4	57.3
OATP1B3 (EG)	46.4	89.4	74.0	49.4
OCT1 (Metformin)	-2.8	67.2	76.4	91.5
OCT2 (Metformin)	-25.5	47.5	34.0	63.6
MATE1 (Metformin)	12.8	49.1	101.6	113.8
MATE2 (Thiamine)	23.0	88.0	93.4	125.9
OAT1 (PAH)	21.5	-25.4	26.9	0.3
OAT3 (ES)	5.6	84.7	16.8	1.8

Values shown are average percent inhibition from two or three independent studies. Negative values indicate no inhibition, where the uptake was greater than DMSO vehicle only. Green indicates that the drug has been shown to be a substrate of the transporter in the literature. Blue indicates that the drug has reported IC_{50} values or has been shown to be an inhibitor of the transporter in the literature.

Supplemental Table 5.2 Pharmacokinetic characteristics for the 25 drugs used in computing the [I] value for I/IC_{50} determinations.

Drug	Dose (mg)	Protein binding (%)	Rb	I_{gut} (μM)	$I_{in,max}$ (μM)	C_{max} (μM)	References/PMID
Azithromycin	2000	12	ND (1)	10681	168	2.80	2154441, 17328583
Baricitinib	4	50	1.32	43	0.64	0.14	Drug label, 24965573, 31832202
Camostat	400	25.8	ND (1)	4016	ND	ND	Drug label
Chloroquine	1000	61	5	7503	24.1	0.92	24687509, 6753885, 6849768
Colchicine	1.5	39	ND (1)	15	0.25	0.02	Drug label, 8930773
Darunavir	800	95	0.58	5843	168	12.7	Drug label, 24644095, 24951533
Favipiravir	2400	54	ND (1)	61106	1530	587	30724789, 26798032
Fingolimod	0.5	99	ND (1)	7	0.10	0.002	Drug label, 15089811
Hydroxy-chloroquine	800	50	7.2	7384	18.3	2.44*	19188392, 3179169, 8803904
Leflunomide	100	99	ND (1)	1480	ND	ND	Drug Bank
Lopinavir	800	98	0.44	5089	197	18.8	Drug label, 15497688
Losartan	150	98.7	ND (1)	1298	22.7	2.65*	Drug label, 17220048
Oseltamivir	300	42	1.42	3841	42.0	0.28	Drug label, 17456583, 23507284
Piclidenoson	2	ND	ND (1)	16	0.29	0.04	15516022
Prazosin	10	97	0.7	104	2.47	0.17*	7398734, 11782904, 7285477
Remdesivir	200	87.9	ND (1)	NA	9.0	9.0	Drug label, EMA compassionate use summary

Drug	Dose (mg)	Protein binding (%)	Rb	I_{gut} (μM)	$I_{in,max}$ (μM)	C_{max} (μM)	References/PMID
Ribavirin	1200	0	60	19656	16.1	11.0	Drug label, 18931138, 2444379
Ritonavir	600	98	0.14	3329	382	15.3	Drug label, 9812178
Ruxolitinib	25	97	ND (1)	326	5.97	0.93	Drug label, 21257798
Sildenafil	100	96	2.12	843	7.32	1.18	Drug label, 11879255, 11879254
Tetrandrine	60	ND	2.33	385	2.66	0.11	25746132, 29100757
Thalidomide	400	60.5	0.91	6196	117	10.9	9499573, 11402635
Tofacitinib	10	40	1	128	2.17	0.20	Drug label, 27129117
Triazavirin	250	95	ND (1)	4382	88.7	21.0	Drug website
Umifenovir	200	89.2	ND (1)	1676	26.7	0.87	32166483, 19446151

*C_{max} scaling factors were used for losartan (1.5), hydroxychloroquine (2), and prazosin (2). ND, not determined; NA, not applicable.

Supplemental Table 5.3 Demographics for on and off groups used in EHR analyses.

Analysis	On drug	Off drug	p-value
Sildenafil			
Main analysis			
% Male	88.1	89.6	0.281
Average age (years)	58.8	58.1	0.22
1) Criteria: exclude lab values taken more than 1 year after first medication order start date			
% Male	87.1	88.5	0.546
Average age (years)	57.8	57.1	0.429
2) Criteria: exclude patients without a diagnosis of pulmonary hypertension			
% Male	58.3	57.8	0.978
Average age (years)	53.9	53.9	0.954
3) Criteria: exclude lab values taken before diagnosis of pulmonary hypertension			
% Male	52.6	52.8	1
Average age (years)	53.2	54.6	0.324
4) Criteria: only include Sildenafil medication orders with dose > 25mg in medication name			
% Male	99.5	99.5	1
Average age (years)	61.3	61.3	1
5) Criteria: exclude male patients			
Average age (years)	52.7	52.7	1
Ritonavir			
Triglyceride			
% Male	83.8	85.9	0.259
Average age (years)	45.9	46.4	0.441
% of patients with statin prescription	7.29	6.65	NA
LDL cholesterol			
% Male	82.6	84	0.524
Average age (years)	46.2	46.5	0.634
% of patients with statin prescription	8.21	8.07	NA
Total cholesterol			
% Male	83.3	85.9	0.167
Average age (years)	45.6	46.1	0.302
% of patients with statin prescription	7.10	6.48	NA

Analysis	On drug	Off drug	p-value
Darunavir			
Triglyceride			
% Male	88.1	85.9	0.344
Average age (years)	51.2	50.2	0.137
% of patients with statin prescription	20.5	8.68	NA
LDL cholesterol			
% Male	88	85.3	0.273
Average age (years)	51.3	50.3	0.131
% of patients with statin prescription	21.3	9.66	NA
Total cholesterol			
% Male	87.9	85.7	0.365
Average age (years)	51.2	50.8	0.593
% of patients with statin prescription	20.9	9.07	NA
Ritonavir and/or Lopinavir			
Total bilirubin			
% Male	83.2	83.7	0.818
Average age (years)	45.7	45.7	0.882
Hydroxychloroquine, Chloroquine			
Main Analysis			
% Male	53.3	55.7	0.240
Average age (years)	63.4	64.0	0.299
1) Criteria: exclude patients with chronic renal disease			
% Male	56.3	56.3	0.513
Average age (years)	62.4	61.9	0.601

Percent male and average age were computed for all analyses. Percent of patients with a statin prescription was computed for ritonavir and darunavir analyses.

Supplemental Table 5.4 Comparison of IC_{50} values from this study to data in the literature.

Drug	Transporter (substrate used for this study)	IC_{50} from this study (µM)	IC_{50} from the literature (substrate used)	PMID
Darunavir	OATP1B1 (ES)	82.5 ± 21.0	3.5 µM (CGamF)	20102298
Lopinavir	OATP1B1 (ES)	0.6 ± 0.1	0.5 µM (CGamF)	20102298
Ritonavir	OATP1B1 (ES)	18.7 ± 1.7	1.6 µM (CGamF)	20102298
Sildenafil	OATP1B1 (ES)	13.3 ± 2.2	1.5 µM (Bosentan)	17496208
Tofacitinib	OATP1B1 (ES)	126 (predicted)	low potential inhibition	NDA 203214
Darunavir	OATP1B1 (EG)	6.2 ± 1.4	3.5 µM (CGamF)	20102298
Lopinavir	OATP1B1 (EG)	0.3 ± 0	0.5 µM (CGamF)	20102298
Ritonavir	OATP1B1 (EG)	0.6 ± 0.15	0.71 µM (CGamF)	12490595
Sildenafil	OATP1B1 (EG)	3.0 ± 0.8	1.5 µM (Bosentan)	17496208
Tofacitinib	OATP1B1 (EG)	39 (predicted)	low potential inhibition	NDA 203214
Darunavir	OATP1B3 (CCK)	7.6 ± 1.3	4.8 µM (CGamF)	20102298
Lopinavir	OATP1B3 (CCK)	4.2 ± 0.6	2 µM (CGamF)	20102298
Ritonavir	OATP1B3 (CCK)	1.6 ± 0.6	3.6 µM (CGamF)	20102298
Sildenafil	OATP1B3 (CCK)	12.8 ± 0.04	4 µM (Bosentan)	17496208
Darunavir	OATP1B3 (EG)	42.9 ± 12.9	4.8 µM (CGamF)	20102298
Lopinavir	OATP1B3 (EG)	2.7 ± 1.7	2 µM (CGamF)	20102298
Ritonavir	OATP1B3 (EG)	0.7 ± 0.2	3.6 µM (CGamF)	20102298
Sildenafil	OATP1B3 (EG)	20.7 ± 1.4	4 µM (Bosentan)	17496208

Drug	Transporter (substrate used for this study)	IC_{50} from this study (μM)	IC_{50} from the literature (substrate used)	PMID
Chloroquine	OCT1 (Metformin)	10.7 ± 10.4	20% inhibition (ASP+) at 50 μM	29061131
Darunavir	OCT1 (Metformin)	6.0 ± 6.6	15.9 μM (TEA)	25914645
Ritonavir	OCT1 (Metformin)	3.8 ± 0.1	5.18 μM (TEA); 14 μM (MPP+)	10681378; 18490433
Prazosin	OCT1 (Metformin)	1.8 ± 2.0	1.56 μM (YM155)	19833842
Chloroquine	OCT2 (Metformin)	103 ± 45.7	1096 μM (MPP+)	19002438
Prazosin	OCT2 (Metformin)	140 (predicted)	80.4 μM (YM155)	19833842
Tofacitinib	OCT2 (Metformin)	209 (predicted)	150 μM (creatinine)	27129125
Chloroquine	MATE1 (Metformin)	0.8 ± 0.8	2.5 μM (Metformin)	21518836
Ritonavir	MATE1 (Metformin)	0.5 ± 0.3	13.9 μM (TEA); 15.4 μM (Metformin); 3.1 μM (MPP+); 4.4 μM (ASP+); 0.08 μM (Metformin)	20053795; 31034908; 23241029
Ritonavir	MATE2 (Thiamine)	12.6 ± 8.2	90 μM (MPP+); 23.7 μM (ASP+)	31034908; 23241029
Camostat	MATE1 (Metformin)	3.4 ± 2.9	2.9 μM (ASP+)	23241029
Camostat	MATE2 (Thiamine)	2.0 ± 1.3	12.7 μM (ASP+)	23241029
Prazosin	MATE1 (Metformin)	0.5 ± 0.2	1.6 μM (ASP+)	23241029
Prazosin	MATE2 (Thiamine)	2.4 ± 0.9	38.4 μM (ASP+)	23241029

Supplemental Table 5.5 Expansion of Table 5.2, showing DDI predictions for each drug with I/IC_{50} for each organ (intestine, liver, and kidney) and their respective transporters.

	Thalidomide	**Tofacitinib**	**Triazavirin**	**Umifenovir**
FDA approval date	1998	2012	Not approved	Not approved
Dose, mg	400	10	250	200
P-gp[1]	**95**	1	**61**	**105**
BCRP[1]	**15**	0.4	**13**	9
OATP2B1[1]	NI	NI	**252**	**481**
OATP1B1[2]	**0.1**	0.03	0.02	**0.57**
OATP1B3[2]	**0.1**	0.003	0.01	**0.44**
OCT1[2]	0.03	0.03	0.004	**2.39**
P-gp[2]	**0.71**	0.01	0.06	**0.18**
BCRP[2]	**0.11**	0.004	0.01	0.02
OATP2B1[2]	NI	NI	**0.26**	**0.83**
OCT2[3]	0.01	0.001	0.003	0.006
MATE1[3]	0.01	**0.12**	0.002	**0.13**
MATE2-K[3]	NI	0.002	0.001	0.02
OAT1[3]	0.03	0.001	**0.26**	0.001
OAT3[3]	0.08	0.002	**0.45**	0.002
P-gp[3]	0.07	0.001	0.01	0.006
BCRP[3]	0.01	0.0004	0.003	0.001
# of transporters inhibited at clinical concentrations	4/11	1/11	5/11	6/11

	Ribavirin	Ritonavir	Ruxolitinib	Sildenafil	Tetrandrine
FDA approval date	1998	2000	2011	1998	Not approved
Dose, mg	1200	600	25	100	60
P-gp[1]	**418**	**13871[a]**	NI	**53**	**102**
BCRP[1]	**29**	**504[a]**	NI	**270**	3
OATP2B1[1]	**12**	**907**	**19**	**22**	NI
OATP1B1[2]	0.01	**12.7**	0.01	**0.1**	**0.11***
OATP1B3[2]	NI	**11.2**	0.008	0.01	0.09*
OCT1[2]	NI	**2.03**	0.02	0.01	**0.31***
P-gp[2]	**0.34**	**31.9[a]**	NI	0.02	**0.7***
BCRP[2]	0.02	**1.16[a]**	NI	0.09	NI
OATP2B1[2]	0.01	**2.08**	0.01	0.01	0.08*
OCT2[3]	NI	0.003	0.003	0.001	0.0001*
MATE1[3]	0.03	**0.66**	0.04	0.02	0.09*
MATE2-K[3]	NI	0.02	0.01	0.003	0.001*
OAT1[3]	**0.11**	0.003	NI	0.00005	0.01*
OAT3[3]	0.01	0.003	0.005	0.002	0.002*
P-gp[3]	**0.23**	**1.27[a]**	NI	0.003	0.03*
BCRP[3]	0.02	0.05[a]	NI	0.02	0.001*
# of transporters inhibited at clinical concentrations	4/11	7/11	1/11	4/11	3/11

	Losartan	**Oseltamivir**	**Piclidenoson**	**Prazosin**	**Remdesivir**
FDA approval date	1995	1999	Not approved	1976	October 2020
Dose, mg	150	300	2	10	200
P-gp[1]	**10**	**87**	0.3	1.5[a]	NA
BCRP[1]	**268**	3	0.1	0.5	NA
OATP2B1[1]	**518**	1	1.3	1	NA
OATP1B1[2]	**0.21**	**0.11**	0.05*	0.002	**0.78**
OATP1B3[2]	**0.16**	**0.12**	0.03*	0.002	**2.72**
OCT1[2]	NI	0.06	0.02*	0.04	**0.11**
P-gp[2]	0.002	**0.55**	0.006	0.001[a]	0.08
BCRP[2]	0.06	0.02	0.003	0.0003	0.04
OATP2B1[2]	**0.12**	0.004	**0.11***	0.001	**0.31**
OCT2[3]	NI	0.0004	0.001*	0.00004	0.006
MATE1[3]	0.0001	0.0005	0.001*	0.01	**2.48**
MATE2-K[3]	0.00005	0.0002	0.003*	0.002	0.07
OAT1[3]	0.003[a]	0.002	NI	NI	NI
OAT3[3]	0.02[a]	0.001	0.005*	0.0002[a]	0.08
P-gp[3]	0.0003	0.004	0.001*	0.0001[a]	0.08
BCRP[3]	0.007	0.0001	0.0004*	0.00002	0.04
# of transporters inhibited at clinical concentrations	5/11	3/11	1/11	0/11	5/11

	Fingolimod	Hydroxychloroquine	Leflunomide	Lopinavir
FDA approval date	2010	1955	1998	2000
Dose, mg	0.5	800	100	800
P-gp[1]	0.1	**143**	2	**2994[a]**
BCRP[1]	NI	5	**327[a]**	**664[a]**
OATP2B1[1]	0.02	7	**18**	**7068[a]**
OATP1B1[2]	0.00001	0.02	NC	**13.2**
OATP1B3[2]	0.000004	0.01	NC	**1.46**
OCT1[2]	0.000002	**0.46**	NC	0.02
P-gp[2]	0.00001	**0.18**	NC	**2.32[a]**
BCRP[2]	NI	0.01	NC	**0.52[a]**
OATP2B1[2]	0.000003	0.01	NC	**5.48[a]**
OCT2[3]	0.00000001	0.007	NC	0.001
MATE1[3]	0.00000001	**0.64**	NC	0.02
MATE2-K[3]	0.000000003	**1.57**	NC	0.01
OAT1[3]	0.0000003	0.006	NC	0.003
OAT3[3]	0.00000002	0.001	NC	NI
P-gp[3]	0.0000002	0.02	NC	**0.22[a]**
BCRP[3]	NI	0.001	NC	0.05[a]
# of transporters inhibited at clinical concentrations	0/11	4/11	2/11	5/11

	Camostat	Chloroquine	Colchicine	Darunavir	Favipiravir
FDA approval date	Not approved	1949	1961	2006	Not approved
Dose, mg	400	1000	1.5	800	2400
P-gp[1]	**115**	**375**	0.4	**365**	**1111**
BCRP[1]	**17**	**13**	0.05	**57**	**69**
OATP2B1[1]	NI	6	NI	**191**	NI
OATP1B1[2]	NC	0.03	0.004	**1.36**	**2.18**
OATP1B3[2]	NC	0.04	0.0004	**0.2**	**3.9**
OCT1[2]	NC	**0.88**	0.005	**1.4**	NI
P-gp[2]	NC	**0.47**	0.004	**0.53**	**12.8**
BCRP[2]	NC	0.02	0.0005	0.08	**0.79**
OATP2B1[2]	NC	0.01	NI	**0.28**	NI
OCT2[3]	NC	0.003	0.00001	0.002	NI
MATE1[3]	NC	**0.46**	0.00003	0.01	**0.33**
MATE2-K[3]	NC	**0.5**	NI	0.02	**0.3**
OAT1[3]	NC	NI	0.0001	0.007	**5.2**
OAT3[3]	NC	0.0001	0.00001	0.02	**3.21**
P-gp[3]	NC	0.02	0.0002	0.04	**4.9**
BCRP[3]	NC	0.001	0.00003	0.006	**0.3**
# of transporters inhibited at clinical concentrations	2/11	5/11	0/11	6/11	8/11

	Azithromycin	Baricitinib
FDA approval date	1991	2018
Dose, mg	2000	4
P-gp[1]	**593**	0.2
BCRP[1]	**34**	0.4
OATP2B1[1]	**26**	0.2
OATP1B1[2]	**2.1**	0.01
OATP1B3[2]	**1.1**	0.01
OCT1[2]	NI	0.01
P-gp[2]	**8.2**	0.002
BCRP[2]	**0.47**	0.003
OATP2B1[2]	**0.36**	0.001
OCT2[3]	NI	0.001
MATE1[3]	0.004	0.002
MATE2-K[3]	0.005	0.01
OAT1[3]	0.04	0.0003
OAT3[3]	0.003	0.005
P-gp[3]	**0.14**	0.0004
BCRP[3]	0.01	0.001
# of transporters inhibited at clinical concentrations	5/11	0/11

[a]Value from literature.
*Protein binding not reported in the literature so $f_{u,p}$ was assumed to be 1.
[1]I_{gut}/IC_{50}
[2]$I_{u,in,max}/IC_{50}$
[3]$C_{u,max}/IC_{50}$
Values in blue are based on predicted IC_{50} values. Values in **bold** meet FDA criteria to consider a clinical DDI study. NI, no inhibition; NA, not applicable; NC, not calculated due to missing C_{max} value.

Supplemental Table 5.6 Evidence from the literature on potential biomarkers of transporter-mediated DDIs.

Drug	Predicted to cause DDI for which transporters? (I=intestine; L=Liver; K=Kidney)	Evidence for transporter mediated DDI	Reference
Azithromycin	P-gp (I, L, K), BCRP (I, L), OATP2B1 (I, L), OATP1B1, OATP1B3	Increased plasma levels of drugs that are substrates of P-gp (e.g. fexofenadine and ximelagatran)	(*26*, *50*)
Chloroquine	P-gp (I, L), BCRP (I), OCT1, MATE1, MATE2	(i) Increased toxicity of azithromycin (P-gp substrate) (ii) Increased metformin level (MATE1, MATE2 substrate) (iii) Decreased creatinine clearance. Potentially due to inhibition of MATE1 and MATE2.	(i) (*36*); (ii) (*51*); (iii) (*52*, *53*)
Hydroxychloroquine	P-gp (I, L), OCT1, MATE1, MATE2		
Darunavir	P-gp (I, L), BCRP (I), OATP2B1 (I, L), OATP1B1, OATP1B3, OCT1	(i) Lopinavir/ritonavir or lopinavir/darunavir increased plasma levels of rosuvastatin (OATPs and BCRP substrates) and fexofenadine (P-gp substrate). (ii) Increased bilirubin levels. Potentially due to inhibition of OATP1B1, OATP1B3. (iii) Lopinavir, ritonavir and darunavir increased cholesterol, LDL and triglyceride levels. Potentially phenocopying the effect of OCT1 reduce function variants and knockout mice. (iv) Remdesivir increased serum creatinine, reduced creatinine clearance. Potentially due to inhibition of MATE1. (v) Remdesivir increased bilirubin levels. Potentially due to inhibition of OATP1B1, OATP1B3.	(i) (*28*-*30*) (ii) (*54*-*57*) (iii) (*58*-*60*) (iv, v) (*61*)
Lopinavir	P-gp (I, L, K), BCRP (I, L), OATP2B1 (I, L), OATP1B1, OATP1B3		
Ritonavir	P-gp (I, L, K), BCRP (I, L), OATP2B1 (I, L), OATP1B1, OATP1B3, OCT1, MATE1		
Remdesivir	OATP2B1 (L), OATP1B1, OATP1B3, OCT1, MATE1		
Umifenovir (Arbidol)	P-gp (I, L), OATP2B1 (I, L), OATP1B1, OATP1B3, OCT1, MATE1		
Sildenafil	P-gp (I), BCRP (I), OATP2B1 (L), OATP1B1	Increased uric acid. Potentially due to inhibition of BCRP.	(*43*, *44*, *62*)

Drug	Predicted to cause DDI for which transporters? (I=intestine; L=Liver; K=Kidney)	Evidence for transporter mediated DDI	Reference
Favipiravir	P-gp (I, L, K), BCRP (I, L, K), OATP1B1, OATP1B3, MATE1, MATE2, OAT1, OAT3	Increased uric acid. Potentially due to inhibition of BCRP, OAT1 and OAT3.	(*63, 64*)

Supplemental Table 5.7 Sensitivity analyses comparing patients prescribed sildenafil vs patients not prescribed sildenafil at a 1:5, 1:10, and 1:20 ratio between the “on” drug and “off” drug groups.

Analysis	Total patients		1:5		1:10		1:20	
Sildenafil	On drug	Off drug	On drug	Off drug	On drug	Off drug	On drug	Off drug
Main analysis	636	53808						
P-value			< 2.2E-16		< 2.2E-16		< 2.2E-16	
Number of patients (#)			636	3180	636	6360	636	12720
Average SUA (mg/dL)			6.84	5.94	6.84	5.94	6.84	5.94
Sub-analysis #1	319	53808						
P-value			2.16E-13		5.85E-14		1.86E-15	
Number of patients (#)			319	1595	319	3190	319	6380
Average SUA (mg/dL)			6.97	5.91	6.97	5.94	6.97	5.92
Sub-analysis #2	175	1483						
P-value			6.12E-07		NA		NA	
Number of patients (#)			175	875	NA	NA	NA	NA
Average SUA (mg/dL)			7.35	6.19	NA	NA	NA	NA
Sub-analysis #3	152	1017						
P-value			6.14E-06		NA		NA	
Number of patients (#)			152	760	NA	NA	NA	NA
Average SUA (mg/dL)			7.41	6.31	NA	NA	NA	NA

Analysis	Total patients		1:5		1:10		1:20	
Sub-analysis #4	183	53808						
P-value			1.15E-08		9.11E-09		2.76E-09	
Number of patients (#)			183	915	183	1830	183	3660
Average SUA (mg/dL)			6.86	6.1	6.86	6.14	6.86	6.1
Sub-analysis #5	76	27659						
P-value			2.88E-11		2.91E-12		6.91E-13	
Number of patients (#)			76	380	76	760	76	1520
Average SUA (mg/dL)			7.29	5.04	7.29	4.99	7.29	4.98

The "on" drug group had significantly higher serum/plasma uric acid levels in each of the analyses, despite the ratio used. Sub-analysis #1 excludes lab values taken more than one year after first medication order start date. Sub-analysis #2 excludes patients without a diagnosis of pulmonary hypertension. Sub-analysis #3 excludes lab values taken before diagnosis of pulmonary hypertension. Sub-analysis #4 only includes Sildenafil medication orders with dose > 25mg in medication name. Sub-analysis #5 excludes male patients. NA, not applicable.

Supplemental Table 5.8 Prescription frequencies of drugs that are substrates for transporters listed in the FDA Drug Development and Drug Interactions: Table of Substrates, Inhibitors, and Inducers.

Drug	Drug_generic_and_trade	count	total	%	Transporter
furosemide	['furosemide', 'lasix']	4055	27130	14.95	OAT1, OAT3 substrate
atorvastatin	['atorvastatin', 'lipitor', 'caduet']	2139	27130	7.88	OATP1B1, OATP1B3 substrate
morphine	['morphine', 'avinza', 'ms contin', 'roxanol', 'mitigo', 'arymo', 'kadian', 'morphabond', 'oramorph']	1687	27130	6.22	OCT1 substrate
famotidine	['famotidine', 'pepcid', 'dyspep', 'fluxid']	1633	27130	6.02	OAT1, OAT3 substrate
metformin	['metformin', 'glucophage', 'fortamet', 'glumetza', 'riomet']	1336	27130	4.92	OCT12, MATE1, MATE2 substrate
simvastatin	['simvastatin', 'zocor', 'flolipid']	347	27130	1.28	OATP1B1, OATP1B3 substrate
digoxin	['digoxin', 'digitek']	332	27130	1.22	P-gp substrate
rosuvastatin	['rosuvastatin', 'crestor', 'ezallor']	249	27130	0.92	BCRP, OATP1B1, OATP1B3 substrate
pravastatin	['pravastatin', 'pravachol', 'selektine']	196	27130	0.72	OAT3, OATP1B1, OATP1B3 substrate
tramadol	['tramadol', 'conzip']	177	27130	0.65	OCT1 substrate
atenolol	['atenolol', 'tenormin']	156	27130	0.58	OCT1 substrate
oseltamivir	['oseltamivir', 'tamiflu']	146	27130	0.54	OAT1, OAT3 substrate
methotrexate	['methotrexate', 'otrexup', 'rasuvo', 'rheumatrex', 'trexall', 'mtx', 'amethopterin']	39	27130	0.14	OAT1, OAT3 substrate
glyburide	['glyburide', 'diabeta', 'glynase', 'glycron', 'micronase']	38	27130	0.14	OATP1B1, OATP1B3 substrate
fexofenadine	['fexofenadine', 'allegra']	33	27130	0.12	P-gp, OATP1B1, OATP1B3 substrate
dabigatran	['dabigatran', 'pradaxa']	22	27130	0.08	P-gp substrate
sulfasalazine	['sulfasalazine', 'azulfidine', 'salazopyrin', 'sulazine']	15	27130	0.06	BCRP substrate, inhibitor

Drug	Drug_generic_and_trade	count	total	%	Transporter
sumatriptan	['sumatriptan', 'imitrex', 'onzetraxsail', 'zembrace', 'tosymra']	15	27130	0.06	OCT1 substrate
repaglinide	['repaglinide', 'prandin']	13	27130	0.05	OATP1B1, OATP1B3 substrate
nateglinide	['nateglinide', 'starlix']	4	27130	0.01	OATP1B1, OATP1B3 substrate
pitavastatin	['pitavastatin', 'livalo', 'nikita', 'zypitamag']	4	27130	0.01	OATP1B1, OATP1B3 substrate
ganciclovir	['ganciclovir', 'cytovene', 'cymevene', 'vitrasert']	2	27130	0.01	OATP1B1, OATP1B3 substrate
adefovir	['adefovir']	0	27130	0.00	OAT1, OAT3 substrate
cefaclor	['cefaclor', 'ceclor']	0	27130	0.00	OAT1, OAT3 substrate
ceftizoxime	['ceftizoxime', 'cefizox']	0	27130	0.00	OAT1, OAT3 substrate

Extracted from the CERNER database during the COVID19 period defined previously. FDA Drug Development and Drug Interactions: Table of Substrates, Inhibitors and Inducers: https://www.fda.gov/drugs/drug-interactions-labeling/drug-development-and-drug-interactions-table-substrates-inhibitors-and-inducers.

5.8 SUPPLEMENTARY INFORMATION

This supplementary text describes the methods used in this study expanding from the main methods section of the manuscript.

Establishment of transient cells

Genes encoding human OATP1B1, OATP1B3, OATP2B1, OCT1, OCT2, OAT1, OAT3, MATE1, and MATE2 were transfected in HEK293 Flp-In cells (ThermoFisher Scientific, Waltham, MA) using Lipofectamine LTX (Life Technologies, Carlsbad, CA) according to the manufacturer's protocol. In brief, 100 ng of DNA and 0.2 µL of Lipofectamine LTX were used for transfection into each well of a 96-well plate (seeding density 40,000 – 45,0000 cells/well). After 48 hours, transiently transfected cells were used for the transporter inhibition studies. Transient cells were used for determining the transporter inhibition at one concentration, 100 µM, unless mentioned otherwise.

Culture of stable cell lines

HEK293 Flp-In cells stably overexpressing human OATP2B1 (*7*), OCT1 (*8*), OCT2 (*9*), OAT1 (*10*), OAT3 (*11*), MATE1 (*12*), and MATE2 (*13*) were grown in DMEM supplemented with 10% fetal bovine serum, penicillin (100 U/ml), streptomycin (100 µg/ml), sodium pyruvate (110 µg/ml), and hygromycin B (100 µg/ml) at 37°C in a humidified incubator with 5% CO_2. HEK293 Flp-In stable cells overexpressing OATP1B1 and OATP1B3 were created using the expression vector, pCMV6-AC-GFP (Catalog number RG222130 for OATP1B1 and RG222317 for

OATP1B3), from OriGene Technologies, Inc. (Rockville, MD). Stable cells were used for determining the inhibition potencies, IC_{50} values, of selected drugs (see next section).

Transporter inhibition studies

Twenty-five COVID19 drugs were screened against 11 transporters at a concentration of 100 μM, except for baricitinib (50 μM) and tetrandrine (10 μM) due to solubility. The substrate used for each transporter is listed in **Supplemental Table 5.1**. For OATP1B1, OATP1B3, OATP2B1, OCT1, OCT2, OAT1, OAT3, MATE1, and MATE2, drugs were screened in cells transiently overexpressing each of the transporters. For P-gp and BCRP, membrane vesicles were used and the vesicular transport assays were performed as reported previously (*14*) with modifications.

Before the uptake, cell culture medium was removed, and cells were washed with warmed Hank's balanced salt solution (HBSS). Inhibition studies were performed in triplicate at 37°C for 10 minutes. Cells were then washed twice with 100 μL ice-cold HBSS buffer and lysed with 100 μL of MicroScint-20 (Perkin Elmer). The 96-well plates were placed on a shaker at room temperature for 1-2 hours. The plates were then read in a MicroBeta2 (Perkin Elmer) using the dual counting mode. Drugs that reduced the uptake of the canonical substrates by more than 50% were considered inhibitors and were further analyzed for IC_{50} determination as described previously (*11*). Drugs that are known inhibitors of a specific transporter were not evaluated further. Stable cell lines overexpressing each of the 9 transporters were used for IC_{50} determination. As recommended by the FDA guidance (fda.gov/media/134582/download), a pre-incubation step was added with OATP1B1 and OATP1B3 cells when determining IC_{50} values. All values were determined in duplicate or triplicate. The IC_{50} values were determined by fitting uptake results to the Hill equation by nonlinear regression (log (inhibitor) vs normalized response) assuming the Hill slope was -1.0 using GraphPad Prism 8. Predicted IC_{50} ($prIC_{50}$) values were determined for some of the drugs using one-point inhibition data from the initial screen (*65*). The equation used to determine $prIC_{50}$ was $V = V/\{1 + [(I)/prIC_{50}]\}$, where V and V_0 are the uptake with and without the inhibitor, respectively, and I is the inhibitor concentration (10, 50, or 100 μM accordingly).

For P-gp and BCRP, membrane vesicles were used and the vesicular transport assays were performed as reported previously (*14*) with modifications. Membrane vesicles (50 μg) overexpressing P-gp or BCRP were added to the uptake buffer containing P-gp substrate (^{3}H-N-methylquinidine) or BCRP substrate (^{3}H-CCK) with and without the inhibitor in a 96-well flat-bottom uptake plate. The uptake buffer was prepared from 50 mM MOPS-Tris, pH 7.0, 70 mM KCl and 7 mM $MgCl_2$. Uptake assays were initiated by adding ATP or AMP to a final concentration of 5 mM. Plates were incubated at 37°C for 5 min with orbital shaking (90 rpm). After 5 min, the uptake was quenched by adding 150 μL of ice-cold wash buffer to each well and the mixture (200 μL) was transferred to a 96-well filtration plate. Vacuum was applied and the vesicles were washed three times with wash buffer. Filters were removed from the filter plate and radioactivity was determined by liquid scintillation counting. Drugs that reduced transporter-mediated substrate uptake by more than 50%, respective to the substrate alone, were considered inhibitors and were further analyzed for IC_{50} determination against P-gp and BCRP using 25 μg membrane vesicles. Drugs with known IC_{50} values were not evaluated. All values were determined in duplicate or triplicate. The IC_{50} values were determined by fitting uptake results to the Hill equation by nonlinear regression (log (inhibitor) vs normalized response) assuming the

Hill slope was -1.0 using GraphPad Prism 8. The Spearman correlation coefficient, r, was determined using GraphPad Prism 8, to compare the IC_{50} values between two transporters.

Prediction of transporter-mediated inhibition

The DDI potential for each drug was evaluated in accordance to the 2020 FDA Drug-Drug Interaction Guidance (https://www.fda.gov/media/134582/download) by calculating the ratio of predicted clinically relevant drug concentration (I) to IC_{50} (I/IC_{50}). The following formulas and cutoff values were used to predict *in vivo* DDI potential:

1) $I_{gut}/IC_{50} \geq 10$
2) $I_{u,in,max}/IC_{50} \geq 0.1$
3) $C_{u,max}/IC_{50} \geq 0.1$

I_{gut} = dose / 250mL

$I_{u,in,max} = f_{u,p} \times (C_{max} + (F_a \times F_g \times k_a \times dose/Q_h/R_b))$

$C_{u,max} = C_{max} \times f_{u,p}$

Where $f_{u,p}$, C_{max}, F_a, F_g, k_a, Q_h, and R_b represent fraction of drug unbound in plasma, maximum plasma concentration, fraction absorbed, intestinal availability, absorption rate constant, hepatic blood flow rate, and blood-to-plasma concentration ratio, respectively. F_a, F_g, k_a, and Q_h were estimated to be 1, 1, 0.1 min^{-1}, and 1.62 L/min respectively.

Electronic health record analyses

1) UCSF Research Data Browser

The UCSF Research Data Browser was utilized to search for patients (irrespective of diagnosis) who had at least one laboratory test value reported for 1) serum/plasma uric acid (“Uric Acid, Serum/Plasma”; 95,207 patients), 2) triglyceride (“Triglycerides, serum”, “Triglycerides, Serum”; 236,990 patients), 3) LDL cholesterol (“LDL Cholesterol”, “Cholesterol, LDL”; 201,965 patients), 4) total cholesterol (“Cholesterol, total”; 249,388 patients), or 5) bilirubin (“Bilirubin, Total”; 428,992 patients). Values reported as an inequality were changed to a numerical value (i.e. < 0.5 mg/dL = 0.5 mg/dL). Lab values with missing values (i.e. DE-IDENTIFIED) and lab values without a lab collection date were excluded. Additionally, patients who did not have sex information or date of birth recorded in the EHR were excluded from the analysis.

For each analysis, patients were divided into two groups depending on their medication prescriptions. Specifically, patients prescribed the drug(s) of interest were grouped into the “on” drug group, respective to each analysis. Search terms for each drug were as follows: “Sildenafil”, “Revatio”, “Viagra”; “Ritonavir”, “Kaletra”, “Norvir”, “Technivie”, “Viekira”; “Darunavir”, “Prezcobix”, “Prezista”, “Symtuza”; “Lopinavir”, “Kaletra”. Only medication orders with an oral route of administration and with a medication order start date were included in the analysis. The remaining patients (i.e. individuals who were never prescribed the drug(s) of interest) were grouped into the “off” drug group. Only patients with one lab value reported in their electronic health record were included in the “off” drug group.

Patients in the "on" drug group were further filtered based on their laboratory collection dates relative to their first and last medication order start dates. Labs collected before the patient's first medication order start date or within 7 days after their first medication order start date were excluded. Additionally, labs collected after the patient's last medication order start date were excluded. A minimum of 7 days between first medication order start date and lab collection date was chosen to allow drug levels to reach steady-state and for an effect to be seen. For patients with more than one lab value, only the lab value closest to the first medication order start date was included. Lastly, patients were age- and sex- matched using the MatchIt package (*15*) in R to be comparable in both groups (**Supplemental Table 5.3**).

For patient population-specific analyses, the UCSF Research Data Browser was utilized to search and extract patients who were diagnosed with pulmonary hypertension and/or human immunodeficiency virus (HIV) since sildenafil and ritonavir/darunavir/lopinavir can be chronically used in these patient populations at doses predicted to cause a clinically relevant DDI, respectively. Patients associated with the following ICD10 codes were included in our analyses: I27.0, I27.2, I27.20, I27.21, I27.22, I27.23, I27.24, and I27.29 for the sildenafil analyses (pulmonary hypertension) and B20 for all other analyses (HIV). Diagnoses with missing diagnosis start dates were excluded. For all analyses involving ritonavir, darunavir, and ritonavir/lopinavir, lab values taken before the initial HIV diagnosis start date were excluded (i.e. labs taken on or after diagnosis start date were included).

2) CERNER Database

The Cerner HealtheDataLab database was used to search Cerner's Real World COVID19 dataset, which includes EMR data from 62 healthcare facilities across the United States from January 2015 to July 2020, for patients who were in the Emergency Room (ER) or admitted to a hospital for COVID19. Deidentified Cerner Real World Data is extracted from the EHR of hospitals in which Cerner has a data use agreement. Encounters include pharmacy, clinical and microbiology laboratory, admissions, and billing information. All admissions, medication orders and dispensing, laboratory orders and specimens are date and time stamped, providing a temporal relationship between treatment patterns and clinical information.

The Cerner Real World COVID19 dataset was utilized to search for the number of patients who have prescriptions for the following drugs, which are known substrates or inhibitors of the transporters, P-gp, BCRP, OATP1B1, OATP1B3, OCT1, OCT2, MATE1, MATE2, OAT1 and OAT3 (https://www.fda.gov/drugs/drug-interactions-labeling/drug-development-and-drug-interactions-table-substrates-inhibitors-and-inducers#table5-1). Search terms included 'Adefovir'; 'Atenolol', 'Tenormin'; 'Atorvastatin', 'Lipitor', 'Caduet'; 'Cefaclor', 'Ceclor'; 'Ceftizoxime', 'Cefizox'; 'Dabigatran', 'Pradaxa'; 'Digoxin', 'Digitek'; 'Famotidine', 'Pepcid', 'Dyspep', 'Fluxid'; 'Fexofenadine', 'Allegra'; 'Furosemide', 'Lasix'; 'Ganciclovir', 'Cytovene', 'Cymevene', 'Vitrasert'; 'Glyburide', 'Diabeta', 'Glynase', 'Glycron', 'Micronase'; 'Metformin', 'Glucophage', 'Fortamet', 'Glumetza', 'Riomet'; 'Methotrexate', 'Otrexup', 'Rasuvo', 'Rheumatrex', 'Trexall', 'Mtx', 'Amethopterin'; 'Morphine', 'Avinza', 'MS Contin', 'Roxanol', 'Mitigo', 'Arymo', 'Kadian', 'Morphabond', 'Oramorph'; 'Nateglinide', 'Starlix'; 'Oseltamivir', 'Tamiflu'; 'Pitavastatin', 'Livalo', 'Nikita', 'Zypitamag'; 'Pravastatin', 'Pravachol', 'Selektine'; 'Repaglinide', 'Prandin'; ‘Rosuvastatin', 'Crestor', 'Ezallor'; ‘Simvastatin', 'Zocor', 'Flolipid'; ‘Sulfasalazine', 'Azulfidine', 'Salazopyrin', 'Sulazine'; ‘Sumatriptan', 'Imitrex', 'Onzetraxsail', 'Zembrace', 'Tosymra'; ‘Tramadol', 'Conzip'. Medication orders with any route of delivery (e.g. oral, intravenous, intramuscular) were included.

The Cerner Real World COVID19 dataset was also queried for patients who had who had at least one positive lab test result for SARS-COV2 by serum, plasma, nasal or other specimens and at least two laboratory test values reported for serum creatinine: one value 0 to 90 days before patient’s first positive SARS-CoV2 lab test result (“Pre”), and another value 7 to 60 days after patient’s first positive SARS-CoV2 lab test result (‘Post’). LOINC code “2160-0” was used to search for serum creatinine values, and only results with a unit of measure of "milligram per deciliter" or "mg/dL" were included. Patients were divided into two groups depending on their medication order history. Specifically, patients were grouped into the “on” drug group if they had an active or complete medication order with “oral”, “intramuscular” or “intravenous” route and the medication order start date that was 0 to 30 days after the date of the first positive SARS-CoV2 lab test result. Those with no record of an order for the medications of interest were assigned to the ‘off’ drug group. Search terms for medications were as follows: “Hydroxychloroquine”, “Chloroquine”, “Aralen”, and “Plaquenil”. For the “on” drug cohort, the serum creatinine value that was reported during a period of 7 to 30 days after the earliest medication start date was used (“Post”). When multiple lab values were found within a defined time frame, the result closest to the time of the first positive SARS-CoV2 lab test was included (**Supplemental Figure 5.1**). Patients with chronic renal disease were filtered out by excluding those with ICD10 codes that begin with “N17” or “N19” or ICD9 codes that start with “584” or

“586”. To identify patients whether patients had creatinine levels that were elevated above the normal range, we used the threshold > 1.1 mg/dL (the upper limit of normal of creatinine for women) > 1.2 mg/dL (the upper limit of normal of creatinine for men) depending on patients’ sex. The MatchIt package (*15*) in R was used to match patients in the drug and control cohorts on propensity score which included age, race, ethnicity, sex, and outcome (mortality) for the main analysis, and the aforementioned covariates as well as medication indication for the analysis on patients without chronic renal disease (**Supplemental Table 5.3**). Indications for treatment with hydroxychloroquine (HCQ) or chloroquine (CQ) include systemic lupus erythematosus (SLE), discoid lupus, rheumatoid arthritis (RA), and malaria, thus the following ICD codes were used to identify patients with these conditions: SLE: ICD10 codes “M32.1”, “M32.8” or “M32.9” or ICD9 code “710.0”; discoid lupus: ICD10 code “695.4” or ICD 9 code “L93.0”; RA: ICD10 code “M06.9” or ICD9 code “714.0”; malaria: ICD10 codes that begin with “B51”, “B52”, “B53”, or “B54” or ICD9 codes that begin with “084”.

5.9 REFERENCES

1. K. Johnell, I. Klarin, The relationship between number of drugs and potential drug-drug interactions in the elderly: a study of over 600,000 elderly patients from the Swedish Prescribed Drug Register. *Drug Saf* **30**, 911-918 (2007).
2. P. S. Patel, D. A. Rana, J. V. Suthar, S. D. Malhotra, V. J. Patel, A study of potential adverse drug-drug interactions among prescribed drugs in medicine outpatient department of a tertiary care teaching hospital. *J Basic Clin Pharm* **5**, 44-48 (2014).
3. S. Cole, E. Kerwash, A. Andersson, A summary of the current drug interaction guidance from the European Medicines Agency and considerations of future updates. *Drug Metab Pharmacokinet* **35**, 2-11 (2020).
4. S. Sudsakorn, P. Bahadduri, J. Fretland, C. Lu, 2020 FDA Drug-Drug Interaction Guidance -Comparison Analysis and Action Plan by Pharmaceutical Industrial Scientists. *Curr Drug Metab*, (2020).
5. M. Khezrian, C. J. McNeil, A. D. Murray, P. K. Myint, An overview of prevalence, determinants and health outcomes of polypharmacy. *Ther Adv Drug Saf* **11**, 2042098620933741 (2020).
6. K. M. Giacomini *et al.*, Membrane transporters in drug development. *Nat Rev Drug Discov* **9**, 215-236 (2010).
7. L. Zou *et al.*, Bacterial metabolism rescues the inhibition of intestinal drug absorption by food and drug additives. *Proc Natl Acad Sci U S A* **117**, 16009-16018 (2020).
8. E. C. Chen *et al.*, Discovery of Competitive and Noncompetitive Ligands of the Organic Cation Transporter 1 (OCT1; SLC22A1). *J Med Chem* **60**, 2685-2696 (2017).

9. Y. Kido, P. Matsson, K. M. Giacomini, Profiling of a prescription drug library for potential renal drug-drug interactions mediated by the organic cation transporter 2. *J Med Chem* **54**, 4548-4558 (2011).

10. L. Zou *et al.*, Molecular Mechanisms for Species Differences in Organic Anion Transporter 1, OAT1: Implications for Renal Drug Toxicity. *Mol Pharmacol* **94**, 689-699 (2018).

11. L. Zou *et al.*, Drug Metabolites Potently Inhibit Renal Organic Anion Transporters, OAT1 and OAT3. *J Pharm Sci*, (2020).

12. M. B. Wittwer *et al.*, Discovery of potent, selective multidrug and toxin extrusion transporter 1 (MATE1, SLC47A1) inhibitors through prescription drug profiling and computational modeling. *J Med Chem* **56**, 781-795 (2013).

13. K. M. Morrissey *et al.*, The Effect of Nizatidine, a MATE2K Selective Inhibitor, on the Pharmacokinetics and Pharmacodynamics of Metformin in Healthy Volunteers. *Clin Pharmacokinet* **55**, 495-506 (2016).

14. L. Zou *et al.*, Interactions of Oral Molecular Excipients with Breast Cancer Resistance Protein, BCRP. *Mol Pharm* **17**, 748-756 (2020).

15. D. Ho, K. Imai, G. King, E. A. Stuart, MatchIt: Nonparametric Preprocessing for Parametric Causal Inference. *2011* **42**, 28 (2011).

16. S. Izumi *et al.*, Substrate-dependent inhibition of organic anion transporting polypeptide 1B1: comparative analysis with prototypical probe substrates estradiol-17β-glucuronide, estrone-3-sulfate, and sulfobromophthalein. *Drug Metab Dispos* **41**, 1859-1866 (2013).

17. M. M. Posada *et al.*, Prediction of Transporter-Mediated Drug-Drug Interactions for Baricitinib. *Clin Transl Sci* **10**, 509-519 (2017).

18. X. Liang *et al.*, Organic cation transporter 1 (OCT1) modulates multiple cardiometabolic traits through effects on hepatic thiamine content. *PLoS Biol* **16**, e2002907 (2018).

19. X. Chu, K. Bleasby, G. H. Chan, I. Nunes, R. Evers, The Complexities of Interpreting Reversible Elevated Serum Creatinine Levels in Drug Development: Does a Correlation with Inhibition of Renal Transporters Exist? *Drug Metab Dispos* **44**, 1498-1509 (2016).

20. M. J. Zamek-Gliszczynski *et al.*, Transporters in Drug Development: 2018 ITC Recommendations for Transporters of Emerging Clinical Importance. *Clin Pharmacol Ther* **104**, 890-899 (2018).

21. M. Niemi, M. K. Pasanen, P. J. Neuvonen, Organic anion transporting polypeptide 1B1: a genetically polymorphic transporter of major importance for hepatic drug uptake. *Pharmacol Rev* **63**, 157-181 (2011).

22. H. Koepsell, Organic Cation Transporters in Health and Disease. *Pharmacol Rev* **72**, 253-319 (2020).

23. A. Yonezawa, K. Inui, Importance of the multidrug and toxin extrusion MATE/SLC47A family to pharmacokinetics, pharmacodynamics/toxicodynamics and pharmacogenomics. *Br J Pharmacol* **164**, 1817-1825 (2011).

24. S. Ito *et al.*, Competitive inhibition of the luminal efflux by multidrug and toxin extrusions, but not basolateral uptake by organic cation transporter 2, is the likely mechanism underlying the pharmacokinetic drug-drug interactions caused by cimetidine in the kidney. *J Pharmacol Exp Ther* **340**, 393-403 (2012).

25. T. Nakada, T. Kudo, T. Kume, H. Kusuhara, K. Ito, Estimation of changes in serum creatinine and creatinine clearance caused by renal transporter inhibition in healthy subjects. *Drug Metab Pharmacokinet* **34**, 233-238 (2019).

26. S. Gupta *et al.*, Pharmacokinetic and safety profile of desloratadine and fexofenadine when coadministered with azithromycin: a randomized, placebo-controlled, parallel-group study. *Clin Ther* **23**, 451-466 (2001).

27. H. Dorani *et al.*, Pharmacokinetics and pharmacodynamics of the oral direct thrombin inhibitor ximelagatran co-administered with different classes of antibiotics in healthy volunteers. *Eur J Clin Pharmacol* **63**, 571-581 (2007).

28. J. J. Kiser *et al.*, Drug/Drug interaction between lopinavir/ritonavir and rosuvastatin in healthy volunteers. *J Acquir Immune Defic Syndr* **47**, 570-578 (2008).

29. D. Samineni, P. B. Desai, L. Sallans, C. J. Fichtenbaum, Steady-state pharmacokinetic interactions of darunavir/ritonavir with lipid-lowering agent rosuvastatin. *J Clin Pharmacol* **52**, 922-931 (2012).

30. R. P. van Heeswijk *et al.*, Time-dependent interaction between lopinavir/ritonavir and fexofenadine. *J Clin Pharmacol* **46**, 758-767 (2006).

31. T. Fiolet *et al.*, Effect of hydroxychloroquine with or without azithromycin on the mortality of coronavirus disease 2019 (COVID-19) patients: a systematic review and meta-analysis. *Clin Microbiol Infect*, (2020).

32. D. M. Roden, R. A. Harrington, A. Poppas, A. M. Russo, Considerations for Drug Interactions on QTc Interval in Exploratory COVID-19 Treatment. *J Am Coll Cardiol* **75**, 2623-2624 (2020).

33. L. S. Nguyen *et al.*, Cardiovascular Toxicities Associated With Hydroxychloroquine and Azithromycin: An Analysis of the World Health Organization Pharmacovigilance Database. *Circulation* **142**, 303-305 (2020).

34. D. M. Roden, R. A. Harrington, A. Poppas, A. M. Russo, Considerations for Drug Interactions on QTc in Exploratory COVID-19 Treatment. *Circulation* **141**, e906-e907 (2020).

35. J. Weiss, G. Bajraktari-Sylejmani, W. E. Haefeli, Interaction of Hydroxychloroquine with Pharmacokinetically Important Drug Transporters. *Pharmaceutics* **12**, (2020).

36. J. M. Scherrmann, Intracellular ABCB1 as a Possible Mechanism to Explain the Synergistic Effect of Hydroxychloroquine-Azithromycin Combination in COVID-19 Therapy. *AAPS J* **22**, 86 (2020).

37. A. Hosomi, T. Nakanishi, T. Fujita, I. Tamai, Extra-renal elimination of uric acid via intestinal efflux transporter BCRP/ABCG2. *PLoS One* **7**, e30456 (2012).

38. K. Ichida *et al.*, Decreased extra-renal urate excretion is a common cause of hyperuricemia. *Nat Commun* **3**, 764 (2012).

39. C. Pattaro *et al.*, Genetic associations at 53 loci highlight cell types and biological pathways relevant for kidney function. *Nat Commun* **7**, 10023 (2016).

40. M. Kanai *et al.*, Genetic analysis of quantitative traits in the Japanese population links cell types to complex human diseases. *Nat Genet* **50**, 390-400 (2018).

41. A. P. Morris *et al.*, Trans-ethnic kidney function association study reveals putative causal genes and effects on kidney-specific disease aetiologies. *Nat Commun* **10**, 29 (2019).

42. A. D. Johnson *et al.*, Genome-wide association meta-analysis for total serum bilirubin levels. *Hum Mol Genet* **18**, 2700-2710 (2009).

43. T. Alici, Y. Imren, M. Erdil, H. Gundes, Gouty arthritis at interphalangeal joint of foot after sildenafil use: A case report. *Int J Surg Case Rep* **4**, 11-14 (2013).

44. W. L. Chen, H. I. Chen, C. H. Loh, Acute gouty arthritis after taking sildenafil: an old disease with a new etiology. *J Rheumatol* **36**, 210-211 (2009).

45. P. R. Ding *et al.*, The phosphodiesterase-5 inhibitor vardenafil is a potent inhibitor of ABCB1/P-glycoprotein transporter. *PLoS One* **6**, e19329 (2011).

46. Z. C. Jing *et al.*, Vardenafil treatment for patients with pulmonary arterial hypertension: a multicentre, open-label study. *Heart* **95**, 1531-1536 (2009).

47. NORVIR [package insert]. North Chicago, IL; AbbVie Inc. https://www.rxabbvie.com/pdf/norvirtab_pi.pdf.

48. S. Mathialagan, B. Feng, A. D. Rodrigues, M. V. S. Varma, Drug-Drug Interactions Involving Renal OCT2/MATE Transporters: Clinical Risk Assessment May Require Endogenous Biomarker-Informed Approach. *Clin Pharmacol Ther*, (2020).

49. X. Chu *et al.*, Clinical Probes and Endogenous Biomarkers as Substrates for Transporter Drug-Drug Interaction Evaluation: Perspectives From the International Transporter Consortium. *Clin Pharmacol Ther* **104**, 836-864 (2018).

50. H. Dorani *et al.*, Pharmacokinetics and pharmacodynamics of the oral direct thrombin inhibitor ximelagatran co-administered with different classes of antibiotics in healthy volunteers. *Eur J Clin Pharmacol* **63**, 571-581 (2007).

51. J. L. Montastruc, P. L. Toutain, A New Drug-Drug Interaction Between Hydroxychloroquine and Metformin? A Signal Detection Study. *Drug Saf* **43**, 657-660 (2020).

52. M. Jallouli *et al.*, Determinants of hydroxychloroquine blood concentration variations in systemic lupus erythematosus. *Arthritis Rheumatol* **67**, 2176-2184 (2015).

53. R. B. Landewe *et al.*, Antimalarial drug induced decrease in creatinine clearance. *J Rheumatol* **22**, 34-37 (1995).

54. L. Deng *et al.*, Arbidol combined with LPV/r versus LPV/r alone against Corona Virus Disease 2019: A retrospective cohort study. *J Infect* **81**, e1-e5 (2020).

55. E. Martinez *et al.*, Early lipid changes with atazanavir/ritonavir or darunavir/ritonavir. *HIV Med* **15**, 330-338 (2014).

56. F. Montastruc, S. Thuriot, G. Durrieu, Hepatic Disorders With the Use of Remdesivir for Coronavirus 2019. *Clin Gastroenterol Hepatol* **18**, 2835-2836 (2020).

57. Y. Wang *et al.*, Remdesivir in adults with severe COVID-19: a randomised, double-blind, placebo-controlled, multicentre trial. *Lancet* **395**, 1569-1578 (2020).

58. L. Dai *et al.*, Impact of Lopinavir/Ritonavir and Efavirenz-Based Antiretroviral Therapy on the Lipid Profile of Chinese HIV/AIDS Treatment-Naive Patients in Beijing: A Retrospective Study. *Curr HIV Res* **17**, 324-334 (2019).

59. P. Debroy *et al.*, Antiretroviral therapy initiation is associated with decreased visceral and subcutaneous adipose tissue density in people living with HIV. *Clin Infect Dis*, (2020).

60. J. M. Molina *et al.*, Doravirine versus ritonavir-boosted darunavir in antiretroviral-naive adults with HIV-1 (DRIVE-FORWARD): 96-week results of a randomised, double-blind, non-inferiority, phase 3 trial. *Lancet HIV* **7**, e16-e26 (2020).

61. Veklury (remdesivir) [package insert], Foster City, CA; Gilead Sciences Inc; 2020. https://www.accessdata.fda.gov/drugsatfda_docs/label/2020/214787Orig1s000lbl.pdf.

62. M. M. Redfield *et al.*, Effect of phosphodiesterase-5 inhibition on exercise capacity and clinical status in heart failure with preserved ejection fraction: a randomized clinical trial. *JAMA* **309**, 1268-1277 (2013).

63. R. Hase *et al.*, Acute Gouty Arthritis During Favipiravir Treatment for Coronavirus Disease 2019. *Intern Med* **59**, 2327-2329 (2020).

64. E. Mishima, N. Anzai, M. Miyazaki, T. Abe, Uric Acid Elevation by Favipiravir, an Antiviral Drug. *Tohoku J Exp Med* **251**, 87-90 (2020).

65. B. Vora *et al.*, Drug-nutrient interactions: discovering prescription drug inhibitors of the thiamine transporter ThTR-2 (SLC19A3). *Am J Clin Nutr* **111**, 110-121 (2020).

CHAPTER 6

Conclusions and Perspectives

This dissertation provides an excellent example of how laboratory experiments, clinical trials, and real world data can be integrated to investigate drug interactions. Here, we present three separate projects across a spectrum of scientific topics, drug-nutrient interactions (DNIs), drug-variant interactions (DVIs), and drug-drug interactions (DDIs), where preliminary *in vitro* data was extended past the bench using clinical trials, pharmacological modelling, and real world data.

In Chapter 2, we focused on characterizing inhibitors of the primary intestinal absorptive transporter for thiamine (ThTR-2) using a multi-faceted approach. A common shortcoming to *in vitro* findings is their translatability to humans; a drug which may inhibit a transporter in cells may not inhibit the transporter clinically. We were able to start addressing this gap by querying electronic health records (EHRs) and observing a drug-induced thiamine deficient signature in patients prescribed inhibitors identified in our screen. However, we were limited by small sample sizes; thiamine pyrophosphate is not a commonly ordered laboratory test. Additionally, comorbidities as well as a lack of a controlled diet confounds our results and makes it difficult to tease apart drug-induced changes versus changes driven by other factors.

Thus, to address some of these concerns and drawbacks, we performed a prospective clinical study in Chapter 3. Prospective clinical trials represent the gold standard for studies of drug interactions. By recruiting healthy volunteers and implementing a thiamine deficient diet, we were able to control covariates which eluded us in the real world analysis in Chapter 2. A randomized crossover design allowed each person to serve as their own control increasing the power of the study. Our findings were contrary to our initial hypothesis, which was that trimethoprim would lower thiamine levels as a result of inhibition of intestinal ThTR-2 mediated thiamine absorption. Instead, we found that trimethoprim increased thiamine levels, possibly as a result of inhibition of the hepatic uptake transporter, OCT1. This finding is one of great interest since inhibition of OCT1 has been associated with increased lipid levels. Once again, we were able to support our *in vitro* findings using EHR data; however, further studies in healthy volunteers and patients diagnosed with HIV are needed to control for variables such as disease state, patient compliance, and genetic variants. Importantly, the study underscores the complexity of drug-transporter interactions, in which drugs may inhibit more than one transporter causing variable effects.

In Chapter 4, we shifted our focus from DNIs to pharmacogenomics, specifically investigating the association between BCRP p.Q141K, allopurinol/oxypurinol, and serum uric acid (SUA). Our study revealed that patients homozygous for the p.Q141K variant had a longer half-life than patients who were homozygous for the reference allele. Additionally, we were able to suggest that enterohepatic circulation of oxypurinol may be affecting the pharmacodynamics of allopurinol. In addition to the costs and length of clinical trials, recruiting patients who were homozygous variant for BCRP p.Q141K was difficult and limited our sample size. However, we were able to build a preliminary PKPD model to identify covariates significantly affecting oxypurinol and SUA concentrations, respectively; this model can be leveraged for future studies and models. Lastly, we were able to use real world data to demonstrate that clinical inhibitors of BCRP associated with increased SUA levels, suggesting the potential of these drugs to cause hyperuricemia and increased risk for gout in susceptible patient populations. A caveat in our EHR analysis that plays a crucial role for this study is that the BCRP genotype of these patients was unknown. Unfortunately, most EHR databases do not currently include genotype information; however, with increasing ease and cost-effectiveness of genetic testing, we are hopeful that patients will be screened for variants in major transporters and enzymes, including BCRP, and this data will be recorded in EHRs for use in patient care as well as research. The study suggested that a pharmacodynamic, rather than a pharmacokinetic, mechanism was responsible for the finding (in several genome-wide association and candidate gene studies) that BCRP p.Q141K associates with poor response to allopurinol.

Lastly, given the time of this dissertation work and the COVID19 pandemic, Chapter 5 focused on elucidating the potential of drugs in clinical trials for COVID19 to cause clinically relevant DDIs, which could lead to potential adverse drug reactions with the use of concomitant medications. Although DDIs are thoroughly investigated throughout the drug development process, the COVID19 pandemic brought upon uncharted territory with the use of drugs in vulnerable patient populations or with concomitant medications that have not been previously studied. Our study identified 21 (out of 25) drugs which were predicted to cause a clinically relevant DDI in patients. Furthermore, we were able to use EHRs from patients not only in the general population but also patients diagnosed with COVID19 to complement our *in vitro* findings. Once again, the use of real world, real patient data allowed us to investigate the applicability and translatability of our findings in the laboratory. Although we were limited by the number of COVID19 patients for our analyses, as more EHR data becomes available, we will be able to account for confounding variables and covariates as well as increase the sample size and robustness of our analyses.

This dissertation focuses on building a bridge between findings in the laboratory and their translation to the clinic. Notably, EHRs are a relatively new source of rich data for research purposes that allows for not only extension of preliminary findings but also hypothesis generation and development. Although there is work to be done and obstacles to be overcome, as discussed in Chapter 1, before the full potential of EHR data can be unlocked and there can be widespread integration, the work presented in this dissertation demonstrates how with increasing standardization and availability, compounded with its low costs relative to clinical trials, EHRs represent a gold mine for patient data and can help bring a real world, real patient component to pharmacological research.

Publishing Agreement

It is the policy of the University to encourage open access and broad distribution of all theses, dissertations, and manuscripts. The Graduate Division will facilitate the distribution of UCSF theses, dissertations, and manuscripts to the UCSF Library for open access and distribution. UCSF will make such theses, dissertations, and manuscripts accessible to the public and will take reasonable steps to preserve these works in perpetuity.

I hereby grant the non-exclusive, perpetual right to The Regents of the University of California to reproduce, publicly display, distribute, preserve, and publish copies of my thesis, dissertation, or manuscript in any form or media, now existing or later derived, including access online for teaching, research, and public service purposes.

DocuSigned by:
Bianca Vora
03C84BA0CA07482...

Author Signature

3/11/2021

Date